Towards the Development of a New Technique for Mastectomy-Scar Electron Beam Treatment Using a Variable Collimator and Computer-Automated Treatment Table Control

by

Musikavanhu Roy Mlambo
04571437

Submitted in fulfilment of the requirements for the degree of

Doctor of Philosophy Medical Physics in the

Faculty of Health Sciences

University of Pretoria
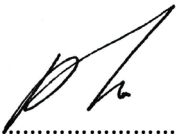
Supervisor: Prof Ado van Rensburg

March 2023

UNIVERSITEIT VAN PRETORIA
UNIVERSITY OF PRETORIA
YUNIBESITHI YA PRETORIA

DECLARATION

I, Musikavanhu Roy Mlambo, hereby declare that this thesis, submitted in fulfilment of the requirements for the degree of Doctor of Philosophy Medical Physics, in the Faculty of Health Sciences, at the University of Pretoria, is entirely my own work unless otherwise referenced or acknowledged. This thesis has not been submitted for qualifications at any other academic institutions.

SIGNATURE: …………/…………………………………………………

DATE: ………………06 March 2023………………………..

ABSTRACT

Breast cancer in women is the most prevalent cancer in both developed and less developed countries, with an incidence of about 2.3 million new cases diagnosed in 2020, which is about 25% of all cancers in women. Several treatment options and techniques are available for the treatment of breast cancer, including surgery, chemotherapy, hormone therapy and radiotherapy, with treatment sometimes involving a combination of these techniques. Nonrandomized studies comparing breast conservation therapy with either electron beam therapy or interstitial implants, showed that there was no statistical difference between the treatment techniques in terms of disease-free survival, cosmesis, local tumour control or morbidity. The use of orthovoltage x-ray beam treatment has also been considered. It has some advantages, such as less shielding requirements and lower equipment costs. However, it has some drawbacks, such as the limitation on the beam penetration, leading to the maximum dose being deposited on the patient's skin, and also requiring longer treatment times because of the lower dose rates. From a South African context, orthovoltage therapy has become obsolete, as the handful of machines are not in operation with a decline worldwide in favour of using linacs. With linacs becoming more widely used and accessible, electron beam therapy remains a mainstay in treating breast cancer compared to other available treatment modalities.

Patients showing locally advanced breast cancer have a risk of both distant and local-regional recurrence. Postmastectomy radiation therapy after surgery reduces the risk of recurrence and improves disease-free and overall survival. A patient undergoing postmastectomy radiotherapy may receive a mastectomy scar electron boost to reduce the risk of local recurrence. Compared with other treatment modalities such as orthovoltage, brachytherapy or photon therapy, electron beam treatment reduces the dose to underlining tissue beyond the target volume and offers a more uniform dose distribution (Khan, 2003). The energy of the electron beam to be used for treatment is determined by the thickness of the breast tissue from the chest wall to the skin (Griem and Hardin, 1998). The physical properties of electron beams make them suitable for chest wall treatment in breast treatment; the crucial motivation for the use of electron beam irradiation is the shape of the depth dose curve. The

electron beam, however, needs to be collimated right down to the patient's surface using applicators and cutouts, which are positioned on the applicator as close as possible to the patient to provide a more customized field shape. Due to the disadvantages of traditional electron beam shaping using cutouts, this study proposes an alternative technique which retains the applicator but replaces the end of the applicator with a variable field shaping device allowing the collimator to deliver the dose over the entire region that would have commonly been treated using a cutout. To achieve the required dose distribution, the new technique makes use of the sliding window technique and incorporates the automated movement of the treatment table. This study aimed to develop a new treatment technique for treating the mastectomy scar using a collimated electron beam and a computer-controlled automated treatment table. The research set out to achieve the following objectives: develop a functional variable field shaping device that will allow treating the mastectomy scar; conduct measurements for the new technique; automate the couch movement for automated patient treatment of breast scar and have a working treatment technique. The proof of concept was carried out in developing a technique for treating mastectomy scars that used a variable collimator and automated treatment table. The treatment technique is an alternative to conventional treatment techniques that use lead and Wood's-alloy electron cut-outs.

Dedication

To my lovely wife Tlatso,
and our children
Roy Jr, Neo and Orefile

In Loving Memory of my father
Seth Thomas Mlambo
(1940 – 2018)

&

My mother
Esnarth Mlambo
(1945 – 2002)

What is man, that thou art mindful of him? and the son of man, that thou visitest him? For thou hast made him a little lower than the angels, and hast crowned him with glory and honour. Thou madest him to have dominion over the works of thy hands; thou hast put all things under his feet.

Psalm 8:4-7

ACKNOWLEDGEMENTS

TABLE OF CONTENTS

ACRONYMS

AAPM	American Association of Physicists in Medicine
DVH	Dose Volume Histogram
EIMRT	Electron Intensity Modulated Radiotherapy
EMET	Energy Modulated Electron Therapy
eMLC	Electron Multileaf Collimator
FLEC	Few Leaf Electron Collimator
FWHM	Full-Width Half-Maximum
HDR-IORT	High Dose Rate Intraoperative Radiotherapy
ICRU	International Commission on Radiation Units and Measurements
IMRT	Intensity Modulated Radiotherapy
IOERT	Intraoperative Electron Radiotherapy
IORT	Intraoperative Radiotherapy
LET	Linear Energy Transfer
MLC	Multileaf Collimator
MU	Monitor Unit
NCR	National Cancer Registry (South Africa)
OAR	Organs at Risk
PBS	Pencil Beam Scanning
PTV	Planning Target Volume
SSD	Source to Surface Distance
TPS	Treatment Planning System
TVT	Tenth Value Thickness
VMAT	Volumetric Modulated Arc Therapy
WHO	World Health Organization

LIST OF FIGURES

LIST OF TABLES

CHAPTER 1

INTRODUCTION AND STUDY ORIENTATION

This section gives a brief overview of the study, with an introduction and orientation of the research. Breast cancer incidences and various breast cancer treatments are also discussed. This is followed by a concise description of the issues the study seeks to address.

1.1 Background

Breast cancer was probably first documented by the Yellow Emperor Huang Di (b. 2698 BCE), with the first operative treatment for breast cancer credited to the Greek physician Leonides (Bland et al., 2018, Roses, 2005). Breast cancer in women is the most prevalent cancer worldwide, with an incidence of about 2.3 million new cases diagnosed in 2020 (Sung et al., 2021). Low and middle-income countries are the most affected by high incidence rates of breast cancer (Love, 2008). Globally in 2020, breast cancer is the fifth leading cause of cancer death, with 685,000 deaths, with 1 in 6 cancer deaths in women and the leading cause of death in 86 % of the countries worldwide (Sung et al., 2021, WCRF International, 2023). Breast cancer has a significant effect on the economy, whereby the incidence of cancer is estimated to have increased by more than 20% and mortality by 14% since 2008 (Ferlay et al., 2013). In 2018 Breast cancer accounted for 12% of all cancers, making it the second most common cancer overall after lung cancer, and 25% of all cancers in women. However, by the end of 2020 it was the world's predominant cancer, accounting for 25.8% of all new cancer cases, with 7.8 million women diagnosed in the past five years living with breast cancer (WHO, 2021, World Cancer Research Fund and American Institute for Cancer Research, 2018). Female breast cancer is in the top three cancers globally in terms of incidence, is the fifth in terms of mortality, and is in the top two in terms of the number of new cases, with incidence rates that surpass other cancers in both developed and developing countries (IARC, 2018). Breast cancer also affects males, accounting for 1% of all breast cancers (Ajithkumar and Eadens, 2011, Jain and Gradishar, 2018). Even though there are fewer studies, postmastectomy radiation therapy in male patients has been shown to significantly increase local recurrence-free

survival (Yu et al., 2012, Jain and Gradishar, 2018, Liu et al., 2015). In some countries in Sub-Sahara, breast cancer is the second leading cause of deaths after cervical cancer (Bray et al., 2018). The National Cancer Registry (NCR) Report of 2019 showed that in South Africa, histologically diagnosed breast cancer accounts for 23.22% of all cancers in women, a decrease of 0.21% from the 2018 report (National Cancer Registry, 2019, National Cancer Registry, 2018). A number of studies have indicated that there are specific risk factors associated with breast cancer and that the high rise of cancer is caused by lifestyle changes and a lack of timely clinical interventions in affected regions (Lacey et al., 2009, World Cancer Research Fund and American Institute for Cancer Research, 2018).

Over the years, there has been an increasing number of breast cancer treatment options that have become available; the following sections below provide an overview of some of these options.

1.1.1 Electron Beam Radiotherapy

The use of megavoltage electrons in conventional radiotherapy for treating cancer began between the 1930s and 1950s, with some centres showing electron therapy as the only alternative cancer treatment (Khan, 2003, Khan et al., 1991). The ICRU (2004) states that the relative biological effectiveness of electrons can be taken to be the same as that of photons. In the early days of electron therapy, clinical electron beams were initially produced by betatrons (Bova, 1995). The first betatron was successfully operated at the University of Illinois in 1941 (Gund and Paul, 1950). The first medical application was also at the same university in the College of Medicine in 1951 (Haas et al., 1954), with the first commercial Siemens betatron for electron therapy installed in Göttingen and Heidelberg, Germany in 1953 (Adams et al., 1995). The modern, more widely used treatment electron beam is produced by a linear accelerator (linac). Prior to 1954, electron beams were also used in radiotherapy under the names cathode rays or beta radiation (Haas et al., 1954, Trump et al., 1940).

Electrons are commonly used in chest wall irradiation for breast cancer, treating skin and lip cancers, and treatment of head and neck cancers, amongst others. Compared with other

treatment modalities such as orthovoltage, brachytherapy or photon therapy, electron beam treatment reduces the dose to underlining tissue beyond the target volume and offers a more uniform dose distribution (Khan, 2003). Electron beam therapy remains to play a crucial role in the treatment of breast cancer. This is due to the inherent properties of electrons and the dose profile, which makes them suitable in the treatment of the chest wall allowing for the sparing of the lungs and heart. Traditionally, cutouts are employed when treating the mastectomy scar, as the electrons require to be collimated close to the patient's skin owing to them being easily scattered. This study sort to eliminate the use of these cutouts, which have a number of disadvantages. The cutouts were replaced by a movable electron collimator. Haussmann et al. (2020) conducted a review of the recent advances in the treatment of breast cancer in radiotherapy, including electron beam therapy. The review considered techniques that included treatment of regional lymph nodes as well as axillary lymph nodes, accelerated partial breast irradiation, hypofractionated post-mastectomy radiotherapy and neoadjuvant radiochemotherapy for the timing of the application of boost therapy as this poses a risk on wound healing and cosmetics. With the advancement of these techniques electron beam therapy remains an integral part in the treatment of breast cancer.

1.2 Overview of Types of Breast Cancer Treatment

There are different types of breast cancer, with the majority of breast cancers originating either in the ducts or in the lobes of the breast, referred to as ductal carcinoma and lobular carcinoma (Wazer and Arthur, 2013, Azodi et al., 2012). A number of treatment options and techniques are available for the treatment of breast cancer. These techniques, amongst others include surgery, chemotherapy, hormone therapy and radiotherapy, with treatment sometimes involving a combination of these techniques. The decision on which treatment to take is very complex and depends on several factors, such as the type of cancer, how advanced it is and patient preferences. Treatment often requires a multidisciplinary team approach and the expertise of the treatment team in decision-making (Buchholz et al., 2013, Kunkler, 2012). A team approach to treating breast cancer with specialists ranging from pathologists, geneticists, surgeons, medical physicists, oncologists, and psychiatrists can reduce mortality and improve the quality of life (Boyle, 2009). This often leads to

multimodality therapy to achieve optimal treatment (Niederhuber, 2005). With surgery, different types of treatment are available, such as segmental mastectomy, radical mastectomy, modified radical mastectomy, extended radical mastectomy, skin-sparing mastectomy, nipple-sparing mastectomy and total or simple mastectomy (Buchholz et al., 2013, Ajithkumar and Eadens, 2011). Segmental mastectomy, also known as lumpectomy or tylectomy, is when the primary tumour with a margin of breast tissue is removed. Radical mastectomy is the removal of the parenchyma breast tissue and pectoralis major muscle with level I/II axillary dissection. Although this can be a mutilating procedure, patients can have disease-free survival of 30-40 years (Kunkler, 2003). Modified radical mastectomy is the removal of the breast tissue plus axillary level I/II dissection. Extended radical mastectomy is radical mastectomy and internal mammary lymph node dissection, which may also include a level III axillary lymph node dissection. Skin-sparing mastectomy is simple or modified radical mastectomy with the preservation of a significant component of the breast skin to optimize the aesthetic result of immediate reconstruction. Nipple-sparing mastectomy involves the preservation of the nipple, which may include the nipple-areola complex. Bilateral mastectomy has also been suggested for patients with unilateral breast cancer but with a high risk of contralateral cancer (Narod, 2014). Simple mastectomy is the surgical removal of the entire breast tissue alone. Simple mastectomy, together with a sentinel lymph node dissection, followed by radiotherapy may be the treatment of choice for locally advanced breast cancer with large tumours (Ajithkumar and Eadens, 2011, Fowble et al., 2010). Breast conservation therapy is also an option for patients with a primary tumour of less than or equal to 4 cm, and enough breast for suitable cosmetic results after the tumour has been excised (Montague et al., 1988).

Patients showing locally advanced breast cancer have a risk of both distant and local-regional recurrence. Clinically occult disease in the operation site and regional nodes result in distant metastases. Locoregional recurrence "is recurrent cancer in the bone, muscle, skin or subcutaneous tissue of the chest wall" (Chao et al., 2002). For patients not getting systemic therapy, locoregional failure occurs in about 25% - 40% of node-positive patients and up to 15% - 20% of node-negative patients (Horst et al., 2012). Postmastectomy radiotherapy is an important part of the multimodal treatment of breast cancer with the goal of reducing the

risk of both locoregional and distant metastases (Alluri and Jagsi, 2018). Postmastectomy radiation therapy reduces the risk of recurrence (Ajithkumar and Eadens, 2011), and improves disease-free and overall survival (Buchholz et al., 2013, Sedlmayer et al., 2011, Fowble et al., 2010, Khan, 2007, Ragaz et al., 2005). Poortmans (2007) reported that radiotherapy reduces the locoregional relapse rate by 70%, with Recht (2009) indicating a reduced locoregional failure rate of 75% in some patients. Postmastectomy radiotherapy is recommended for the treatment of the chest wall, supraclavicular, axillary and appropriate draining regional nodes (Khan, 2007). It is indicated for patients with four or more positive nodes and T3 and T4 tumours (Barrett et al., 2009). Studies show that the use of radiotherapy improves local control rates (Harris et al., 2012). The technique should deliver adequate radiation to the treatment region with minimal radiation to the critical structures such as the heart and lungs (Magee et al., 1991). Several techniques are used to treat the chest wall and internal mammary lymph nodes; more commonly, they include extended tangent photon fields, partially wide photon tangent fields, electrons-only fields or a combination of both electron and photon fields. This research work focused on developing a new postmastectomy radiotherapy treatment technique using electrons.

1.3 Statement of the Problem

Postmastectomy radiotherapy is usually prescribed for breast cancer patients. The administration of chest wall locoregional radiotherapy after mastectomy or breast-conserving cancer surgery, can significantly increase local tumour control and overall survival (Jansson et al., 1998, Salguero et al., 2009). The most common site for recurrence is the mastectomy scar (Kunkler, 2012). A patient undergoing postmastectomy radiotherapy may receive a mastectomy scar electron boost to reduce the risk of local recurrence (Motwani et al., 2006). The boost field comprises of en face electrons encompassing the scar with a 3 - 5 cm margin (Vassil and Tendulkar, 2012). A boost is used firstly to treat the scar, as this is likely to have the most residual microscopic disease and also to counteract the effects of hypoxia resulting from treating the large field (Stevens, 2005). Currently, the Medical Physics department at Steve Biko Academic Hospital treats scars by giving an electron boost, which is done by marking the skin and adding a 3 cm margin around the scar, similar to what is suggested by

Chao et al. (2002) and (Khan and McNeese, 1999), with an electron dose of 10 - 20 Gy at 2 Gy per fraction prescribed to 90% depth dose. Unlike photons, the dose prescription point for electrons is relative to a dose at a point in water (Hogstrom et al., 2000). For chest wall treatment, it is important to minimize the dose to the heart and lungs, which are organs at risk (OAR) (Chao et al., 2002). It has been reported that there is a correlation between cardiac deaths with irradiation of tumours in the breast (Jansson et al., 1998, Fowble et al., 2010).

As electrons traverse matter, they undergo elastic or inelastic collisions with the atomic electrons as well as elastic or inelastic collisions with the nuclei (which is the predominant process) due to Coulomb force interactions; this results in the electrons suffering multiple scattering. The inelastic collisions result in ionization and excitation for interactions with atomic electrons and bremsstrahlung production for interactions with the nuclei. Electrons are negatively charged and have a small mass, which is approximately about 1/2000th the mass of a proton or neutron. As they travel through the medium, they are either attracted or repelled by positive or negative charges, and because of their small mass, they are easily deflected from their original path. As a result of the scattering of the electrons, the electron beam needs to be collimated right down to the patient's surface. As the electrons pass through the scattering foil, other elements of the linear accelerator head as well as the air between the patient and the exit window, as shown in Figure 2.2, the electrons are scattered. Collimation is required to have a clinically acceptable penumbra. The electron beam penumbra is defined as the distance between the 80% and 20% dose points on the central axis at a specified depth of maximum dose. The conventional collimators for photon beams can be used for electron field-shaping (Mueller et al., 2018; du Plessis et al., 2006). For electrons, the collimation from the linac head right down to the patient needs to have an acceptable clinical beam profile, as the angular fluence of the electrons is affected by the collimating system (Van der Merwe, 1994).

In conventional electron beam therapy, applicators or cones attached to the treatment unit head are used to collimate the beam, such that the field of the electron beam is defined at a distance away from the surface of the patient for non-extended SSD treatments. Conventional field shaping of electron beams to conform the therapeutic dose surface of the electron beam to the target volume is always achieved with electron applicators (cones) in

conjunction with cutouts (or blocks) with or without bolus to modify beam energy and intensity. The cut-outs, as shown in Figure 1.1, which are placed on the applicator as close as possible to the patient, provide a more customized field shape. These patient-specific cutouts are constructed from toxic Wood's alloy, also known as Cerrobend which is molten during fabrication. The molten metal, as well as the Styrofoam used in the process of the cutout construction, generate harmful toxic fumes to which hospital staff making the cutouts can be exposed (Eldib et al., 2013, Boyer et al., 2001). The use of such cutouts and beam modifiers is time-consuming since customization is required for each patient, and their manual placement implies an inherent inaccuracy (Salguero et al., 2009, Strydom et al., 2005) and is a source of error if not placed in the correct orientation. The use of these cut-outs also requires that mould-room equipment be retained, which is becoming irrelevant with the use of modern radiotherapy treatment modalities, techniques and technologies.

Figure 1.1 *Typical electron cutouts made from Cerrobend that are used for the treatment of mastectomy scars.*

In circumventing the use of cutouts, the use of an electron multileaf collimators (eMLC) has been suggested and developed (Eldib et al., 2013, Salguero et al., 2009, Gauer et al., 2006,

Jansson et al., 1998) however, it might be seen to be cumbersome or impractical. Due to the disadvantages of traditional electron beam shaping using cutouts, an alternative technique was proposed. The proposed solution retained the existing applicator and replaced the end of the applicator with a variable field shaping device, whilst delivering the dose over the entire region that would have normally been treated using a cutout. To achieve the required dose distribution, the new technique attempted to use the sliding window technique by Spirou and Chui (1994).

Although the new technique is for chest wall treatments, it is possible to extend its use for the treatment of other sites, such as the internal mammary chain and the head and neck treatment sites requiring electron beam treatment.

1.4 Rationale

Radiotherapy plays an important role in achieving local-regional tumour control by treating subclinical microscopic disease after surgery (Zagars, 2010). Despite the electron beam having a distinct advantage over other radiotherapy modalities, Hogstrom and Almond (2006) have argued the need for new innovative technologies for electron beam therapy to remain relevant. In addressing this, this study sought to develop a new technique for electron beam therapy for treating mastectomy scars. Most of the suggested electron beam therapy techniques only consider the aspect of electron beam collimation and beam shaping; therefore, this study incorporated the use of the treatment table movement. The use of an automated treatment table allows for the mastectomy scar to be treated with an adequate dose distribution with a minimum burden to the radiotherapy staff and machine treatment time.

1.5 Aim and Objectives

1.5.1 Aim

The aim of this study was to develop a new treatment technique for treating the mastectomy scar using a variable collimated electron beam and a computer-controlled automated treatment table.

1.5.2 Objectives of the Study

This research set out to achieve the following objectives:

    i.   Develop a functional variable field-shaping device to treat the mastectomy scar.

    ii.   Conduct measurements for the new technique.

    iii.   Automate the couch movement for patient treatment of mastectomy scar.

    iv.   Have a working treatment technique.

1.6 Ethical Considerations

No patients or test animals were used during the course of this research. All tests and measurements that might have required a real patient were conducted using a water, plastic phantom or Rando phantom, which is an anthropomorphic phantom.

1.7 Outline of the Thesis

Chapter 1 gives a brief overview of the subject matter and discusses breast cancer treatment. This is followed by the theoretical background for electron beam therapy and a review of various radiation treatment techniques for breast cancer in Chapter 2. The methodology section is in Chapter 3; it looks at the characterisation and collimation of the electron beam, as well as the automation of the treatment table. The experimental results on the electron beam parameters, computer-controlled couch and variable collimator are presented in

Chapter 4 and discussed in Chapter 5. The final chapter, chapter 6, has the conclusion and suggested recommendations.

CHAPTER 2

LITERATURE REVIEW AND THEORETICAL

BACKGROUND

The theoretical background and a comprehensive summary of previous literature related to this study are presented in this section. An overview of the various radiotherapy treatments, including electron beam radiotherapy, is given. The electron beam virtual source and electron beam characteristics are also considered.

2.1 Contextual background

Breast cancer is a disease that has plagued human society for centuries. The ancient Egyptians had knowledge of breast cancer, as evidenced in the translation J.H. Breasted of the Edwin Smith Papyrus (Baum, 1986, Ariel and Cleary, 1987). As already indicated, several treatment options have been proposed, with electron beam radiotherapy being one of them. Electron beams have been used for various treatment sites, such as total skin irradiation, medulloblastoma craniospinal irradiation, eye treatment, and intraoperative. The first documented breast cancer patient to be treated using radiation and the first fractionated treatment (18 eighteen daily one-hour exposures) was treated by Emil Herman Grubbe (b. 1875), three weeks after the announcement of the discovery of x-rays by Wilhelm Roentgen in 1895 (Bland et al., 2018, del Regato, 1996).

Over the years, there has been some concern over the possibility of low-dose radiation-induced contralateral breast cancer (Barrio and Cody, 2018). A 20 twenty-year follow-up on the B-04 study, a randomized trial by the National Surgical Adjuvant Breast and Bowel Project (NSABP) in 1971, suggested that breast surgery followed by radiotherapy did not result in radiation-induced breast cancer (Barrio and Cody, 2018). The trial looking at total mastectomy without radiation, lumpectomy only, and lumpectomy with radiation showed no difference in the overall survival, disease-free survival and distant–disease–free survival in the three

patient groups. The results showed that radiotherapy after breast surgery is a viable treatment option for patients with breast cancer (Fisher et al., 2002)

2.1.1 Bolus and wedged electron fields

When treating, bolus can be used for a number of reasons, such as increasing the skin dose, replacing missing tissue compensation, conforming the dose to the target volume and sparing the normal tissue (Gerbi et al., 2009). The bolus should be made of a material that is equivalent to tissue in both scattering and stopping power. Mahdavi et al. (2016) assessed a thermoplastic bolus of varying thicknesses for chest wall irradiation using electrons. In that study, they got adequate dose homogeneity for the CTV. The use of the bolus, however, requires a lot of preparation time, and the setup for the different days could lead to the introduction of air gaps. Perkins et al. (2001) used an electron bolus made of polystyrene-like wax material. The bolus, which followed the patient's contour, was fabricated using a milling machine. Perkins et al. (2001) found that although the technique reduced dose heterogeneity, the skin dose was higher than that of conventional techniques when the bolus was used for the whole treatment course, it resulted in erythema and desquamation. They also found the use of the bolus to be laborious and prolonged the treatment process. The use of bolus to get better dose distribution was also considered by Su et al. (2014), who explored the use of 3D printed bolus modulated electron radiation therapy (MERT) dose distributions.

Low et al. (1992) conducted a study where they looked at custom bolus with the intention of getting dose coverage of the target volume and dose homogeneity whilst avoiding critical structures. They used operators to transform a set of bolus thicknesses into another; these operators were in three groups, namely creation, modification, and extension operators. Fan lines extending from the virtual source to the patient skin surface give the thickness of the bolus, which the operator can use to modify and extend the bolus shape. They were able to demonstrate the use of the operators in getting a custom design of a particular bolus, to improve the dose distribution whilst sparing critical organs.

Lief et al. (1998) achieved electron wedged fields with sharper penumbra by modulating the beam from a racetrack Microtron accelerator using a narrow scanning elementary beam. They

obtained wedged profiles with angles as much as 70° and an increase of homogeneity of 70% for the modulated beam. Smyth et al. (2013) looked at trajectory optimization for single arc dynamic couch rotation Volumetric modulated arc therapy (VMAT). The Trajectory optimization for DCR–VMAT was achieved using ray tracing and a graph search algorithm. The plans resulted in a significant reduction of dose to the OAR compared to doses in conventional coplanar VMAT techniques.

2.1.2 Prescription, reporting and recording of electron beam therapy

The AAPM Task Group 70 report by Gerbi et al. (2009) incorporates developments arising from the introduction of the AAPM Task Group 51 report (Almond et al., 1999), which ushered dose to water calibration. As a protocol, it re-introduces the concept of lateral dose build-up ratio for small and irregular electron fields, which were initially described by Khan et al. (1998). The performance of the treatment planning system algorithm should be tested at least once where there are heterogeneities or surface irregularities. The report by Task Group 70 highlighted the need for the treatment planning system vendor to provide documentation with peer-reviewed articles describing the theory and implementation of these tests for the particular algorithm. The prescription, reporting and recording of electron beam therapy should follow the recommendations of AAPM TG70, such as the electron beam should be specified to include the energy of the beam, the field size, the nominal SSD and beam modifying devices like the bolus. Also, the target dose should be at a depth of maximum dose on the central axis or central part of the open field, with the 90% isodose level encompassing the target volume; and the prescription point should not be in a high-dose gradient region.

2.1.3 Electron beam relative dosimetry

Shiu et al. (1994) evaluated the application of the AAPM task group 25 report by Khan et al. (1991), for the linac electron beam central axis dose. The data showed that at nominal SSD, as the field size decreased, there was an increase in surface dose relative to the maximum dose, and the therapeutic depth decreased because of loss in side-scatter equilibrium, which was more pronounced for higher electron beam energies. The higher energy of 20 MeV at an

extended SSD of 110 cm, for a field size of 6 × 6 cm^2, gave the most significant difference of 5.5% between the measured percentage depth dose and that calculated as specified by Task Group 25. They suggested that the differences are due to a substantial number of electrons that are scattered off the edges of the applicator and x-ray collimators. There was no definite trend of how the output varied with electron beam energy. The output factor depends largely on the x-ray collimator settings than on the field size (Mills et al., 1982, Biggs et al., 1978). Shiu et al. (1994) were successfully able to implement the AAPM task group 25 for most of the electron beam configurations.

2.2 Various Other Radiation Treatment Techniques

Besides conventional linac-based external radiotherapy, there are other treatment methods that are available, which include the following but are not limited to helical tomotherapy, proton therapy, brachytherapy, intensity-modulated radiation therapy (IMRT), electron arc therapy, electron intensity-modulated radiation therapy (EIMRT), and volumetric modulated arc therapy (VMAT). There is increasing interest in treating breast cancer using IMRT with the potential to reduce dose to the lung and heart, and improving target volume coverage as the volumes are often complex and irregular (Khan, 2007); with IMRT planning either using forward planning or inverse planning techniques (Buchholz, 2005). Brachytherapy (low dose rate or high dose rate) can be given in conjunction with external beam therapy as a boost (Nam and Marks, 2009). Interstitial high dose rate brachytherapy, which places radioactive sources in the breast, is an alternative treatment (Khan, 2007, Motwani et al., 2006, Nag and Scruggs, 2013). Interstitial brachytherapy can be delivered after surgery to the whole residual breast parenchyma and may include the tumour bed boost using either low-dose-rate, pulse dose rate or high dose rate brachytherapy (Montemaggi et al., 2008, Chao et al., 2002). Permanent seed implants using Palladium-103 can also be used for breast cancer treatment (Stewart et al., 2013). Intraoperative radiotherapy (IORT) is another treatment method that can be used for the treatment of breast cancer. It involves the delivery of a dose of radiation in the tumour bed during surgery. The IORT treatment methods include perioperative high dose rate brachytherapy (HDR-IORT), intrabeam low-kV IORT that uses a miniature driven low-kV energy x-ray source and intraoperative radiotherapy with electrons on a linac (IOERT) (Gunderson et al., 2010, Sedlmayer et al., 2011). IORT given as a boost has been shown to

significantly prevent local recurrence (Calvo et al., 2008). The use of protons in radiotherapy or the treatment of cancer was first proposed in 1946 by Robert R. Wilson (b. 1914), also known as the "father of proton therapy" (Wilson, 1946, Giap and Giap, 2012). Despite the cost of proton therapy being an order higher than conventional radiotherapy, there is a lot of research and innovation to reduce these costs and improve the delivery of proton therapy (Mohan and Grosshans, 2017). Breast cancer treatment using proton therapy may be for patients with complex anatomy that could be difficult to treat, such as unfavourable cardiac anatomy and permanent bilateral implants (MacDonald et al., 2013, Laramore et al., 2008). Electron arc therapy can also be used for treating the chest wall after mastectomy (Klein and Kashani, 2013). The use of electrons in radiotherapy has some distinct advantages due to the physical properties, which are discussed in the sections that follow.

As far back as the 1920s, Keynes (1928) showed the effectiveness of locoregional tumour control of breast cancer using radium needles (Pierquim and Grimard, 1989). Postoperative radiotherapy seeks to reduce local-regional recurrences and improve survival when there is metastatic dissemination originating from regional nodes (Tubiana and Sarrazin, 1987). Postmastectomy radiotherapy is given to treat subclinical remnants of the tumour after surgery, resulting in long-term control of the disease and disease-free overall survival for breast patients (Buchholz et al., 2010, Haffty, 2003). Postmastectomy irradiation can decrease locoregional occurrence by as much as 67% (Vinés et al., 2003).

Loganadane et al. (2017) evaluated the loco regional control of women with breast cancer treated by postmastectomy conformal electron beam radiation therapy (PMERT). They mapped patterns of loco regional recurrences, comparing them with ESTRO and RTOG guidelines, and found that recurrences are uncommon for patients undergoing PMERT and of those with recurrences, it was due primarily to the aggressive nature of the disease and not the insufficiency of the radiation. Kirova et al. (2007) developed a technique to eliminate the hot spots of the standard technique they had used for over 20 years at their institute. The technique used a single field that included both the chest wall and internal mammary chain volumes to avoid hotspots at the junction. They found that their technique had low early toxicity and was able to improve the homogeneity and conformality as well as reduce hotspots.

Toscas et al. (2010) considered the dosimetric pros and cons of boost treatments using dynamic conformal arcs (DCA), IMRT, VMAT and Intensity-modulated proton therapy (IMPT). They suggested that shallow treatment targets using energies between 9 and 12 MeV could be sufficiently treated with electrons. Lief et al. (2005) have looked at accelerated contaminant boost IMRT as a way of reducing overall treatment times for breast cancer patients, by reducing the number of fractions from 23 – 25 fractions to 15 fractions over three weeks. The doses are typically 40.5 Gy in 2.7 Gy fractions to deliver doses that are biologically equivalent to conventional treatments. The results showed less acute skin reaction than conventional fractionation. Some clinical trials have not shown any differences between hypofractionation and standard fractionation (Gaffney, 2013). More recently, Shah et al. (2021) also did a review on breast treatment using radiotherapy. They reviewed studies on single-fraction intraoperative radiotherapy, hypofractionated whole breast irradiation and partial breast irradiation after breast-conserving surgery. The data are in favour of hypofractionated radiotherapy for breast treatment, including radiotherapy after breast reconstruction.

Ashenafi et al. (2010) have proposed helical tomotherapy as an alternative to using electron beams, as the Hi-Art II system does not offer electron beam therapy. The tomotherapy plans had better PTV dose homogeneity in the chest wall and internal mammary nodes, with the potential for better cosmesis. Rong et al. (2012) evaluated helical tomotherapy dosimetry for the treatment of postmastectomy patients, which also included simultaneous integrated boost (SIB) in the scar region using strip bolus. The strip bolus allowed for better setup reproducibility, and increased dose uniformity to the scar PTV, with the TLD dose indicating that the scar PTV received 100.7% of the prescription dose where the strip bolus was used. Ito et al. (2011) evaluated skin doses of mastectomy patients treated using helical tomotherapy. They used a bolus of 1 cm with the TLDs placed on the skin surface beneath the bolus. They found that many of the TLD doses were within 5% of the TLD doses calculated by the treatment planning system.

Another modality for post-mastectomy radiotherapy using protons is intensity-modulated proton therapy (IMPT). IMPT is similar to conventional photon IMRT were different fluences are combined to give an overall homogeneous and conformal dose to the

target, with the advantage of the depth for the Bragg peak of each beamlet being modulated (Lomax et al., 2005). Jimenez et al. (2013) looked at the delivery of post-mastectomy radiation therapy using protons without delaying breast reconstruction until after radiation for patients with bilateral implants. The study compared the treatment plans for IMPT versus the plans for 3D conformal therapy. Not delaying reconstruction has the potential to provide psychological benefits to the patient. The study considered thirty plans consisting of ten IMPT plans, ten 3D photon/electron conformal plans and ten photon conformal plans. The plans were designed to give a 95% target coverage to a dose of 50.4 Gy. The IMPT plans had better homogeneity and better sparing of the normal tissue and the organs at risk. IMPT using proton pencil beam scanning (PBS) was found to have better homogeneity and be capable of minimizing both long-term cardiovascular morbidity and mortality. Depauw et al. (2015) have also looked at using IMPT for patients with or without breast implants. A single proton pencil beam scanning field was optimized to ensure adequate target coverage and sparing of OAR. The pencil beam IMPT plans using a single PBS field had better nodal coverage and cardiac sparing and shorter overall treatment time compared to passive scattering and conventional photon or electron beam therapy. One concern of proton therapy for breast treatment; however, is that proton beams do not have dose buildup, this can result in an increase of chest wall skin toxicity (Depauw et al., 2015).

Despite electron beam arc therapy being time-consuming with the need for physics support and requiring the fabrication of patient-specific immobilization, it remains a viable chest wall treatment technique when compared to using photon beams (Rodrigues et al., 2013). Gaffney et al. (2001) evaluated the twenty years of experience using electron beam arc therapy at the University of Utah in Salt Lake City, USA. From February 1980 to December 1998, they treated 156 postmastectomy breast cancer patients with electron beam arc therapy. The follow-up was sixty-eight months for living patients and fifty-five months for all patients. The results showed that electron beam arc therapy had good locoregional, control rate and modest acute and late toxicity. The technique allowed for the inclusion of internal mammary lymph node chain with low dose to the heart and lung.

Since the start of clinical use of volumetric modulated arc therapy (VMAT) in 2008, the use of this treatment technique for breast cancer treatment has not been extensively published as

shown in a review by Cozzi et al. (2017). They looked at sixty-seven articles, sixty-one of which were related to treatment planning, and six were clinical. The two main groups were divided into subcategories which included the risk of VMAT secondary cancer induction, VMAT boost treatment, bilateral breast irradiation, hybrid techniques and knowledge-based planning, amongst others. They concluded that although VMAT is simpler and faster to deliver and offers improved treatment plans in some cases, however, more clinical studies were required to confirm better clinical outcomes. Xia et al. (2018) advocate that the treatment of breast cancer using IMRT or VMAT does not need to be routinely used; it should rather be considered when non-IMRT/VMAT plans have been taken into account. These techniques can be used in certain cases to limit the dose to OAR and improve conformality.

A study by Fogliata et al. (2017) looked at VMAT techniques with a trade-off between improving target dose homogeneity and healthy tissue receiving low dose levels that could give rise to a possible risk of future late toxicity and secondary cancer induction. They compared two planning strategies for dual-partial-arc VMAT, where a full, partial arc was used and the other a partial arc with avoidance sectors, with the dose rate forced to zero for the avoidance sectors. The plan with the partial arc with avoidance sectors had lower doses to the contralateral structure doses and had better delivery efficiency as it had 11% less MU.

There is a growing interest in modulated electron beam radiation therapy (MERT) for both intensity modulation and energy modulation. MERT is electron beam radiation delivered similarly to IMRT for photon beams. The use of MERT for the treatment of superficial targets has the possibility to conform electron dose distributions and offer lower exit doses and less scatter to normal tissues, including the lungs, heart and contralateral breast. Alexander et al. (2011) compared MERT using a few leaf electron collimator (FLEC), with conventional electron beam therapy and VMAT. They used a FLEC designed by Al-Yahya et al. (2007). The FLEC was made of two automated pairs of trimmer bars, which allowed for step-and-shoot modulated electron fields. A copper plate of 1.2 cm thickness was used for the trimmers, as it is lighter and able to stop high energy electrons and produce lesser bremsstrahlung photons compared to tungsten and lead. Al-Yahya et al. (2007) used energy-modulated electron therapy (EMET) to achieve conformal dose distributions. Alexander et al. (2011) found that MERT had better

conformity and lesser lung dose indices ($p < 0.05$), compared to VMAT and conventional electron beam therapy.

du Plessis et al. (2006) characterized electron beams delivered using a double-focused photon MLC without an electron applicator. The electron beam energies of 6, 9, 12, 15 and 18 MeV were characterized in terms of penumbra, range, target coverage, scatter, bremsstrahlung and field abutment. The optimal penumbra for all electron beam energies was at 60 cm SSD. A dose gradient of 40 cGy cm^{-1} was achieved with segmented abutted fields sparing tissue beyond the distal region, which is better than megavoltage photon beams.

Jin et al. (2008) considered delivering MERT using a photon MLC on a linac without the electron applicator with a shortened SSD of 60 cm, following the study by du Plessis et al. (2006). They found that the in-house Monte Carlo-based treatment planning system agreed to within 1% per millimeter with the measured film dose distribution. There was a 1.4% difference between the point dose measurement with the ion chamber and the Monte Carlo calculation. Ma (2004) developed an in-air magnetic collimator with a cylindrical magnet which had a magnetic field of about 0.6 T along its central axis. Measurements were done with 6-15 MeV electron beams. Ma (2004) found that the collimated electron beams had narrower beam penumbra and offered better skin-sparing with increased output at the d_{max} when compared to conventional electrons.

Rodrigues et al. (2013) developed a conformal electron beam therapy technique known as dynamic electron arc radiotherapy (DEAR). The technique delivers radiation whilst the gantry and couch motion, and the dose rate is modulated to get the required dose distributions. They used the Varian TrueBeam linac, which has a Developer Research Mode, that allows users to move couch, gantry and collimator simultaneously to create any incident beam trajectory. The user is able to access the linac via the native XML language. The developer mode allows for the capturing of an incident beam trajectory log file that can be analyzed. The DEAR dose distributions for curved surfaces had better penumbra and uniformity compared to that of static fields on flat surfaces.

Various studies have looked at the comparison between VMAT and helical tomotherapy, and one such study is by Nichols et al. (2014). They looked at the plans of patients treated with helical tomotherapy and compared them with those using partial VMAT arcs. The comparison parameters included dose homogeneity and conformity index, the tumour control probability (TCP), normal tissue complication probability (NTCP) and secondary cancer complication probability (SCCP). The plans from both techniques had comparably acceptable plans, with the VMAT plans having a better conformity index (p < 0.01) and better OAR sparing for low doses less than 5 Gy. Also, the VMAT plans were delivered in much less time, up to 66% less in some cases. Although the results showed good dose distribution for VMAT, they acknowledged the need for further evaluations using thermoluminescent dosimeters, to ensure adequate skin dose to mitigate the risk of recurrence in the chest wall.

The occurrence of male breast cancer is rare, making it less than 0.5% in males and constitutes 0.7% of all male cancers, with radiotherapy given after mastectomy (Dixon and Sainsbury, 2012). Liu et al. (2015) acknowledged the need for treatment guidelines for male breast cancer that are not simply an extension of those for female breast cancer. There is also support for both radical and conservative surgery, including or excluding radiotherapy in male breast cancer (Crichlow and Evans, 1987).

Iktueren et al. (2012) assessed the peripheral dose outside the treatment field for various electron applicators and energies, including how it was affected by beam obliquity. They used an Advanced Markus ion chamber in a water-equivalent slab at varying depths, including d_{max} up to a distance of 20 cm from the central axis, for gantry angles of 0°, 10° and 20°. The measurements were compared to those from the treatment planning system. They found that the peripheral dose can be as high as 4.1% of the central axis dose for 15 MeV beams, which can translate to 2 Gy for a patient getting a treatment dose of 50 Gy. These kinds of peripheral doses have a bearing on both deterministic as well as stochastic effects when considering radiation effects.

The study by Gosselin et al. (1994) looked at the centrally shielded electron beams. They used Cad-free 95 electron shielding fusible alloy of varying width, of 1.2 cm thickness. They found that doses at shallow depths are more affected by the central shield, with the relative dose

under it increasing with depth due to the scattering of the electrons from the open field. They recommended that the dose estimation under the central shield measurement should be done in a phantom under a similar clinical setup of the actual treatment.

Other emerging breast cancer treatment techniques include radiofrequency ablation, cryoablation, stereotactic excision, vacuum-assisted core biopsy and the use of nanotechnology (Huston and Simmons, 2005, Andres, 2009). Also, the use of molecular biomarkers in radiotherapy allows for personalized treatment regimens for patients undergoing radiation therapy, as different subtypes of cancer respond differently to radiation (Dandapani, 2017).

2.3 Electron Beam Radiotherapy

2.3.1 Electron beam production and transport

In 1973 Karzmark and Pering (1973) reviewed the principles and technology of linear accelerators. They also provided a summary of the development of major enhancements in features and technological advancements by various manufacturers prior to 1970. The modern linear accelerators (linacs) have not varied much since then and are more widely used for treating with electron beams. The electron beam comprises electrons from an electron gun, which are accelerated by microwave power to the required energy in a high vacuum waveguide structure. In the accelerating waveguide, the velocity of the electrons is almost constant as their velocity is close to the velocity of light. Any gain in kinetic energy can be taken to be a result of an increase in the electron mass, with the gain in relativistic mass given by

$$m/m_o = (1-\beta^2)^{-\frac{1}{2}}$$

2.1

where β is the ratio of the velocity of the electron to the velocity of light c, m_o is the rest mass of the electron, and m is the mass of the electron at velocity v. Thus, the kinetic energy E_k (expressed in MeV) gained by the electron is proportional to the difference between the rest and relativistic mass $(m-m_o)$ as given by

$$E_k = eV = (m - m_o)c^2$$

The electron beam is a pulsed beam, with the servo-control system such that the electron beam current is about one milliamp during the pulse; this is to keep the dose rate at a safe level (Greene, 1986, Klevenhagen, 1985). This is a significantly smaller dose rate than that required for the photon beam. When the electrons exit the waveguide window, the pencil beam is only about 1-2 mm wide (Bova, 1995). The beam then passes through a dual-foil scattering system, where the first foil spreads the beam as it exits the electron window; the second foil, which is a few centimeters away from the first one, is used to flatten the beam (Bova, 1995). When compared to a single foil scattering system, a dual-scattering one gives better flatness and steep dose fall-off beyond the depth of maximum dose, with minimum energy degradation. High beam stability is required in the electron treatment mode, as a small energy variation may cause a significant depth dose shift, which can be detrimental to closely laying critical structures; a 10% change in a high-energy electron beam can result in an 80% isodose shift and 7 mm for a 20 MeV beam (Klevenhagen, 1985). A non-diverging monoenergetic beam from an ideal flattening system would still be degraded by a collimator, especially for small fields due to electrons scattered by the collimator (Lax and Brahme, 1980).

2.3.2 Electron beam interactions

With the clinical electrons, we are interested in knowing how the electrons behave after the electron source before the patient and inside the patient. For clinical use of the electron, the pencil beam that emerges from the accelerator vacuum window can be spread either by electromagnetic steering or by multiple scattering foils (Jayaraman and Lanzl, 1996). The interactions of the electron beam with the medium are characterized by the stopping and scattering power of the medium (Van der Merwe, 1994). In calculating the dose, it is important to know the energy of the electron beam in choosing the correct energy-dependent factors, such as the stopping powers and the perturbation correction factors. The energy loss that the electrons experience as they pass through the material is characterised by the stopping power. The stopping power of a medium is defined as the average energy loss per unit path length of a charged particle (ICRU, 1970). A more useful quantity is the mass stopping, which is independent of the density of the material that the electrons are traversing.

Because of the two main types of energy losses, the mass stopping power has two components, the one due to the collisional inelastic collisions with atomic electrons, and the radiative stopping power that results from the radiative losses of the electrons interacting with the electric field of the nucleus. The total stopping, $(S/\rho)_{tot}$, power is therefore given by

$$(S/\rho)_{tot} = (S/\rho)_{rad} + (S/\rho)_{col}$$

2.3

Where $(S/\rho)_{rad}$ is the radiative stopping power and $(S/\rho)_{col}$ is collisional stopping power. The energy loss due to ionization and excitation is deposited close to the electron track, i.e. "imparted locally", whilst that due to bremsstrahlung radiative losses is absorbed further along the track (Klevenhagen, 1993).

When considering absolute dose measurement, the farmer ionization chamber is considered to be the gold standard for accurate clinical measurement of radiation dose. The absorbed dose in a medium is measured with an ionization chamber based on the Bragg–Gray theory. The theory provides a means of determining the absorbed dose at a point in the medium, which is normally water, in relation to the mean absorbed dose in the detector, which is air equivalent for an ionization chamber. Thus, according to the Bragg–Gray theory, the dose in the medium is given by

$$D_{med} = \overline{D}_{air} s_{med,air}$$

2.4

where D_{med} is the absorbed dose at the medium, $\overline{D}_{air}$ is the mean absorbed dose in the detector (air), and $s_{med,air}$ is the proportionality factor known as the medium/air mass (collision) stopping power ratio. The stopping power ratios for electrons in the clinical range of about 0.2 MeV to 20 MeV vary with energy and depth in water. The depth ionization curves, therefore, need to be corrected with the appropriate stopping power ratios when determining the electron depth dose curves.

The biological effectiveness of electrons is not different from that of megavoltage photon beams, and thus electron beams have no biological advantage over photons. The specification of the electron beam quality is specified at various points in its beam transportation. Four

23

parameters are used to characterize the beam, namely the maximum energy E_{max}, the mean energy $\overline{E}$, the energy spread Γ, and the most probable energy. These parameters are specified at the accelerator window as the electron beam exits the linac, at the phantom surface as the beam enters the phantom medium, and lastly in the phantom medium. The energy of the beam as it exists the linac is almost mono-energetic, and the energy spread increases as the electron beam interacts with the air, the collimators and the phantom.

The production of neutrons due to electrons is much less than that due to photons since the electron electrodisintegration cross-section for the electrons is approximately two orders of magnitude smaller (Schaeffer et al., 1982, NCRP, 1984, Expósito et al., 2013). Electron beams of energies 10-20 MeV can generate neutrons either as the generated bremsstrahlung or electrons directly interact with the electron scattering and collimating system. However, the generated neutron levels are low. A survey for neutron contamination was conducted in the department using a neutron detector, with no neutrons being detected for all energies.

2.3.3 Electron beam collimation

To get the desired flatness and limit the electrons interacting with the lower part of the applicator, the use of collimating jaws used for the x-ray beam is implemented. Whilst photon beams diverge linearly to give increasing field sizes with distance, the beam divergence for electrons is not so straightforward as they do not obey the same rules of geometry that photons obey. As can be seen in Figure 2.1, the higher beam intensity lines move towards the beam central axis, and the low-intensity lines diverge with increasing distance. As a result, the field size should be larger than that that encompasses the target covered by the 90% isodose line, especially for the higher electron beam energies (Jayaraman and Lanzl, 1996)

Electrons experience collision and radiation energy losses like any charged particles whilst also changing their direction of travel as they interact with the electric fields associated with the nucleus and orbital electrons of the material they are passing through; this is a result of electron-nuclear or electron-electron scattering.
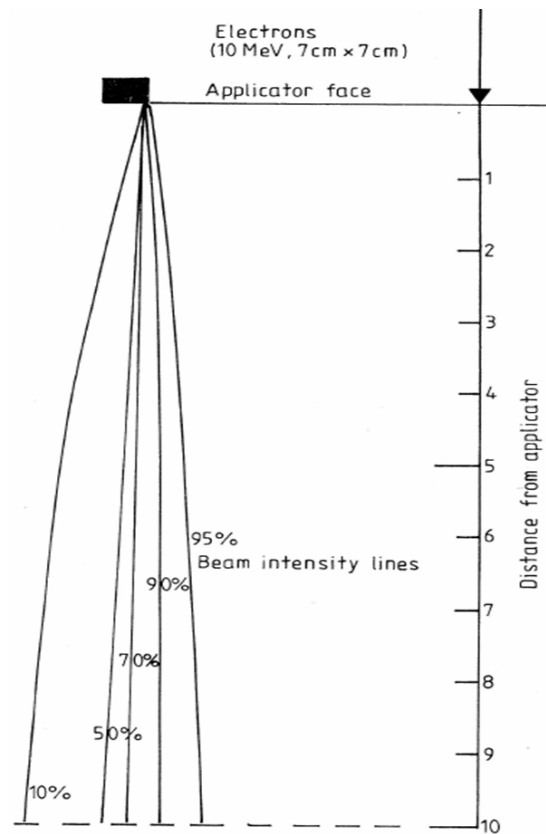
Figure 2.1 *Variation of the radiation field boundaries with the applicator to surface distance. Source:*
(Klevenhagen, 1985)

Electrons striking the primary collimator are scattered, resulting in an electron beam edge with a large penumbra (Jayaraman and Lanzl, 1996). The steady dose fall-off is a result of range straggling, with the maximum range being that of primary electrons that have suffered less angular scattering. Even for a monoenergetic electron beam incident on a medium, the statistical variation of the interactions and energy loss results in energy straggling (Jayaraman and Lanzl, 1996).

In an electron-electron interaction, the primary electron is considered to have higher energy and the secondary electron the lower energy. Some of the factors that affect the electron beam dose distribution include the interactions that contribute to the energy loss of primary electrons, the presence of bremsstrahlung in the electron beam, the effect of beam divergence on the inverse-square law, and the production of secondary electrons (Jayaraman and Lanzl, 1996). The effect of lateral motion of electrons in material and collimator scattered

electrons on the therapeutic range of small fields was considered by Lax and Brahme (1980). They also discussed the various contamination in the electron beam due to the collimation.
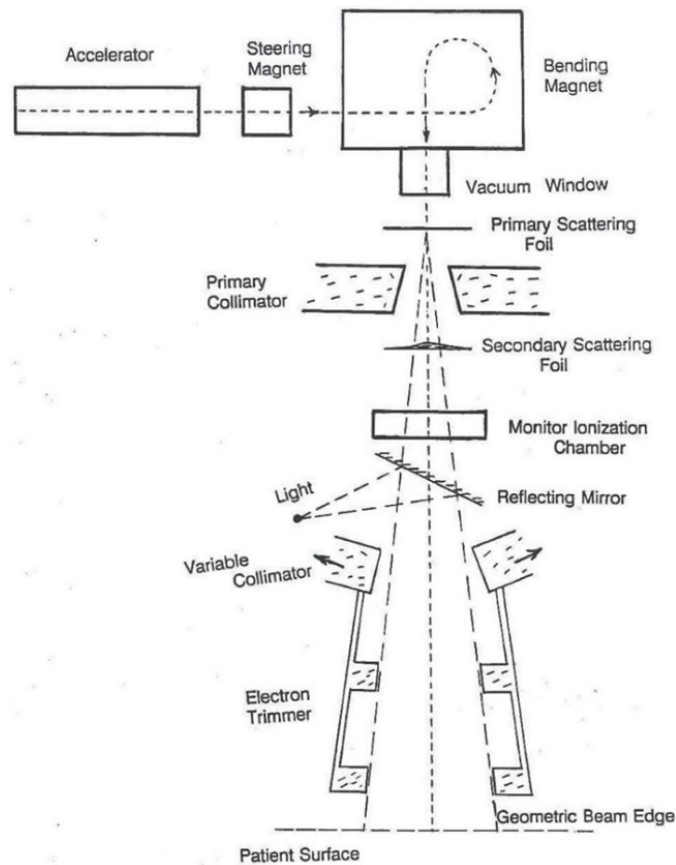
Figure 2.2 *Different elements comprising an electron beam delivery system. Source: Jayaraman and Lanzl (1996)*

Kurup et al. (1995) looked at the output factors for irregularly shaped electron fields. They found that the calculated output factors were within 1% of the measured output of most irregular fields and were within 2% for extremely elongated fields. The calculated outputs were calculated using a scatter air ratio (SAR) method similar to the empirical method used for photons. Richert et al. (2007) came up with a technique for improving the field matching of multiple abutted fields using an electron applicator that was able to vary the source-to-collimator distance (SCD) for varying energies. The technique uses a varying air gap between the patient surface and the collimator for different electron energies to increase the width of the penumbra, resulting in an improved homogeneity across the segmented electron fields. They were able to get a dose variation of ±5% across the abutment regions of the segmented-field electron conformal therapy.

2.3.4 Electron Beam Characteristics

The clinical electron energies ranging from 5 to 25 MeV are used for treating superficial tumours which are less than 5 cm deep. Higher clinical energies of up to about 40 MeV can also be used, with this upper limit corresponding to the beam penetration for the human body (Greene, 1986). However, beyond 25 MeV, the thickness of the scatterer increases as the square of the energy of the electron beam (Bova, 1995). In determining the physical characteristics of the electron beam, dosimetry measurements of the relative spatial distribution and quantitative absolute measurements are conducted. When looking at the central-axis depth-dose curve, as shown in Figure 2.3, the tail end D_x is the dose from x-ray contamination. The x-rays are due to bremsstrahlung interactions produced when the electron beam interacts with the various components in the linac head, such as the scattering foil, mirror, beam-defining collimators, air as well as the patient. Photon contamination is usually acceptable for regular electron beam treatments. The bremsstrahlung background is usually about 1-3.0% of the total beam intensity, depending on the electron energy linac design (Klevenhagen, 1985). R_p is the practical range, which can be approximated by E_0/2 in centimeters where E_0 is the most probable energy of the electron beam at the phantom surface, R_p increases with increasing energy. R_q is the tangent to the curve where the point of inflection intersects the maximum dose level. G_0 is the reduced dose gradient, as shown in Figure 2.3; it increases with decreasing field size, and decreases with energy and can be used to compare the electron beam quality from different linacs (McNeese et al., 1999). G_0 is given by the equation,

$$G_0 = \frac{R_p}{(R_p - R_q)}$$
2.5

An electron beam should ideally have the sharpest dose fall off beyond the therapeutic range, with R_q as close as possible to R_p to give a large dose gradient.

One way of determining the electron energy at the phantom surface of the medium is to use the range method. Where the most probable energy, $(E_p)_0$ at the surface is associated with the practical range R_p, and the mean energy $\bar{E}_0$ at the surface is associated with the depth at which the dose is 50% of the maximum dose, R_{50} (Khan, 2003). The surface dose is usually

defined as the dose at a depth of 0.5 mm (Gerbi, 2006, Bova, 1995). Lower electron energies have lower surface doses compared with higher energy beams, with a 6 MeV beam having a surface percentage depth dose of about 70-75% as compared to about 95% for a 20 MeV. This is due to lower energy electrons being scattered at wider angles (Gerbi, 2006). When the field size is smaller than the practical range of the electron beam energy, there is an increase in surface dose, and the D_{90} moves towards the surface. This effect is a result of the loss of side scatter equilibrium and is more pronounced for higher electron beam energies and decreases with increased SSD (Hogstrom et al., 2000). Donmez Kesen et al. (2014) have compared measured electron beam data and compared it with data from the treatment planning system calculated using a pencil beam algorithm. They found percentage differences of as much as 21% between the calculated and measured data when using film for measurements. Because the dose-response curve for film depends less on the electron beam energy, it has a high spatial resolution and is recommended by the AAPM for relative dosimetry (Donmez Kesen et al., 2014).

The shape of the electron beam isodose curves is dependent on the field size, beam energy, beam collimation and SSD. However, the shape of isodose curves in the penumbra region (20% to 80% isodose curve) does not change significantly with field size. For abutted electron fields, the shape of the penumbra affects the dose in the overlap regions. For field sizes where there is lateral equilibrium, an extended SDD has the effect of decreasing the width of the area covered by the 90% isodose curve and having more dose outside the field edge. This becomes more important when considering the best SDD to use for the new technique since the small field segments do not have lateral equilibrium.

The D_{90} or the D_{80} isodose levels are usually taken as the therapeutic depth for electron beam treatment. As a rule of thumb, the depth of the 90% and the 80% depth dose is approximately E_0/3.2 cm and E_0/2.8 cm in water, respectively, where E_0 is the most probable energy in MeV of the electron beam on the surface. The electron energy should be chosen such that either the 90% or the 80% isodose level covers the distal end of the target volume plus 5 mm beyond, and the depth dose maximum is positioned at the center of the PTV (ICRU, 2004). Choosing the correct energy of the treatment beam is more critical for electrons than photons, due to the sharp dose fall-off after the 90% dose level. Beam energy modulation should be

considered to ensure there is good coverage of the treatment volume, with the depth to be treated determined from the CT scan. The use of bolus for beam energy modulation has been looked at by various authors (Eldib et al., 2013, Kudchadker et al., 2002, Ma et al., 2003).

The central-axis depth dose is measured with respect to flat surfaces and thus should not be used for curved surfaces without corrections. Beam obliquity results in the maximum dose moving upwards to shallow depths whilst reducing the depth dose at larger depths (Jayaraman and Lanzl, 1996). The technique involves treating the chest wall, which has a curved surface; it is important to keep the incidence of the electron beam perpendicular to the patient's surface to avoid the beam obliquity effect. The depth of maximum dose decreases as the angle of incidence increases, with a significant change in the shape of the depth dose curve for angles of incidence greater than 60°. This necessitates the measurement of beam obliquity. One method to correct for beam obliquity is to use the obliquity factor. The obliquity factor is the dose enhancement factor defined as the ratio of the dose at a point in phantom on the central axis of a beam, that is incident at an angle to the dose at the same point and depth along the central axis with the beam incident perpendicular to the surface (Khan, 2003).
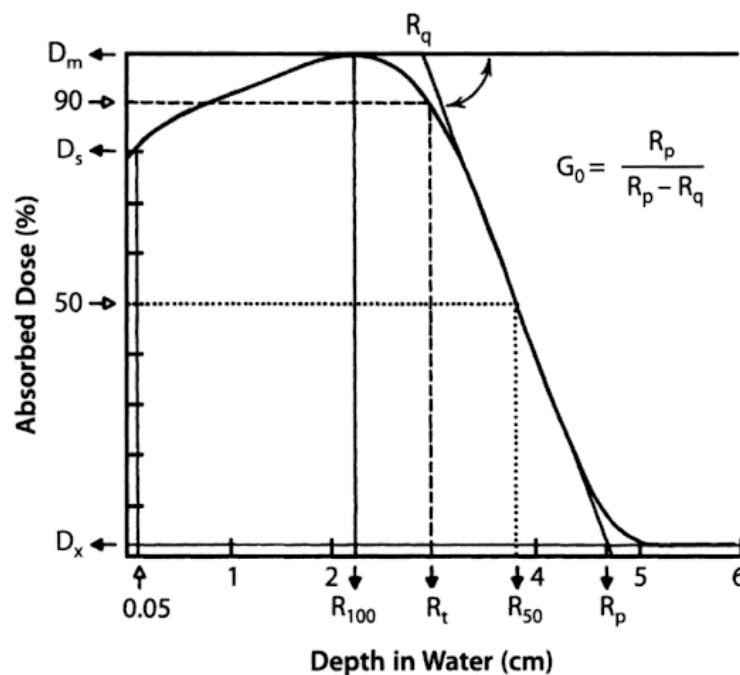
Figure 2.3. *Central-axis depth–dose curve for an electron beam with parameters indicated that can be used to characterize electron beams. Source: Gerbi (2006)*

Electron beams exhibit characteristics that are beneficial in radiotherapy. Electrons of energies below 20 MeV have a plateau of a few centimeters depth (about 6 cm for a 20 MeV beam), followed by a sharp dose fall-off; with higher energies losing this distinct sharp fall-off. The shape of the depth dose curve offers the use of a single treatment beam. Another useful characteristic is that the energy absorption for electrons is not dependent on the density of the absorbing material but instead on the electron density, making the energy absorption in bone or soft tissue more or less the same. It is because of the physical properties of electron beams, which make them more suitable for chest wall treatment in breast treatment, the major attraction of electron beam irradiation being the shape of the depth dose curve, as shown in Figure 2.3 above. The finite range of the electrons allows for a region of uniform dose, also called the "plateau region", followed by a rapid dose fall-off beyond the tumour, in contrast to photons that are absorbed exponentially and thus have no finite range (Johns and Cunningham, 1983, Hogstrom et al., 1981). The rapid dose fall-off allows for sparing of the non-target tissues beyond the tumour and offers a distinct clinical benefit when compared to conventional X-ray modalities (Zackrisson and Karlsson, 1996, Khan, 2003, Bova, 1995). These properties, including the well-defined ranges of electron beams and a narrow penumbra at shallow depths, allow for the reduced dose to organs at risk (OARs) (Salguero et al., 2009).

2.3.5 Small Fields

Over the more recent past, the use of small fields in radiotherapy treatment techniques has increased due to advances in the field of dosimetry; the size of the field is determined by the lateral range of the charged particles (Alfonso et al., 2008).   A new protocol for small-field dosimetry has been developed for photons (AAPM and IAEA, 2017); however, one for electrons still needs to be established. Small fields whose area is small compared to the range of the electrons in the material, will not have a build-up due to the electrons scattering away from the central axis with very little scattering back. The depth doses for the small fields vary substantially with field size when compared to larger field sizes. For the same energy, the depth dose for small field sizes falls off considerably slower than for larger fields, with the

higher depth doses moving towards the surface and increased surface dose. There is a decrease in dose build-up due to a reduction in lateral scatter.
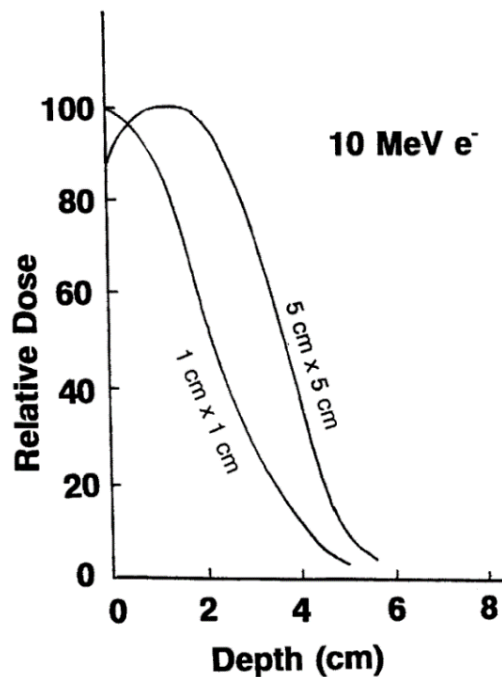
Figure 2.4 *Dependence of depth dose on field size for two narrow electron beams. Source: Jayaraman and Lanzl, 1996).*

Donmez Kesen et al. (2014) found that for electron fields smaller than the range of the lateral scatter equilibrium, the pencil beam algorithm does not accurately calculate the depth dose and monitor units (MU)s, especially for fields of 5 cm diameter or less. It has now been established that Monte Carlo based calculation algorithms give a more accurate dose calculation than other algorithms.

Lillicrap et al. (1975) conducted a study on narrow electron beams where at the phantom surface, they have a small divergence and small diameter compared to the range of the primary electrons. They used an evacuated collimator, which produced a 2.5 mm pencil electron beam for energies of 4 and 10 MeV. The narrow beams had sharper dose fall compared to broader beams, with the dose distribution becoming broader with depth as the electron were scattered more.

31

2.4 Virtual Source Position for Electrons

Unlike the X-ray beam, the electron beam does not come from a physical point but rather appears to come from a point known as the virtual source. The term "virtual electron source" was coined in 1965 by W. Pohlit (Klevenhagen, 1993). The virtual source is used to calculate the dose rate at extended distances. As the pencil electron beam passes through the various components in the linac head, the beam spreads out into a broad beam that appears to diverge from the virtual source. However, magnetically scanned electron beams do not require the use of a virtual source (Sandison and Huda, 1989). The virtual source position is dependent on the electron beam energy and applicator field size, as these are affected by the changes in the scattering conditions and collimating jaw settings (Al Asmary and Ravikumar, 2010, Thomas, 1988, Rosenberg, 2007, Mayles et al., 2007). The ICRU defines the virtual source as the "source, when placed in vacuum at some distance s_{eff} from the phantom surface (z = 0), produces exactly the same electron fluence at z = 0 as the real beam". The virtual source position is specified by three factors namely the mean-square radius of the source; the mean-square angular spread of the source; and the effective SSD (ICRU, 1984, Jamshidi et al., 1986).

The position of the virtual source is important for corrections in the treatment planning system and the inverse square law (ISL) corrections (Schröder-Babo, 1983). For small fields, the inverse square law does not predict the variation of output with SSD, requiring the virtual source distance to determine dose changes with distance (Khan, 2003). Various methods have been proposed to ascertain the virtual source position of the electron beam. These include using grids, the multi-pinhole camera, the inverse slope method, the inverse square law method, the full-width at half-maximum (FWHM) method and the power-law method. These methods can be done using ionization chambers, diodes or film in air, in water or solid phantoms (Khan, 2003, Mayles et al., 2007).

One method, the inverse square law method, makes use of taking dose measurements in a phantom whilst varying the air gap (0 - 15 cm) between the phantom and electron applicator (Strydom et al., 2005). The inverse square law method measurements can be done in either the phantom or in air. Jamshidi et al. (1986) measured and calculated the virtual source

distance for a Varian Clinac-2500 using the multi-pinhole camera method. They found that the multi-pinhole camera method is similar to that by Schröder-Babo (1983) and was in agreement with the FWHM method. Ravindran (1999) showed that there is a variation in the virtual SSD for machines with the same energy and applicator size, and thus the virtual source position should be measured for each individual machine. The FWHM method used by Ravindran (1999) was different from that used by Thomas (1988), in that the measurements were done in water, whereas the others were in the air.

The position of the virtual source depends on a number of factors, namely the source-to-collimator distance, the energy of the electron beam and the field size. As the electron beam interacts with the accelerator window, scattering foil, electron monitor chamber, electron applicator and air, as it reaches the patient, it appears to originate from the virtual source. One of the methods employed to determine the virtual source position is to extrapolate the plot of the root of the inverse of the central axis readings against the SCD (Sandison and Huda, 1989). Al Asmary and Ravikumar (2010) obtained results that were similar for both the inverse square law (ISL) and the Inverse Slope (IS) methods. Lief and Lutz (2000) compared two methods to determine the effective source size. They looked at using a multi-slit camera made from parallel aluminium plates with plastic strip spacers, and a pinhole camera. Yudelev et al. (1982) used the inverse square law, obtaining readings at positions ranging from 95 cm to 160 cm from the electron window with a chamber in a polystyrene phantom.

Sweeney et al. (1981) looked at determining the virtual source position of fixed electron applicators with a 20 MeV electron beam, and the effect of varying the primary collimator jaw settings. They used the power-law method in establishing the virtual source position. Thomas (1988) used a method described by Almond (1976) to determine the virtual source position. Measurements were made in the air using a chamber at various distances from the end of the electron applicator. Another inverse slope method is that of Khan et al. (1978). The method proposed the determination of what they termed the "'effective source'-to-cone end distance" denoted by *f. This method was more suitable than that proposed in ICRU (1974) Report 21, as measurements were conducted in more clinically relevant conditions of collimation and phantom scatter.

2.5 Abutted Electron Fields

The abutted fields should be such that the dose distribution is uniform with minimum hot or cold spots in the overlapping regions, especially for beams with converging central beam axes. For conventional electron beams, to achieve this, a gap between the electron fields can be used however, this might be dependent on the curvature of the chest wall being treated. For treatment fields with one energy, and since the technique is sliding window, gaps will not be required to get a dose distribution that has acceptable high-dose and low-dose regions. The required gap was considered for segments that have different energies. The technique is recommended to treat the postmastectomy chest wall, which is a curved body surface. For treatment planning purposes, to get an idea of the dose distribution, several stationary beams might have to be used or direct measurements taken (Gerbi, 2006). The ICRU Report No. 71 (2004) recommends that Level 3 for dose and volume evaluation be used to report evolving techniques, as was the case for the new technique. Level 3 includes a comprehensive description of the "data required to perform electron beam therapy effectively and safely" (ICRU, 2004), including heterogeneous corrections used and dose-volume histograms (DVH). Electron beam treatment planning is important to optimize the treatment that will give an adequate dose to the PTV whilst sparing the OARs. Suggestions and recommendations were made as to what features are needed in the treatment planning systems, for the implementation of this technique.

Ulin and Palisca (1996) looked at two types of scattering foils to get better uniform dose distribution for single and abutting fields. The first was made from mylar with the aim of increasing the dose to the chest wall medial and lateral borders. The other was made of lead foil with the purpose of increasing the electron beam penumbra. The mylar compensator made from different layers of mylar was used to scatter the electrons outwards toward the edges, thereby increasing the dose at the edges for a single 6 MV beam irradiating the chest wall as a result of the reduced dose caused by beam obliquity and inverse square. The second scattering foil was made from three layers of lead, for abutting fields with a hinge angle

between 0° and 68° for beam energies of 6, 9 and 12 MeV. The compensators were able to provide better dose homogeneity in the target, with the lead foil offering better results.

Vatanen et al. (2009) have looked at eMLC leaf front face shaping and angles, for narrow electron fields. Their study showed that the shape of the leaf front affected the electron angular and energy distribution and depth dose profiles of the narrow beams. They also looked at whether leaf scatters from different leaf materials had an effect on the dose build-up. There was little difference in the angular and energy distributions for steel, brass and tungsten eMLC leaves. The face angle of 15° increased the scattering and builds up the dose, which gave a better flatness for abutting narrow beams. Ravindran et al. (2002) developed an electron multileaf collimator with the leaves made from Lipowitz alloy, with a leaf thickness of 16 mm to reduce the maximum dose to 5%. They found an increase in surface dose for the eMLC due to "in scatter" of the electrons, the highest increase was 5% for the lower electron beam energy of 5 MeV and 2% for a 14 MeV beam. They also found that the edges of the beam profiles have a steep gradient of dose with a smaller penumbra for the eMLC.

Compared to photons, placing a wedge material in an electron field increases the scattering and significantly degrades the energy of the beam. Kurup et al. (1993) looked at using polystyrene electron wedges to improve dose uniformity at the edges of abutting fields, by increasing the beam penumbra. They reported beam penumbra as a function of sheet thickness, field size and beam energy. They were able to get better dose uniformity with an energy degradation of 5% for a 6 MeV beam, and 6.5% for the 20 MeV beam.

A literature review of field abutment was included as this is an aspect to be considered for adjoining electron fields. However, in this study an in-depth analysis of this aspect was not conducted.

2.6 Electron Beam Treatment Planning

Electron beam models and calculation algorithms should accurately describe the beam's behaviour as it traverses the medium. The model should be able to reproduce the dose distributions that are similar to those experimentally obtained in a water phantom, as well as

correct doses where there might be surface irregularities and heterogeneities of different densities such as lung, bone, air cavities.

Knowledge-based treatment planning has its origins in artificial intelligence and includes machine learning. Machine learning is a technology that uses computer algorithms to emulate human intelligence. In radiotherapy, it has the potential of optimizing and automating contouring and treatment planning, doing physics quality assurance, image-guided radiotherapy and many more (Naqa et al., 2015). Wang et al. (2017) considered IMRT knowledge-based planning for breast cancer patients. Knowledge-based treatment planning aims to eliminate poor and sometimes wrong clinical trade-offs, to achieve the best possible plan for the given technique using the knowledge of prior plans. They were able to improve IMRT plans with knowledge-based planning, allowing the transfer of planning expertise from experienced planners to less experienced ones.

A second check on the MU calculation is essential to ensure the correct and accurate delivery of therapeutic radiation dose, and the guidelines for the appropriate action levels applied (Stern et al., 2011). When calculating the MU for an electron plan on a TPS, it is important to ensure the correct grid size, as a way of eliminating possible errors in the calculation (Stern et al., 2011)

Whilst CT to electron density conversion is more relevant for CT-image based treatment planning for photon beams, in the case of electron beams, conversion to total stopping power and mean angular scattering power is more important for dose calculation using pencil beams (Huizenga and Storchi, 1985, Hogstrom et al., 1981). With improved algorithms such as those using Monte Carlo techniques, this is less of an issue. Xu et al. (2009) have compared the measured data on a Varian linac to that calculated on a TPS using the Varian Eclipse electron Monte Carlo (eMC) algorithm. They found the eMC algorithm to be more accurate than earlier electron algorithms. Xu et al. (2009) also determined that for small fields up to 3 cm, limiting cutout sizes for an electron field should be approximately E (MeV)/2.5 in centimeters of water as given by Lax and Brahme (1980), Khan (2003) was not applicable with eMC.

Gibbons et al. (2014) recommended that the normalization depth for electrons be the depth of maximum dose along the central axis as in a water phantom at the same SSD. The protocol written by Gibbons et al. (2014) provides a formalism for the manual calculation of monitor units for electron beams, where the MU at the nominal SSD is calculated using

$$MU = \frac{D \cdot 100\%}{D_0' \cdot PDD(d, r_a, SSD_0) \cdot S_e(r_a, SSD_0)} \qquad 2.6$$

where the PDD is normalized to the depth of maximum dose for the treatment field size, r_a, and S_e is the dose output for a field size (applicator and insert).

The electron output as given by Gerbi et al. (2009) is

$$S_e(r_a, SSD) = \frac{D/MU(d_m(r_a), r_a, SSD)}{D/MU(d_m(r_0), r_0, SSD_0)} \qquad 2.7$$

$$= \frac{D'(d_m(r_a), r_a, SSD)}{D_0'} \qquad 2.8$$

where D/MU is the dose per MU, $d_m(r_a)$ is the depth of maximum dose for the treatment field size, r_a, and $d_m(r_0)$ is the depth of maximum dose for the reference field size, r_0.

For MU calculations at extended SSD, the following equation is used

$$MU = \frac{D \cdot 100\%}{D_0' \cdot PDD(d, r_a, SSD) \cdot S_e(r_a, SSD_0) \cdot ((SSD_{eff}(r) + d_0)/(SSD_{eff}(r) + d_0 + g))^2} \qquad 2.9$$

where g is the difference between the treatment SSD and the calibration SSD, and SSD_{eff} is the effective source to surface distance. In the case of the air gap technique, the MU is calculated using the following equation

$$MU = \frac{D \cdot 100\%}{D_0' \cdot PDD(d, r_a, SS) \cdot S_e(r_a, SSD_0) \cdot ((SSD_0 + d_0)/(SSD_0 + d_0 + g))^2 \cdot f_{air}(r_a, SSD)} \qquad 2.10$$

Where g is the difference between the treatment SSD and the calibration SSD, and f_{air} is the air-gap correction factor.

2.6.1 Collision Avoidance

Humm et al. (1995) looked at collision detection and avoidance of treatment planning. They developed software that had a graphical interface that analytically verified collisions based on the known dimensions of the treatment machine. The planner was able to visualize the position of the patient in relation to the gantry on the "room's eye view" of the graphical user interface throughout the whole process of developing a treatment plan. Becker (2011) created gantry-couch collision charts for Varian linacs, and Becker et al. (2013) created gantry-couch collision charts for Siemens and Elekta machines. Elena et al. (2003) developed a technique and computer program that was able to detect possible collision of the gantry and couch and signal avoidance of potential problematic treatment beams. However, the program did not check for collisions when moving in between treatment fields. The technique involved the use of analytical geometry.

CHAPTER 3

RESEARCH METHODOLOGY

In developing the new technique for treating the mastectomy scar with electrons, a number of tests and measurements were conducted for this study. The Siemens Oncor Impression was the linac used to carry out the measurements. The Siemens Oncor Impression is a klystron based linac with both photon and electron energies, that had a 58 multi-leaf collimator (mlc). The IBA Blue Phantom^2 and the IBA control unit were used, with the IBA Markus chamber as a reference chamber and the PTW Advanced Markus-34045 chamber as the field chamber. With a common control unit (CCU) which incorporates a built-in pressure & temperature sensor and two independent electrometers with a bias of +400 V. Measurements were made in air for 2 × 2 cm, 4 × 4 cm, 6 × 6 cm, 8 × 8 cm and 10 × 10 cm field sizes. The nominal electron energies used were 5, 7, 8, 10, 12 and 14 MeV, for 2 × 2 cm, 4 × 4 cm, 6 × 6 cm, 8 × 8 cm field sizes. GafChromic EBT film was also used for measurements. For certain electron dosimetry measurements, film was used as it is recommended because of its high spatial resolution and weak electron energy dependence (Khan et al., 1991, Su et al., 2007, Donmez Kesen et al., 2014).

3.1 Electron Beam Characteristics

The shape of the electron beam isodose curves is dependent on the field size, beam energy, beam collimation and SSD. However, the shape of isodose curves in the penumbra region (20% to 80% isodose curve) does not change significantly with field size. Some of the measurements that were carried out in this study included the following: measurements to determine the effects of oblique incidence on electron dose distribution, surface dose dependence on field size, depth of maximum dose for small fields, the effect on therapeutic depth for small fields, and the effect on depth of maximum penetration, as these effects are dependent on field size. For field sizes where there is lateral equilibrium, an extended SDD has the effect of decreasing the width of the area covered by the 90% isodose curve and giving more dose outside the field edge.

3.1.1 Variation of dose with SSD

Measurements were conducted in water to determine how the dose of different field sizes varied with SSD. The IBA Blue Phantom[2] water tank was used, with an Advanced Markus chamber with the effective point of the chamber at d_{max} of the electron beam energy being measured. The relative dose was measured with the water tank at different SSD. The position of the water tank was varied for a possible SSD range of 100 cm to 112 cm. Measurements were for 5, 7, 8, 10 and 12 MeV, for 2 × 2 cm, 4 × 4 cm, 6 × 6 cm, 8 × 8 cm and 10 × 10 cm field sizes.

3.1.2 Beam Obliquity

The technique involves treating the chest wall, which has a curved surface; it was important to keep the incidence of the electron beam perpendicular to the patient's surface to avoid beam obliquity effect. The depth of maximum dose decreases as the angle of incidence increases, with a significant change in the shape of the depth dose curve for angles of incidence greater than 60°, beam obliquity measurements were therefore done.
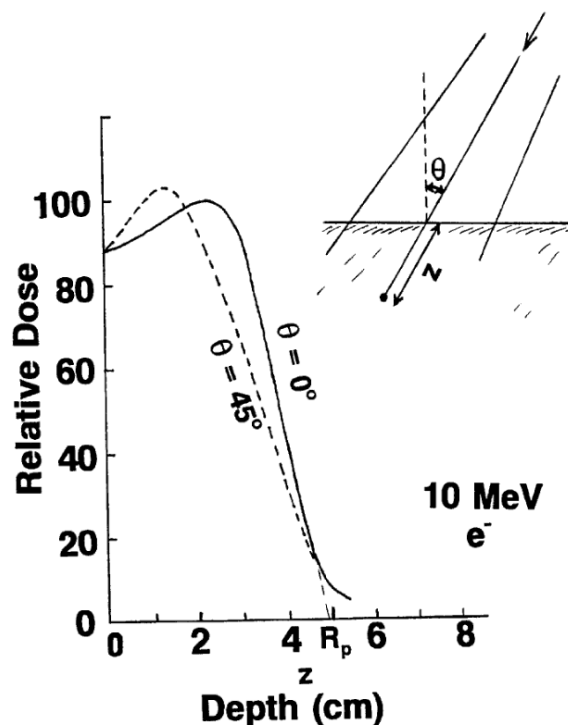

Figure 3.1 *Comparison of the central-axis depth-dose curves for 10-MeV electrons at normal incidence and incidence at 45° with respect to the entrance surface. Source: Jayaraman and Lanzl (1996)*

The measurements were conducted with the angle of incidence, as shown in Figure 3.1, with the depth of measurement in the direction of the beam as indicated by the *z*-direction. The effect of increasing the air gap for extended SSD, results in the edges of the field being diffuse. Thus, the curvature of the body was followed to ensure a relatively constant SSD.

3.1.3 Virtual Source Position

3.1.3.1 Inverse Square Law Methods

Two approaches were employed for determining the virtual source position using the inverse square law methods measurements. For one method, the measurements were conducted in-air whilst the other measurements were done using a water phantom. Both methods measurements were made using an IBA Blue Phantom[2] and Advanced Markus chamber, for field sizes of 2 × 2 cm, 4 × 4 cm, 6 × 6 cm, 8 × 8 cm and 10 × 10 cm. The nominal electron energies were 5, 7, 8, 10, 12 and 14 MeV. For the in-air method, measurements were done with the chamber at -5, 0, 5, 10, 15, 20, 25 and 30 cm from the end of the applicator. For the water measurements, the Advanced Markus chamber was at d_{max}. They were done with the air gap between the water phantom and applicator at 0, 5, 10, 15, 20, 25 and 30 cm. The virtual source position is determined by plotting the inverse of the square root of the electrometer readings and finding the intercept of the straight line.

3.1.3.2 Inverse Slope Method

The virtual source position was also evaluated using the inverse slope method with both in-air and in-phantom measurements. The virtual source position was determined using a method similar to that described by Thomas (1988). The in-air measurements were taken at different separations between the Advanced Markus chamber and the applicator, at a separation of 0, 5, 10, 15, 20, 25, 30, 35 and 40 cm. For the in-phantom measurements, a farmer chamber was placed in a 20 cm × 20 cm × 20 cm polystyrene phantom with the chamber at reference depth. Measurements were at different separations between the phantom and the applicator, at a separation of 0, 5, 10, 15, 20, 25, 30, and 35 cm.

The inverse slope method is based on the inverse square law and the following equation,

$$\sqrt{\frac{Q_0}{Q_S}} = 1 + \left[\frac{1}{(VSP_{eff}+d)}\right] s \qquad\qquad 3.1$$

where Q_0 is the collected charge with no separation and Q_S is the collected charge with separation s, VSP_{eff} is the virtual source position and d is the depth of measurement. The plot of the square root of the quotient of the charge readings with no air gap to the readings of the charge with separation of the air gap, $\sqrt{\frac{Q_0}{Q_S}}$, against the separation s, gives a linear plot. The gradient of this line, as represented in equation 3.1 is given by

$$slope = \frac{1}{(VSP_{eff}+d)} \qquad\qquad 3.2$$

Therefore the virtual source position is given by the inverse of the slope as

$$VSP_{eff} = \frac{1}{slope} - d \qquad\qquad 3.3$$

3.1.3.3 Full-Width Half-Maximum (FWHM) Method

The virtual source position was determined using the method described by Ravindran (1999). Measurements were done using an IBA Blue Phanton^2 water tank. The PTW 0.02 cm^3 Advanced Markus electron chamber was used as the field chamber for measurements, with another Markus chamber used as the reference chamber. A standard 10 × 10 cm fixed size electron applicator was used; the distance from the target to the end of the applicator is 95 cm, leaving a gap of 5 cm when the patient surface is at an SSD of 100 cm.

3.2 Electron Beam Collimation

A consequence of the physical characteristics of electrons is that they need to be collimated from the point of production, all the way down to as close as possible to the patient's surface.

3.2.1 Effect of primary jaw field size

The primary jaw or collimator settings have an effect on the electron beam profiles. The default jaw settings for the primary collimator for the Siemens linac when using electron applicators are 19 × 19 cm and 22 × 22 cm, depending on the standard applicator that is

inserted. An investigation into whether primary jaw settings less than 19 x 19 cm would have an effect on the electron beam was conducted. Measurements were conducted to see how the primary jaw opening has a bearing on the electron beam at the patient level. This was done for different jaw field sizes and electron energies and for different applicator sizes. Beam profiles were measured at depths of R_{100}, R_{90} and R_{50} for the various electron beam energies.

3.2.2 Electron Transmission

To determine the thickness required for the collimating jaws of the variable collimator, transmission measurements were conducted for varying thicknesses. Electron transmission curves were measured by placing the steel plates made from Cerrobend of varying thickness at the end of a standard 10×10 cm electron applicator. Cerrobend was used for these measurements as it was readily available in the department. The tenth-value thickness (TVT) of the steel is about twice that of Cerrobend (Jayaraman and Lanzl, 1996, Tellili et al., 2017); thus, the required thickness of the required steel would be twice that of Cerrobend. Measurements were done in a water phantom at 100 cm SSD, using an Advanced Markus with the effective point at a depth of 0.5 cm. The setup is shown in Figure 3.2.
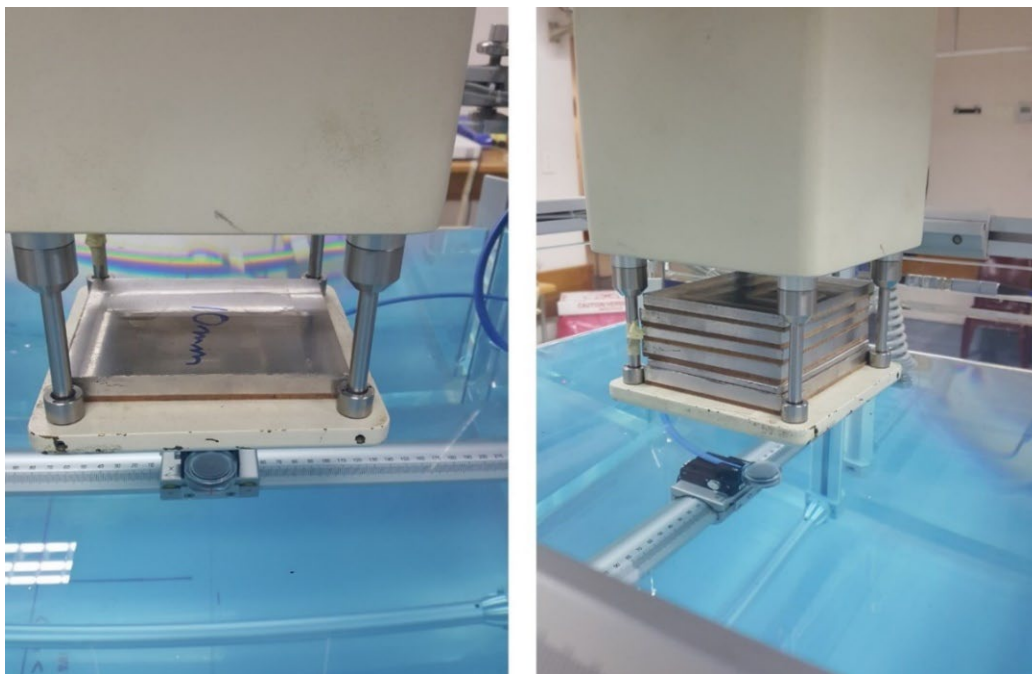
Figure 3.2 *Setup used for measuring the transmission of Cerrobend.*

As a guideline, the thickness of lead in millimeters required to reduce the dose to 5% of the maximum is half the electron beam energy in MeV (Klevenhagen, 1993).
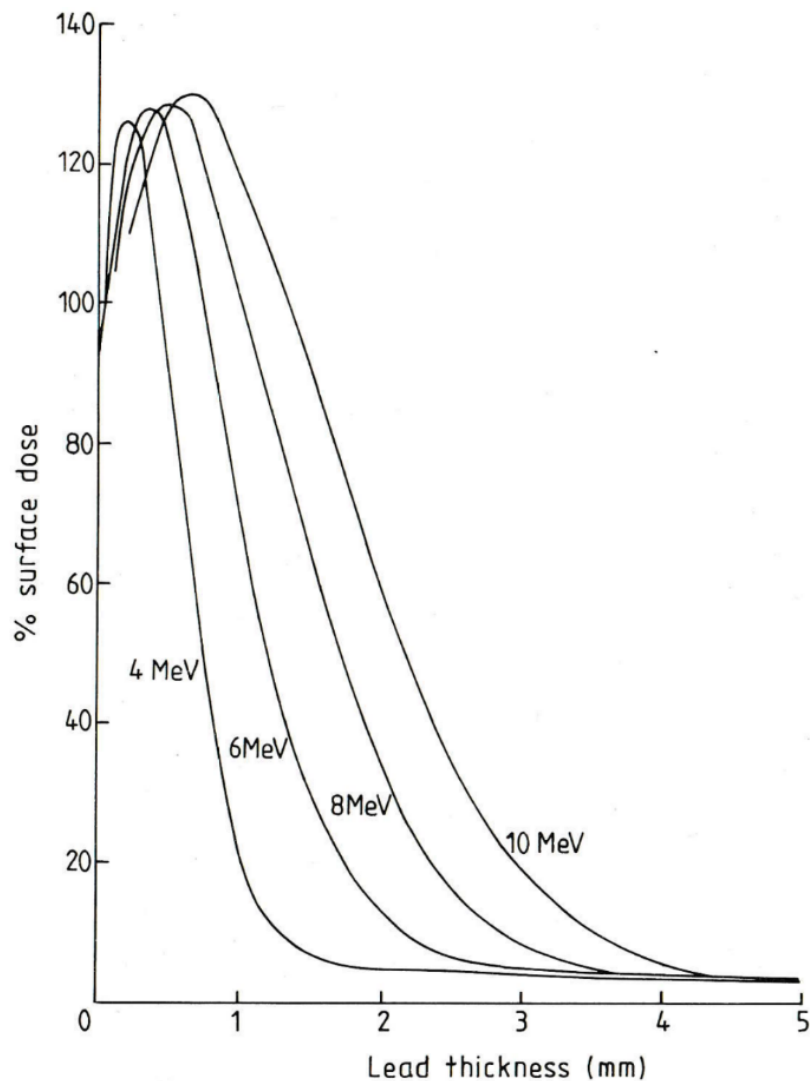
Figure 3.3 *Electron transmission curves for lead. Source: Klevenhagen (1985)*

The correct thickness of the shielding material is required. Inadequate shielding can result in increased surface dose, as indicated in Figure 3.3 above, as a result of bremsstrahlung and forward scattered electrons (Klevenhagen, 1985). Electron transmission measurements were conducted to determine the required thickness of the steel.

3.2.3 Variable field-shaping collimator

A 3-D model of the electron variable field-shaping collimator was constructed using CAD software, from which a 3D plastic model was made. A working model was machined using

mild steel, which is more rigid than lead, or Wood's alloy. For electron field sizes less than 10 × 10 cm, the variable collimator was used for the dosimetric measurements. The motors to drive the collimators for the variable field-shaping were considered, as well as the motor controller. The motors that were chosen were the Maxon high-precision pencil motors that were controlled by an Arduino Uno R3.

The variable collimator allows for the treatment of different segments with different energies. Bolus was not used for beam energy modulation in this study. The modulation of the beam will be accomplished by treating the scar in segments to allow for the change of beam energy in between the segments. Should a bolus be needed to increase the surface dose beyond the 80% to 90% and limit the lung dose (Chao et al., 2002), it needs to be tissue equivalent both in stopping power and scattering power.

When a patient is undergoing breast treatment, the patient lies on the breast board that is placed on the treatment table, similar to the one shown in Figure 3.4.

Figure 3.4 *Patient lying supine on a breast board. Source: Bellon et al. (2016)*

The patient lies such that the scar can be seen, as shown in Figure 3.5. Daily patient setup changes should be taken into consideration by using 2D or 3D patient position verification.
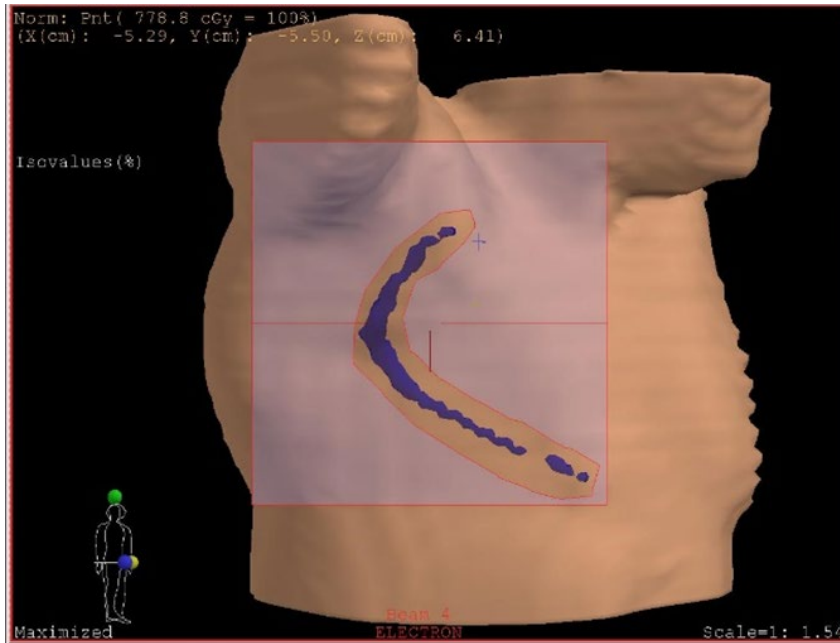
Figure 3.5 *3D surface rendering of the patient with breast scar as seen from a treatment planning system.*

The movement of the variable field-shaping collimator uses the sliding window technique. The sliding window technique has both jaw collimators moving unidirectionally from one end to the other, at different speeds. The jaws produce a fluence profile that is represented by a piecewise linear function consisting of segments of straight lines (Spirou and Chui, 1994). Each segment is delivered, as shown in Figure 3.6.
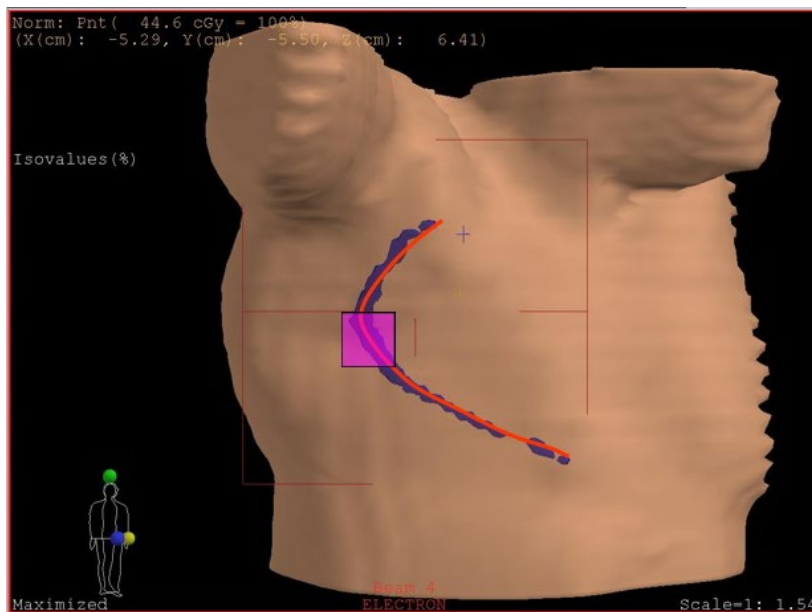
Figure 3.6 *An individual segment being delivered.*

The dimensions of the variable collimator were chosen to allow the collimator to be fitted on a 10 × 10 cm standard electron applicator; however, the use of the variable collimator is not limited to a 10 × 10 cm standard electron applicator but can be used on the other electron applicators to treat larger areas. For a scar similar to the one in Figure 5.1, the dose distribution was represented by a dose profile, as shown in Figure 3.7; the profile or sections of which needed to be monotonic, with the profile comprising of discrete points. The assumption was that the profile varied linearly between these points, and thus the velocity between these points would be constant.
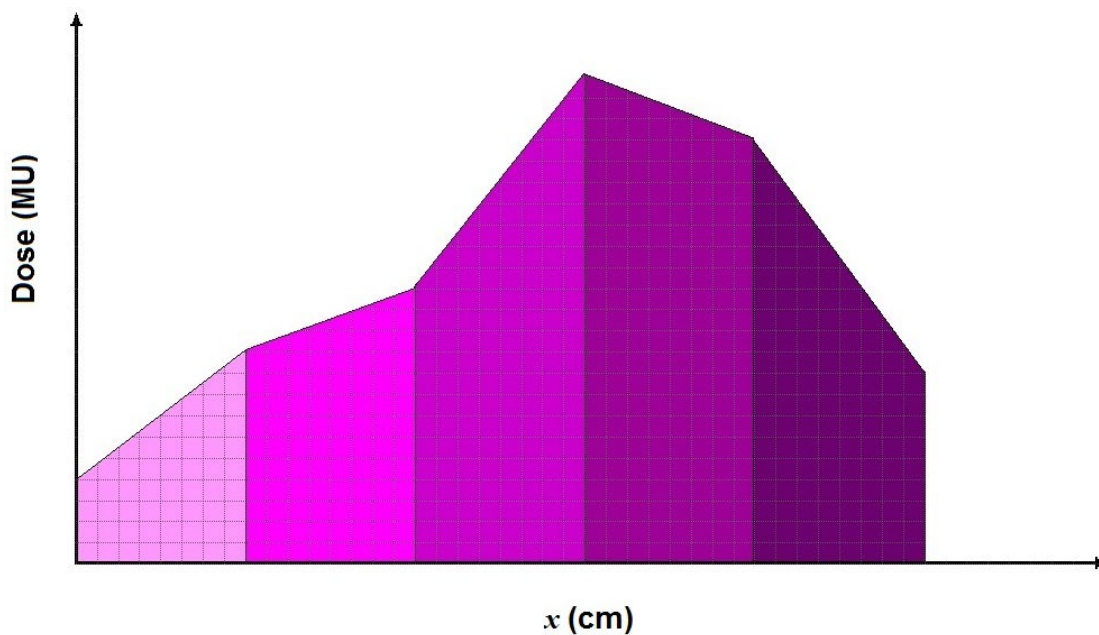
Figure 3.7 *Dose profile for electron scar boost*

A simple dose distribution in the form of a 'wedge' is shown in Figure 3.8, where the dose across the field was generated by the moving collimating jaws. Thus, each of the segments in Figure 3.7 was represented by a wedge.

From Spirou and Chui (1994), the following equations were used to describe how the dose distribution is obtained using a pair of collimating jaws.

For a particular wedge section, the dose rate is given by

$$Dose\ rate\ = \frac{v}{V_{cr}}$$

3.4

Where the dose rate is in units of MU/min, v is the mechanical velocity of the jaw in cm/s, and V_{cr} is the critical velocity given as the inverse of the slope in units of cm/MU. If the dose rate is known, and the slope is known, then the velocity of the jaw can be determined; this can be seen in the scenario presented in Figure, 3.8 jaw-2 remains stationary whilst jaw-1 moves at maximum velocity.
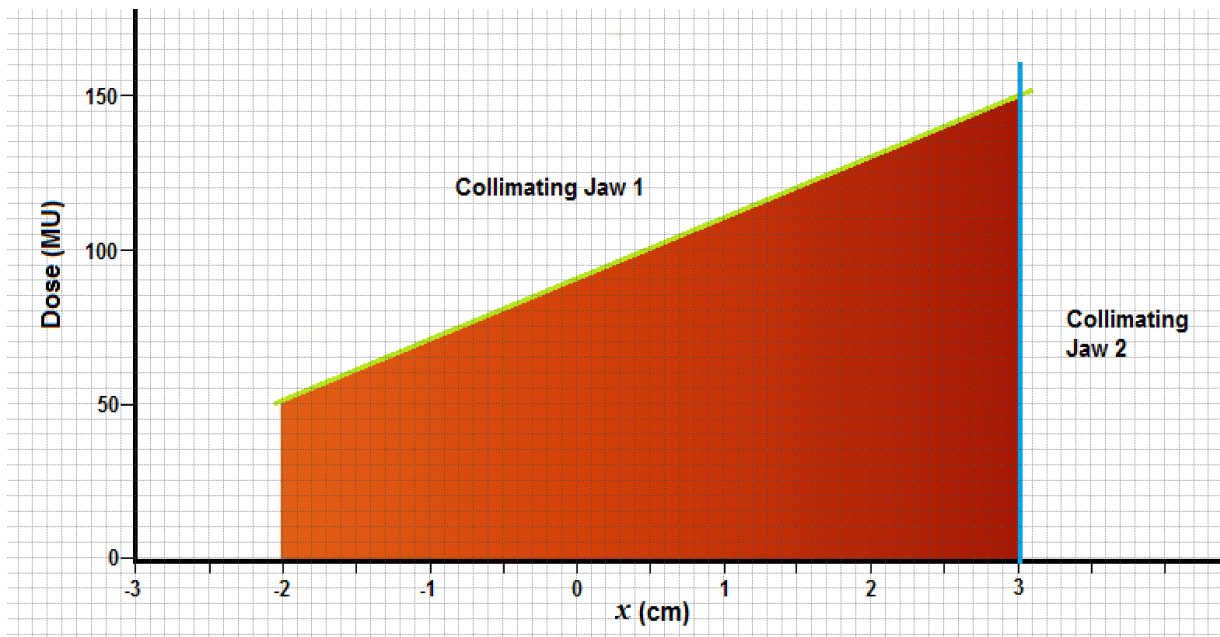
Figure 3.8 *'Wedge' dose distribution generated by two collimating jaws.*

The algorithm used for controlling the motion of the pair of collimating jaws followed the work by Spirou and Chui (1994). The dose distribution calculated by the planning system is represented by the intensity profile $I(x)$. The profile is in the form of a piecewise linear function, with N discrete points. The accumulative beam-on time in MU at position x for the two jaws (shown in Figure 3.9) jaw-1 and jaw-2, is given by the monotonic functions $I_1(x)$ and $I_2(x)$ respectively.

The field intensity produced by the jaws is in the form of a Heaviside step function:

$$I_1(x) = \begin{cases} 0 & if \ x < x_0 \\ D & if \ x > x_0 \end{cases} \qquad 3.5$$

and

$$I_2(x) = \begin{cases} 0 & if\ x > x_0 \\ D & if\ x < x_0 \end{cases} \qquad\qquad 3.6$$

where D is the beam-on field intensity in MU. The intensity profile is then given by

$$I(x_i) = D_1(x_i) - D_2(x_i)\ ,\ \text{where } i = 1,....,N \qquad\qquad 3.7$$
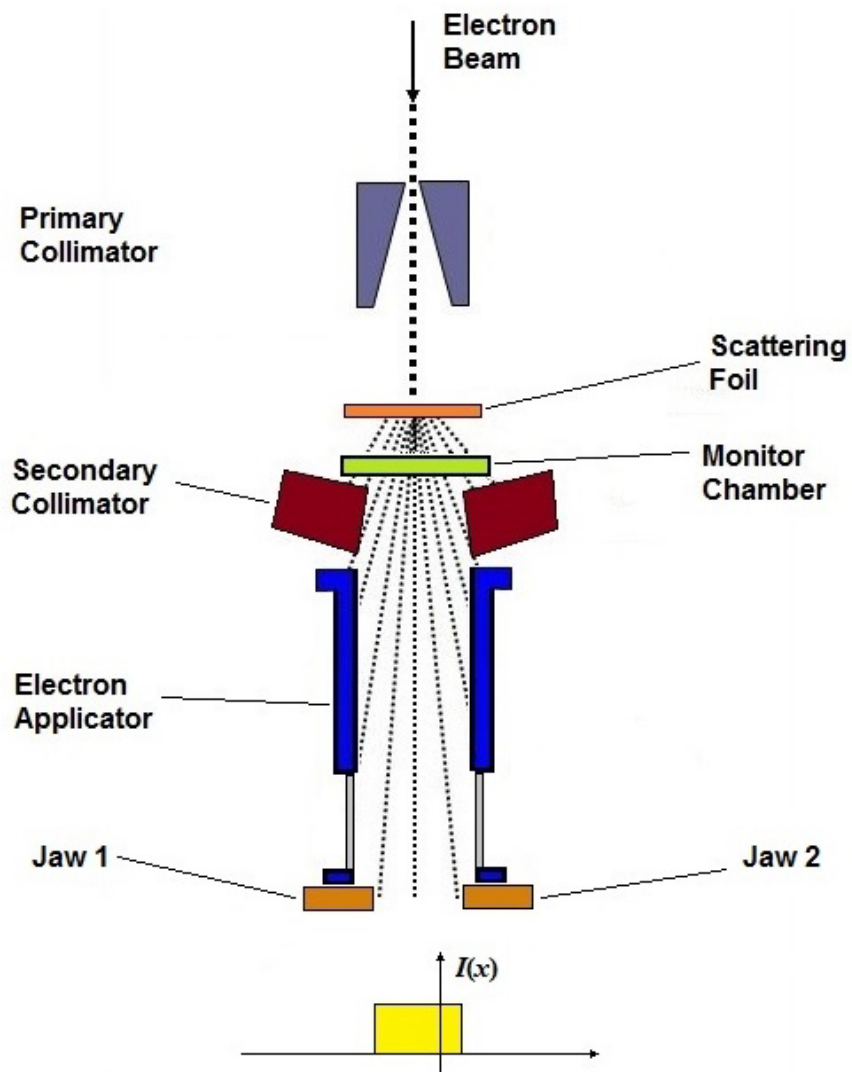
Figure 3.9 *Electron applicator with collimating jaws.*

One of the jaws is assumed to be able to move at a maximum speed between adjacent points, and $I(x_{i+1}) \geq I(x_i)$, as shown in Figure 3.10.
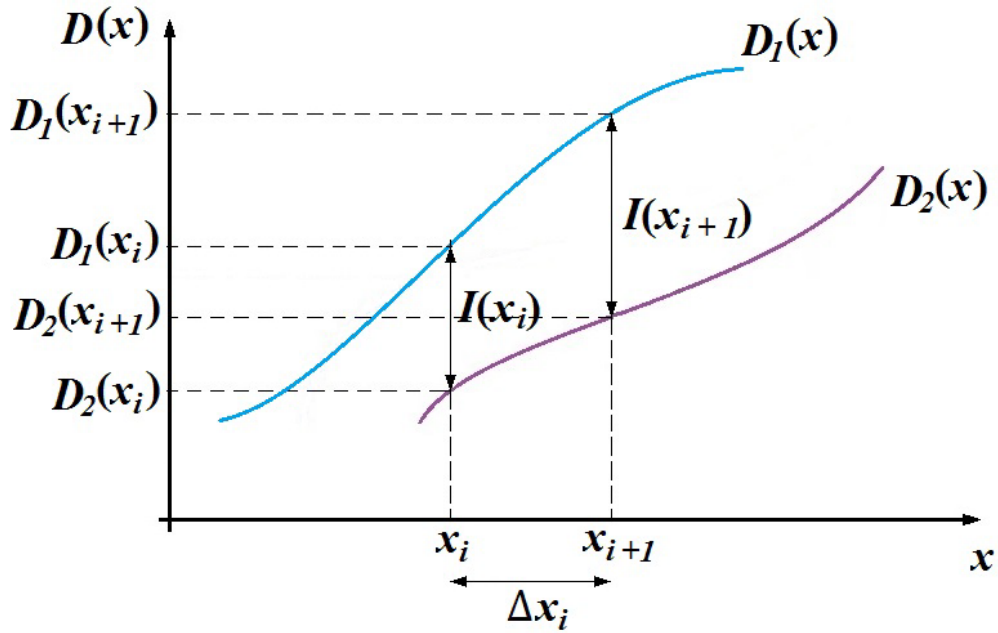
Figure 3.10 *The relationship between I(x), D1(x), and D2(x) at the points x_i and x_{i+1}. Both D1(x) and D2 (x) are piecewise linear.*

Then,

$$D_2(x_{i+1}) = D_2(x_i) + \frac{\Delta x_i}{V_{max}}$$ 3.8

and

$$D_1(x_{i+1}) = D_2(x_{i+1}) + I(x_{i+1})$$ 3.9

In the case where $I(x_{i+1}) \ngeq I(x_i)$, then

$$D_1(x_{i+1}) = D_1(x_i) + \frac{\Delta x_i}{V_{max}}$$ 3.10

and

$$D_2(x_{i+1}) = D_1(x_{i+1}) + I(x_{i+1})$$ 3.11

Where V_{max} is the maximum speed in cm/MU, and Δx_i is the distance travelled in the ith - segment, $x_{i+1} - x_i$.

The individual segments are delivered as indicated in Figure 3.11, with the summation of the dose coverage and the appropriate margin around the scar.
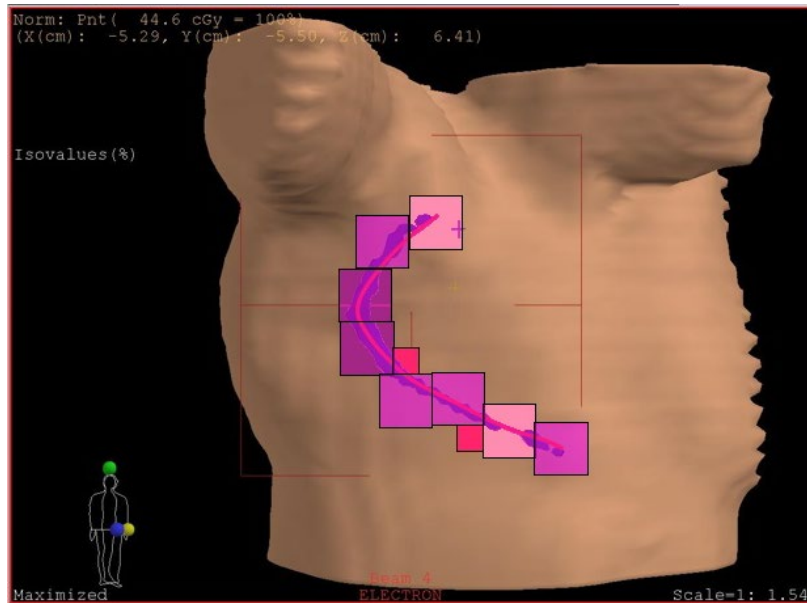
Figure 3.11 *Dose delivery of segments of varying lengths and energy.*

The Siemens Oncor was able to deliver electron beams at a dose rate of 300 MU/min. For the sliding window technique where the two jaws start at the same position for each segment the maximum speed, V_{max}, in cm/MU should be less than the critical speed, V_{cr}. Thus, the mechanical speed of the jaws was expressed by

$$V_{cr} > \frac{v}{5} \hspace{3cm} 3.12$$
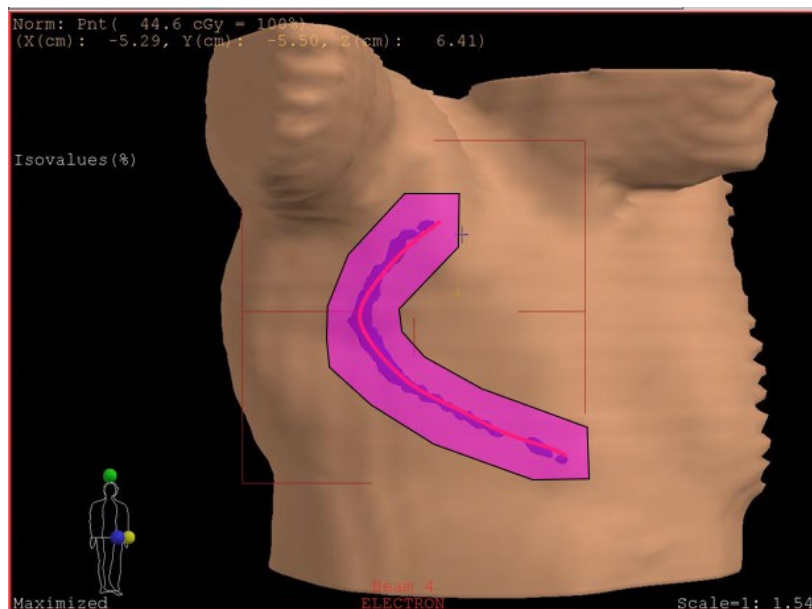
Figure 3.12 *Summation of segments with a margin around the scar.*

3.3 Automated Couch Movement

3.3.1 Couch Movement

The optimal treatment of the scar requires the movement of the treatment couch, the collimator as well as the gantry, all of which are automated. This study looked at automating the treatment couch movement. The software was used to control the movements of the motorized couch.

The treatment couch used was a Siemens ZXT table that was installed on one of the linacs in the department. The ZXT treatment table, as shown in Figure 3.13, has a microcontroller that is used to control the table movements. The table movements, except for the column rotation, are monitored by encoders and potentiometers. The encoders are used to control the longitudinal, lateral tabletop and isocentric motors (Siemens Medical Solutions USA, 2004). The table has a vertical range of 110 cm, longitudinal range from 0 cm to 90 cm, lateral range of ± 25 cm, column (eccentric) rotation range of 180° in either direction, an isocentric rotation range of ± 120° and a maximum posterior field size of 57 cm × 57 cm when the table is at the lowest position (Siemens Medical Solutions USA, 2005). The table lateral, longitudinal and isocentric movements are manual or motorized, whilst the vertical movement is only motorized, and that of the column (eccentric rotation) is motorized. The table movement was stopped by a software limit, limit switch or mechanical limit, as indicated in Table 3.1.

A serial line RS232 interface to the controller was used to send the signals to move the table via the laptop that was linked to the couch. The serial cable with a DB-9 connector for the PC connection was used. Only three pins, pin 2 (RxD - receive data), pin 3 (TxD - transmit data) and pin 5 (GND - ground), were used since communication with the table is asynchronous as no clock signal is used. The input and output baud rates were set to 9600. Position errors were generated by comparing the data from the encoders with that from the potentiometers. A 20 mA current loop format for serial communications had the advantage that there were no line losses due to voltage drop, as a result of line resistance and also provided a simple form of networking.
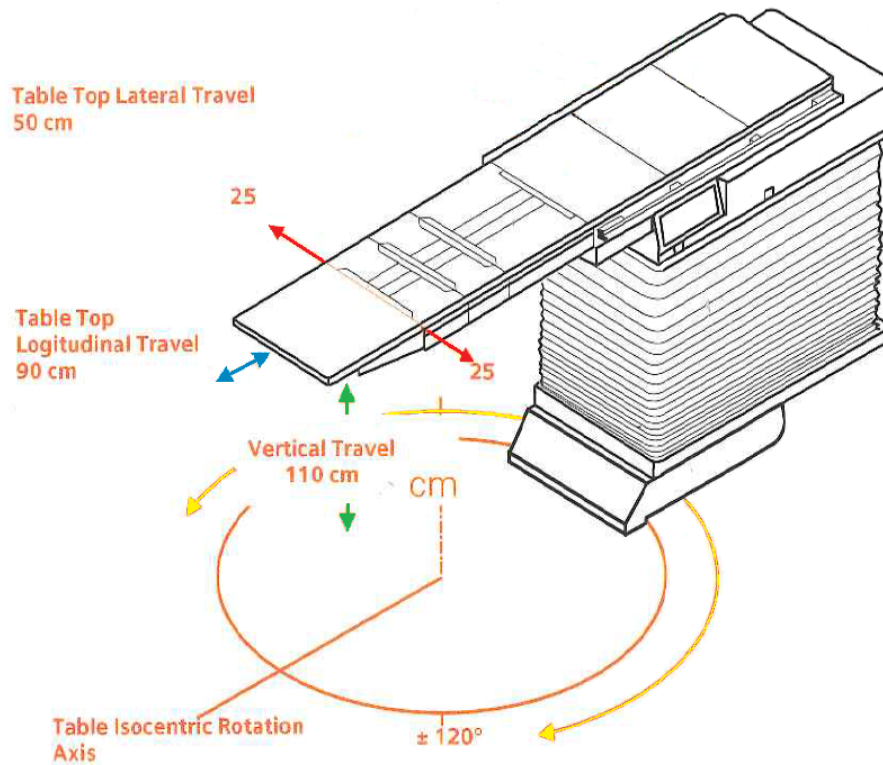
Figure 3.13 *Siemens ZXT treatment table. Source: (Siemens Medical Solutions USA, 2005)*

The software was used to move the treatment table in four directions, namely vertically, laterally, longitudinally and isocentrically, as shown in Figure 3.13 above. The software code was written using the C language.

Table 3.1   *ZXT Table Movement Data. Source: (Siemens Medical Solutions USA, 2005)*

Movement	Direction	Total Movement	Motorized Movement	Software Limit Position	Limit Switch Position	Mechanical Limit Position
Tabletop Longitudinal	To Gantry	1016 mm	900 mm	900	902	905
	From Gantry			0	998	995
Tabletop Lateral	Right	520 mm	500 mm	250	255	260
	Left			750	745	740
Table Vertical	Up	1170 mm	1100 mm	558	538	none
	Down			658	none	668
Isocentric Rotation	CW	260º	240º	120º	121º	124.5º
	CCW			240º	239º	235.5º
Column Rotation	CW	380º	none	none	none	178º
	CCW			none	none	182º

3.3.2 Digitization of Path for Couch Movement

The movement of the couch needed to follow a certain path corresponding to the length and curvature of the scar being treated. The method of digitizing the path to be followed by the couch, made use of a pointer, as shown in Figure 3.14. The couch with the "patient" was moved in incremental steps so that the pointer stayed on the scar for the entire length of the scar for different table, collimator and gantry positions. The position of the table height, lateral position and longitudinal position was captured, as well as the collimator rotation and gantry rotation positions.

Figure 3.14 *Pointer used to digitize that path to be followed by the couch.*

Figure 3.15 shows the digitization using the pointer and Rando phantom. The coordinates of the position of the table height, lateral position and longitudinal position were used to move the table accordingly.
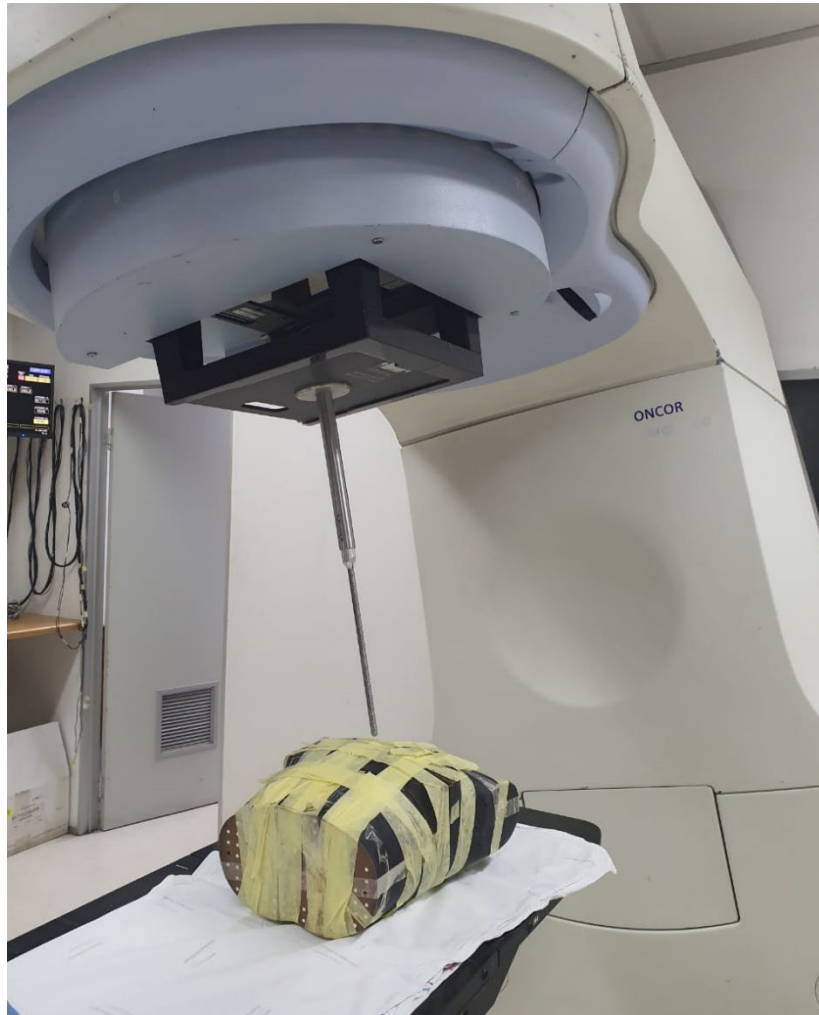
Figure 3.15 *Pointer used to digitize that path to be followed by the couch using a Rando phantom.*

The couch with the patient (which in our setup was a phantom) was moved in incremental steps, with the pointer staying on the scar for the entire length of the scar for different table, collimator and gantry positions. Positions that were captured were marked by the yellow, white and green crosses, with the yellow and white crosses marking the beginning and end of the scar. As the couch was moved, the gantry was also manually moved to ensure that the pointer remained normal to the surface of the patient to minimize the effects of beam obliquity, allowing for a 5 cm gap between the patient surface and the applicator. The pointer followed the path indicated by the red line in Figure 3.16. The table positions, collimator and

gantry positions for each point marked with a cross were captured. The captured table positions provided the coordinates indicating the path the table would move.
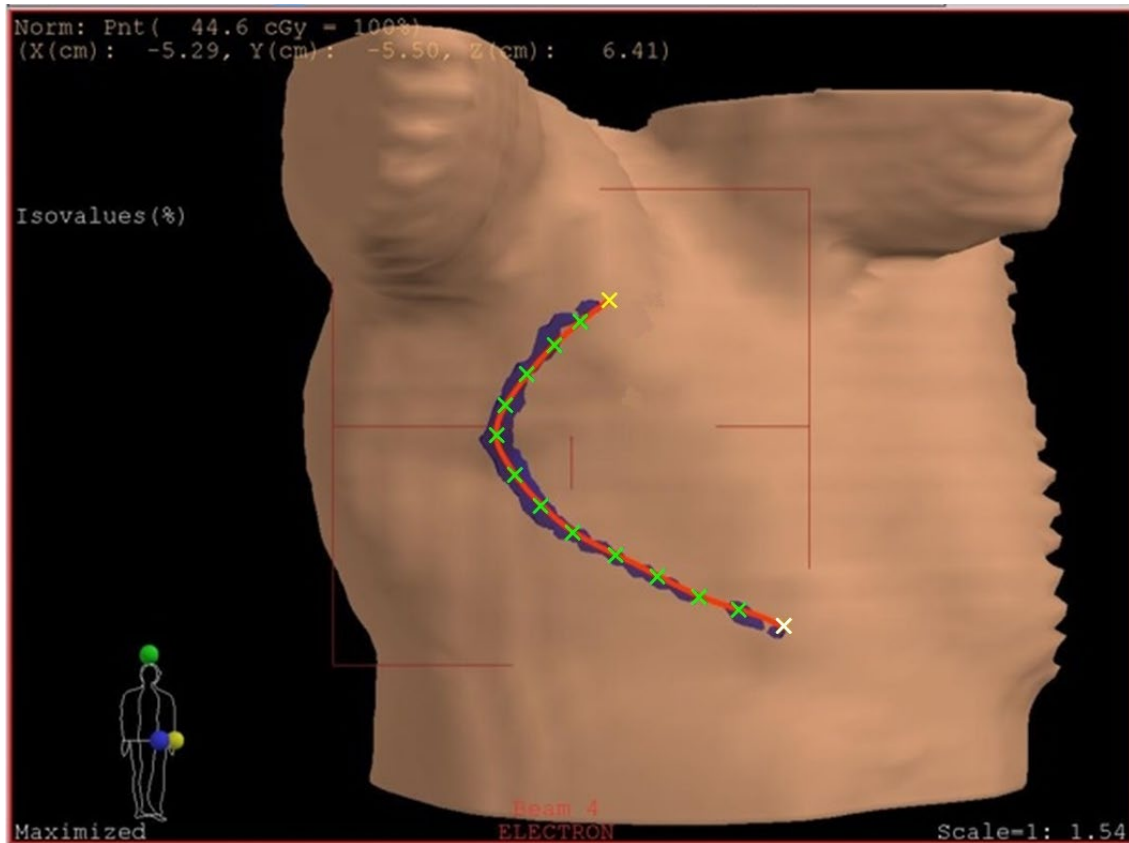
Figure 3.16 *The points used for digitizing the path for the table movement are indicated by the crosses.*

3.4 Collision Avoidance

The Siemens linac gantry rotates about the isocenter in a 180° clockwise or 180° counterclockwise direction through a nominal angle of 360°. An overtravel of about 10° in either direction is allowed when the gantry position is at 180°, as shown in Figure 3.17.
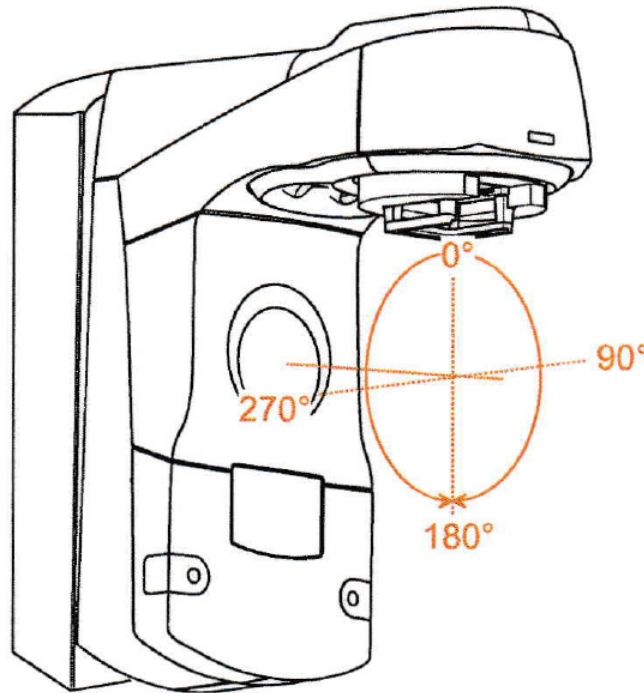
Figure 3.17 *Clockwise and counterclockwise rotation of the gantry. Source: (Siemens Medical Solutions USA, 2005).*

The movement of the couch is as shown in Figure 3.13. The treatment couch has an isocentric rotation range of ± 120°. The table was at position -20 cm (IEC table configuration), which is 20 cm below the table isocenter position indicated as the "0" position, and for lateral table position of 0 cm. To check for collisions, the treatment couch was first moved at increments of 10°, followed by the gantry to the maximum possible angle for each incremental change of the treatment couch. The possible range of rotation of the couch without colliding with the gantry was noted.

3.5 Treatment of Rando Phantom

For the treatment simulations, the Rando phantom was used as the "patient". The Rando phantom is an anthropomorphic phantom in the shape of a human torso, made up of tissue-equivalent material to simulate human tissues such as muscle, bone and lung. The phantom is composed of cross-sectional slices, which have a matrix of holes to allow for the placement of film or other dosimeters, such as thermoluminescent dosimeters (TLD). Mastectomy scars vary in length, as shown in Figure 3.18. A marking that was 12 cm long was made across the

chest of the phantom to resemble a typical mastectomy scar, as indicated in Figure 3.19. A wire was then taped on the entire length of the scar to indicate where the scar was on the scanned CT images. The Philips Brilliance Big Bore CT scanner in the department was used to scan the phantom, as shown in Figure 3.20. The scanned images were sent to an Elekta Monaco treatment planning system for planning.
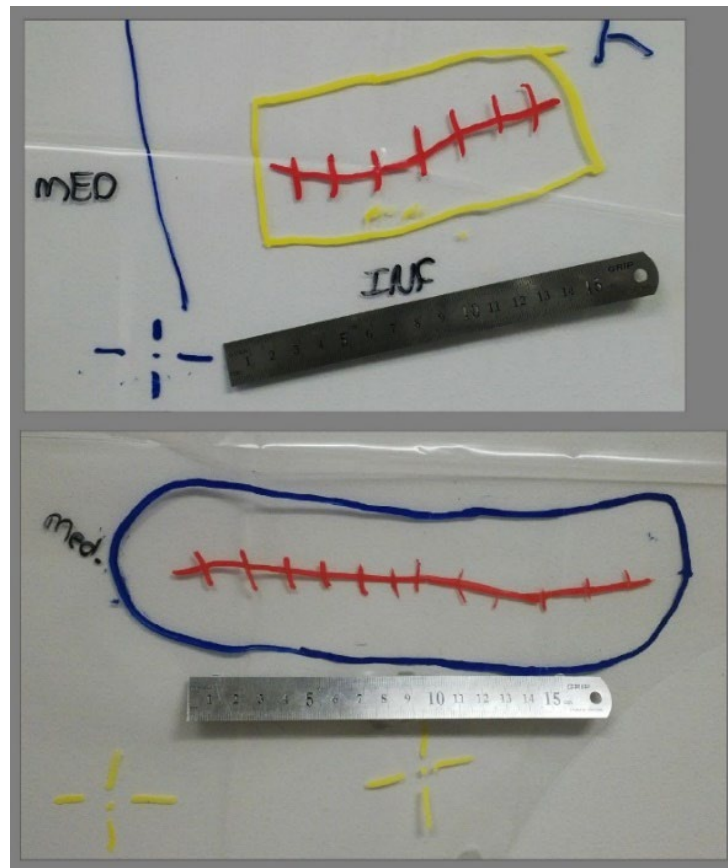
Figure 3.18 *Tracings on transparent plastic of the mastectomy scar cut-out for making the moulds of the Cerrobend electron cutouts.*

The electron plan was created using the Monaco treatment planning system, which uses an electron Monte Carlo algorithm for electron plans. A forward plan was made to give 2 Gy in one fraction to deliver 90% of the dose to the target volume at a depth of 3.5 cm. The scar was 12 cm long with a margin of 4 cm. The treatment plan consisted of three segments, with the first 4 cm of the scar being planned with a 5 MeV electron beam, followed by the next using a 10 MeV electron beam, with the last by electron 14 MeV beam to indicate treatment at varying depths.

Figure 3.19 *Rando phantom with "mastectomy scar" indicated by the white line.*

Figure 3.20 *Scanning of the Rando phantom in the Big Bore CT scanner.*

For the treatment of the Rando phantom, the couch was moved to follow the path traced out on the "patient", with gantry and collimator in the appropriate positions to treat the area, that would typically have been treated using a lead cutout.

The results of the various measurements that were conducted are presented in the following chapter.

CHAPTER 4

RESEARCH RESULTS

In the following section, the findings of the study are presented. These results comprise of the measurements for electron beam characterisation and virtual source position, as well as work done on the variable collimator and treatment couch.

4.1 Electron Beam Characteristics

Measurements for 5 MeV, 7 MeV, 8 MeV, 10 MeV, 12 MeV and 14 MeV were done using a Siemens Oncor, with a 58 multi-leaf collimator for the variable collimator 2 × 2 cm, 4 × 4 cm, 6 × 6 cm, 8 × 8 cm and 10 × 10 cm standard applicator field sizes. Depth ionization curves were converted to depth dose curves using the recommendation in the AAPM Task Group 51 protocol (Almond et al., 1999). An Advanced Markus ion chamber and GafChromic EBT film were used for measurements.

4.1.1 Typical Electron Beam Data

The results of the various electron beam parameters for the measured beams are shown in Table 4.1. The results are of measurements for different collimation jaw openings for the variable electron collimator.

Table 4.1 *Beam parameters for 5 MeV, 7 MeV, 8 MeV, 10 MeV, 12 MeV and 14 MeV electron beams.*

Energy (MeV)	Field Size (cm)	Most Probable Energy Ep0 (MeV)	Surface Dose (% of Peak Dose)	Depth of dose (mm)					Practical range Rp (mm)	Rq (mm)	X-ray Contamination Dx (%)	Gradient G
				Peak Dose	90%	80%	50%	10%				
5	2x2	5.26	56.4	9.5	14.5	16.3	20.2	25.4	25.4	14.6	0.3	2.4
	4x4	5.34	63.6	10.9	15.1	16.7	20.1	25.2	25.8	14.6	0.4	2.3
	6x6	5.22	70.6	10.7	15.0	16.5	19.9	24.9	25.2	14.5	0.4	2.4
	8x8	4.96	87.6	11.0	14.3	16.0	19.3	24.2	23.9	14.1	0.6	2.4

61

	10x10	4.99	84.1	10.0	14.3	15.8	19.1	24.0	24.0	14.1	0.8	2.4
7	2x2	7.17	46.1	9.5	18.2	20.9	26.2	33.3	35.0	17.5	0.5	2.0
	4x4	6.91	68.1	15.3	20.6	22.5	27.1	33.3	33.7	20.3	0.4	2.5
	6x6	6.84	72.4	15.4	20.5	22.7	26.8	33.2	33.3	20.6	0.5	2.6
	10x10	6.61	87.0	13.6	19.5	21.6	26.0	32.1	32.1	19.6	0.9	2.6
8	2x2	8.31	53.3	10.8	20.0	23.3	30.4	39.1	40.6	20.0	0.5	2.0
	4x4	8.08	70.1	17.7	24.4	26.7	32.1	39.2	39.5	24.2	0.6	2.6
	6x6	8.02	73.8	19.1	24.6	26.9	32.0	39.2	39.2	24.5	0.6	2.7
	10x10	8.08	84.0	11.4	14.3	15.8	19.2	23.9	24.4	14.8	1.0	2.3
10	2x2	9.84	59.0	9.6	21.1	25.4	34.9	46.0	48.3	21.2	0.8	1.8
	4x4	9.7	715.0	20.9	29.1	32.2	38.5	46.5	47.6	29.1	0.9	2.6
	6x6	9.73	74.0	22.9	30.1	32.7	38.6	46.5	47.7	29.5	1.0	2.6
	8x8	9.36	85.9	38.1	29.2	32.2	38.1	46.3	45.9	29.3	0.9	2.7
	10x10	9.53	89.5	20.0	28.8	31.5	37.6	45.7	47.3	28.1	1.0	2.5
12	2x2	11.55	64.9	9.6	23.2	28.3	39.8	55.3	56.8	22.2	0.9	1.6
	4x4	11.72	72.4	24.7	34.8	38.9	46.6	56.9	57.6	35.3	1.1	2.6
	6x6	11.53	74.9	26.4	36.6	40.1	47.1	56.8	56.7	36.9	1.1	2.9
	10x10	10.99	91.9	25.4	34.5	37.9	45.0	54.6	54.0	35.6	1.4	2.9
14	2x2	12.3	65.8	9.5	24.0	29.4	42.0	59.9	60.5	22.3	1.3	1.6
	4x4	12.54	72.4	23	36.8	41.2	50.0	61.8	61.8	37.8	1.4	2.6
	6x6	12.54	74.5	27.9	39.3	43.2	50.8	61.7	61.7	39.5	1.6	2.8
	8x8	11.89	86.0	49.1	37.5	41.7	49.1	59.3	58.5	37.9	1.4	2.7
	10x10	12.24	91.9	25.6	36.8	41.0	48.7	58.4	60.3	36.5	1.3	2.5

4.1.2 Variation of dose with SSD

The measurements to determine how the dose for different field sizes and energies varies with SSD, are shown in Figure 4.1 to Figure 4.4 below.
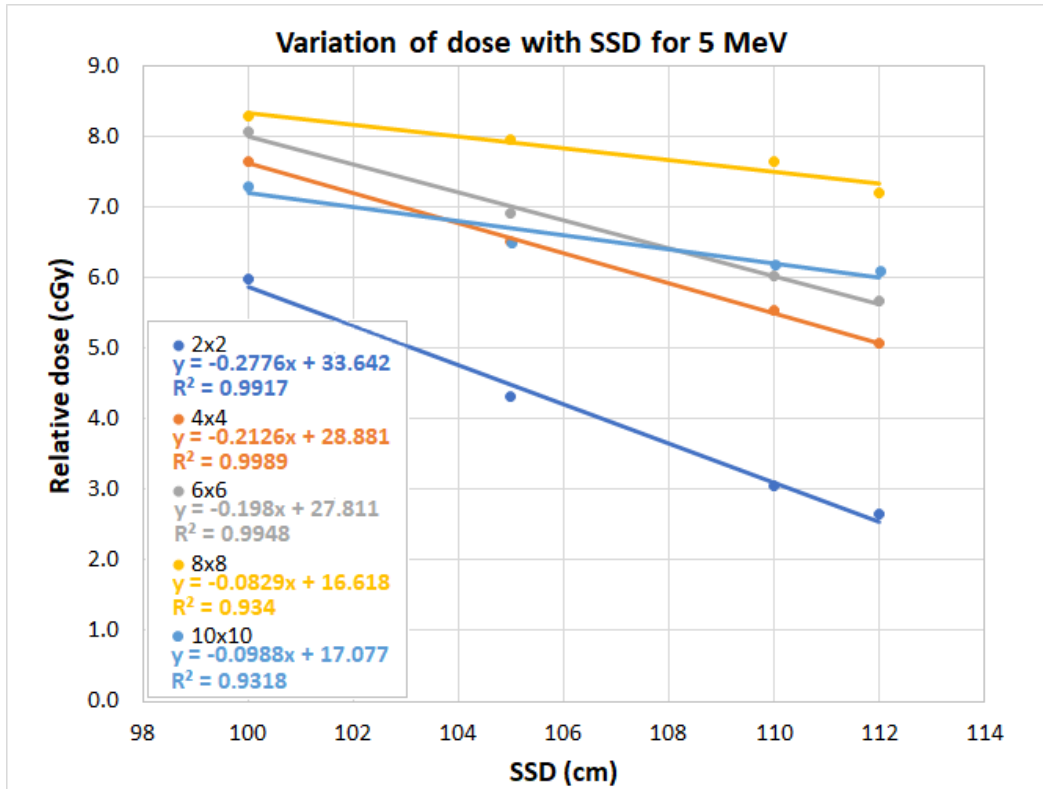
Figure 4.1 *Variation of dose with SSD for a 5 MeV electron beam.*
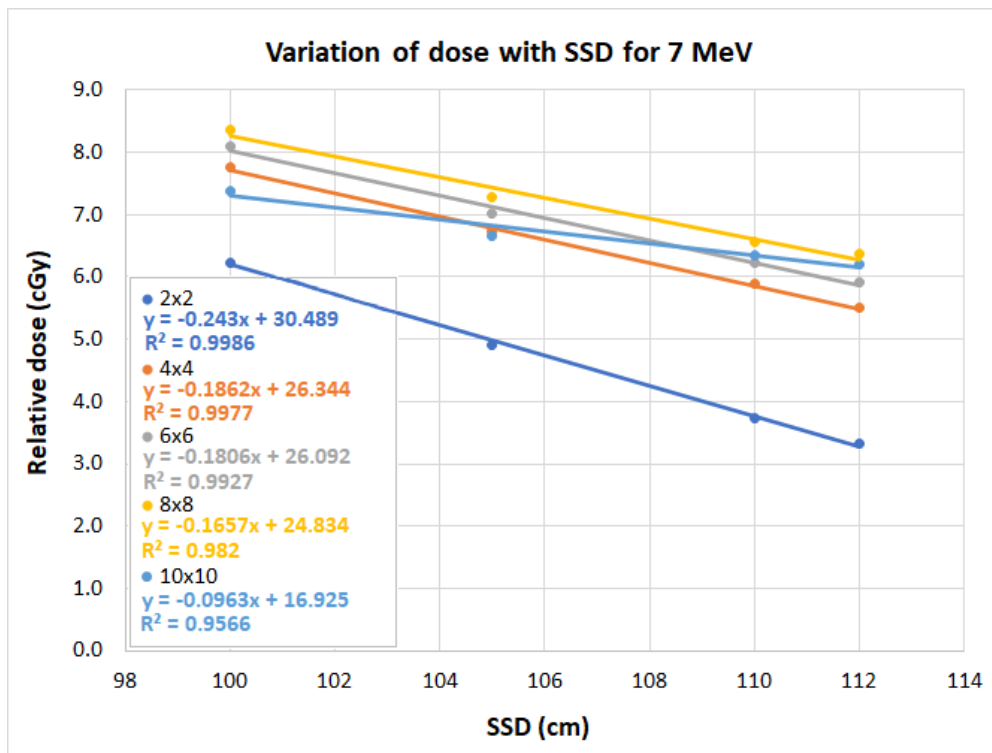

Figure 4.2 *Variation of dose with SSD for a 7 MeV electron beam.*
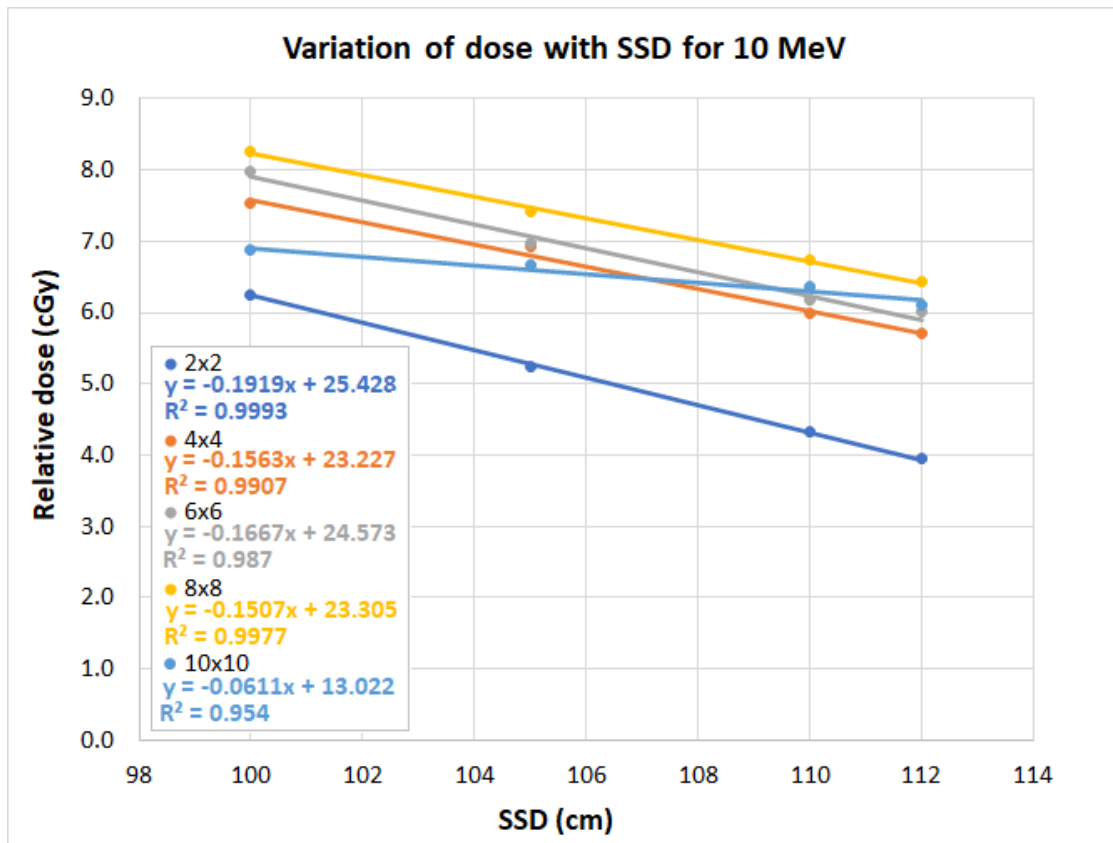
Figure 4.3 *Variation of dose with SSD for a 10 MeV electron beam.*
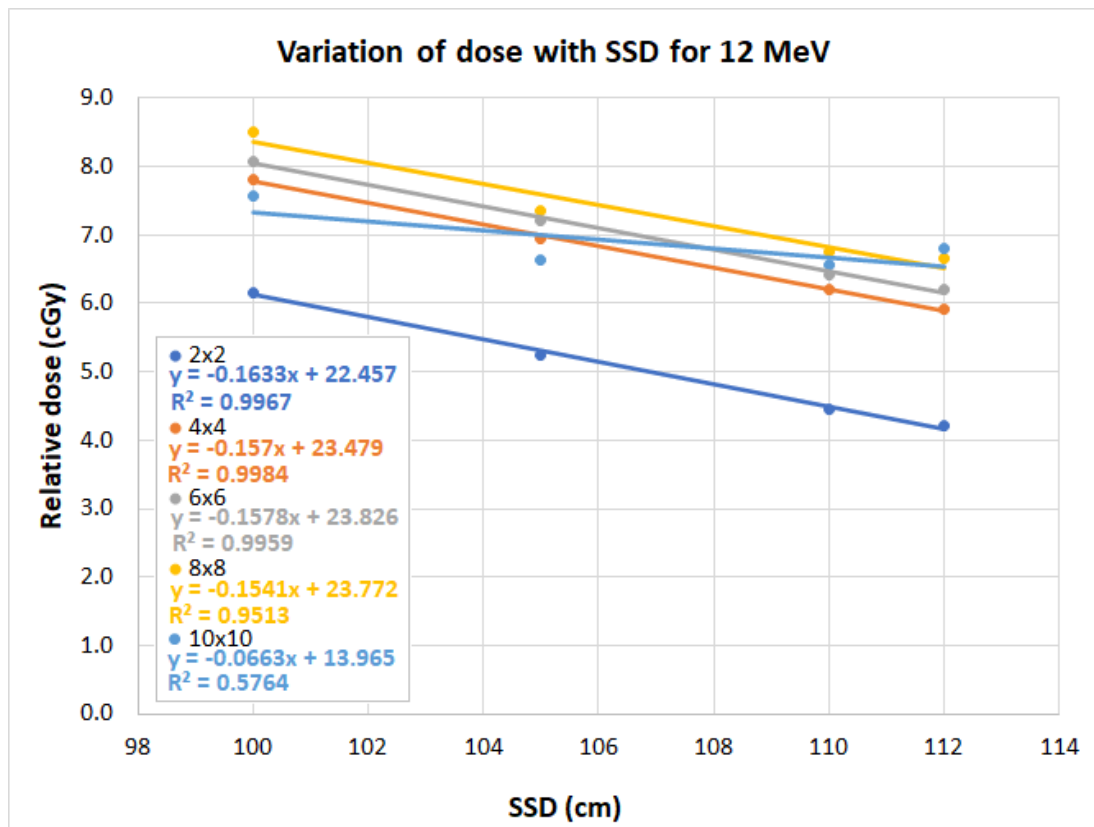
Figure 4.4 *Variation of dose with SSD for a 12 MeV electron beam.*

4.1.3 Beam Obliquity

Beam obliquity measurements were done at 100 cm SSD for beam energies 5, 10 and 14 MeV, for 2 × 2 cm, 4 × 4 cm, 6 × 6 cm, 8 × 8 cm and 10 × 10 cm field sizes, at gantry angles 0°, 15°, 30°, 45° and 60°. The depth dose measurements followed the gantry angle, and were in the direction of the beam axis, as indicated in Figure 4.5.
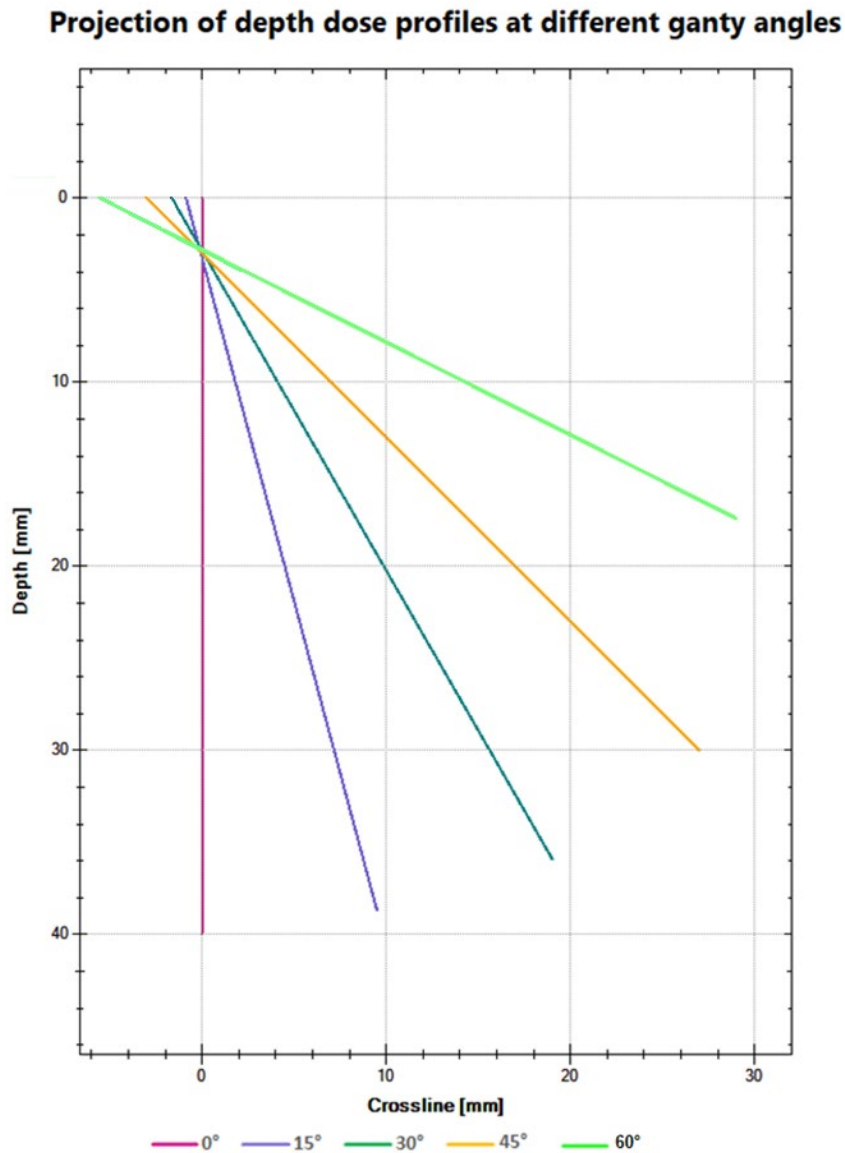
Figure 4.5 *Projection of depth dose measurements at different gantry angles.*

Figure 4.6 to Figure 4.11 shows the effect of beam obliquity for different field sizes and energies.

Figure 4.6 *Obliquity depth dose curves for (a) 5 MeV electron beam with 2 × 2 cm field size, (b) 10 MeV electron beam with 2 × 2 cm field size.*
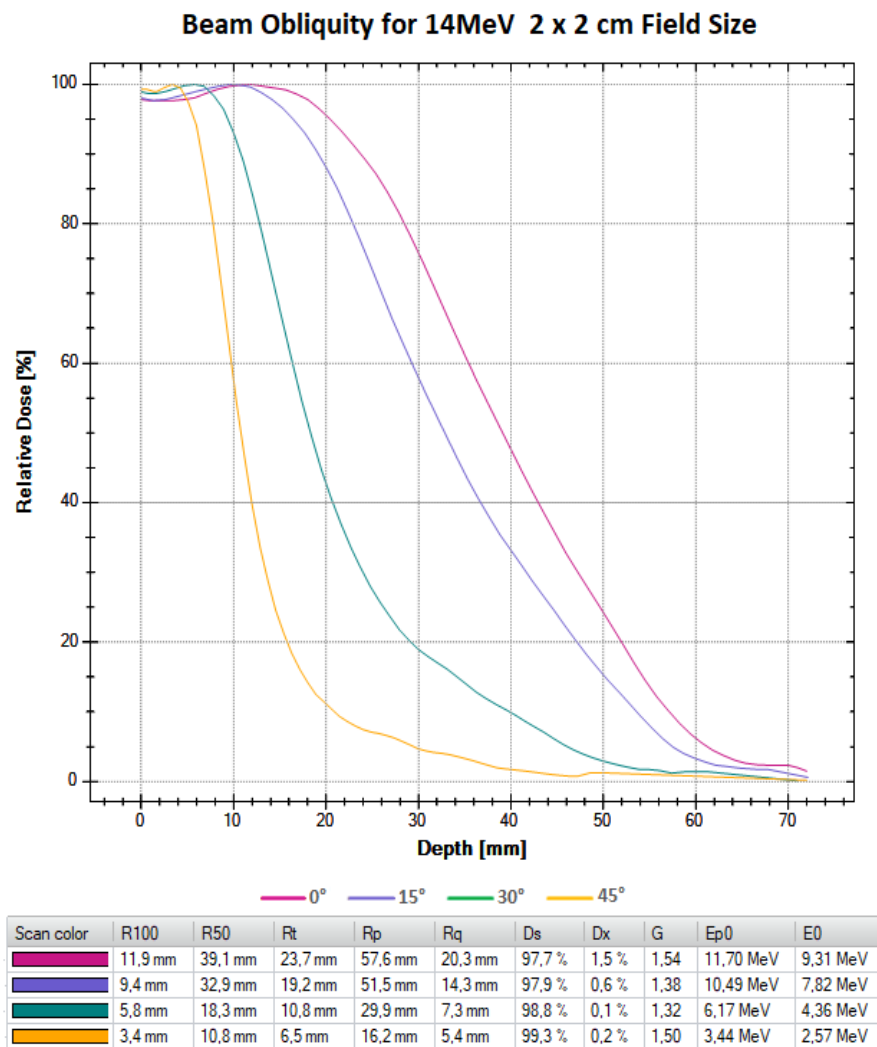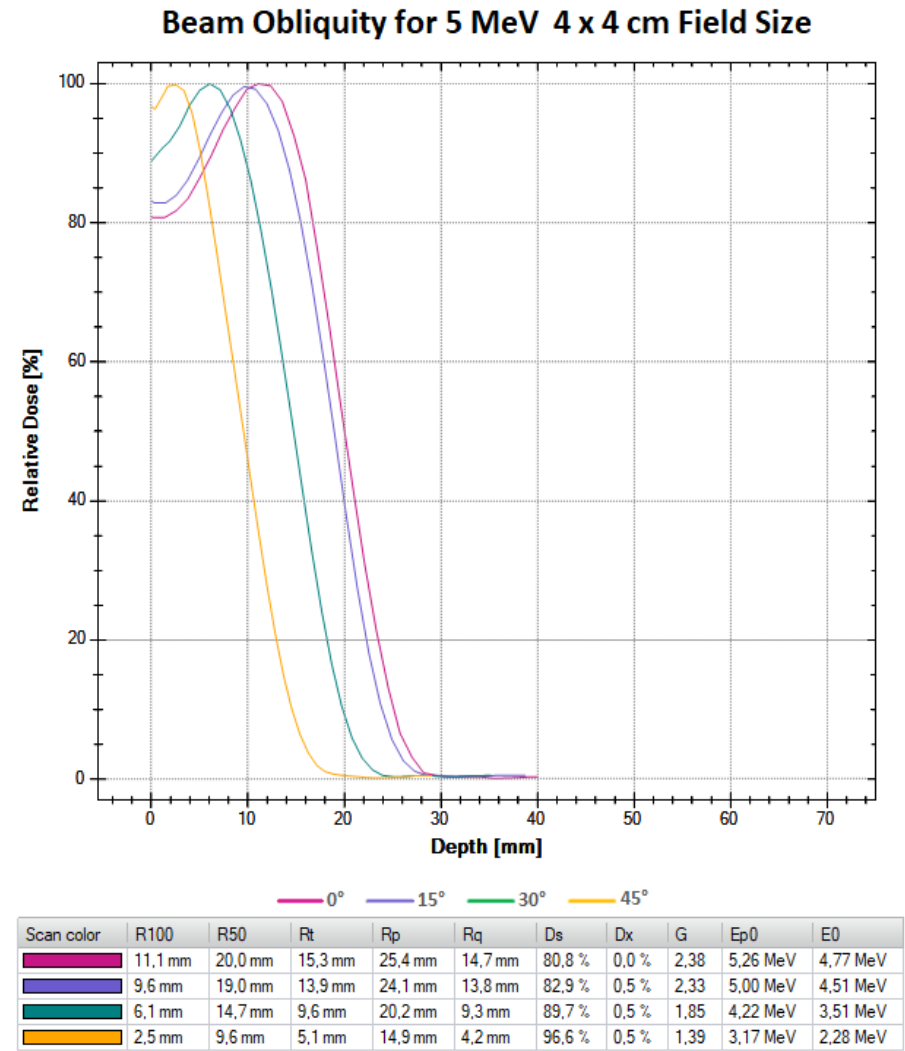
Figure 4.7 *Obliquity depth dose curves for (a) 14 MeV electron beam with a 2 × 2 cm field size, (b) 5 MeV electron beam with a 4 × 4 cm field size*

Beam Obliquity for 10 MeV 4 x 4 cm Field Size

Scan color	R100	R50	Rt	Rp	Rq	Ds	Dx	G	Ep0	E0
(pink) 0°	20,2 mm	38,8 mm	29,1 mm	48,4 mm	29,1 mm	89,7 %	0,0 %	2,50	9,87 MeV	9,23 MeV
(purple) 15°	16,1 mm	35,8 mm	25,2 mm	45,7 mm	25,5 mm	91,2 %	1,3 %	2,26	9,33 MeV	8,52 MeV
(teal) 30°	9,8 mm	26,9 mm	16,3 mm	38,7 mm	14,7 mm	93,3 %	1,1 %	1,61	7,93 MeV	6,41 MeV
(orange) 45°	5,1 mm	16,3 mm	9,0 mm	26,2 mm	6,3 mm	91,5 %	1,5 %	1,31	5,43 MeV	3,88 MeV

(a)

Beam Obliquity for 14 MeV 4 x 4 cm Field Size

Scan color	R100	R50	Rt	Rp	Rq	Ds	Dx	G	Ep0	E0
(pink) 0°	19,4 mm	48,5 mm	35,2 mm	61,0 mm	35,8 mm	94,6 %	0,5 %	2,43	12,38 MeV	11,55 MeV
(purple) 15°	15,2 mm	44,0 mm	28,9 mm	58,7 mm	29,2 mm	95,1 %	0,5 %	1,99	11,93 MeV	10,48 MeV
(teal) 30°	13,1 mm	32,6 mm	20,1 mm	49,4 mm	15,9 mm	-	0,2 %	1,47	10,07 MeV	7,76 MeV
(orange) 45°	5,6 mm	17,6 mm	10,0 mm	28,6 mm	7,0 mm	93,7 %	0,0 %	1,32	5,91 MeV	4,19 MeV

(b)

Figure 4.8 *Obliquity depth dose curves for (a) 10 MeV electron beam with 4 × 4 cm field size, (b) 14 MeV electron beam with 4 × 4 cm field size.*
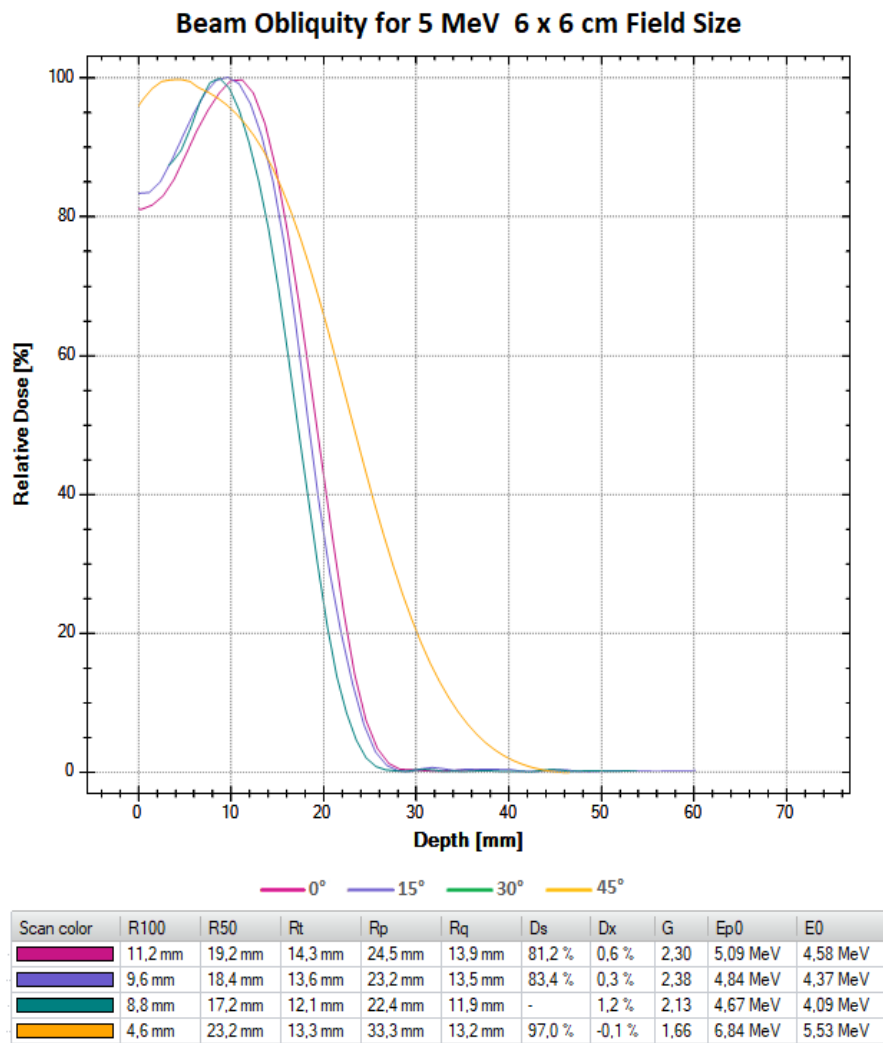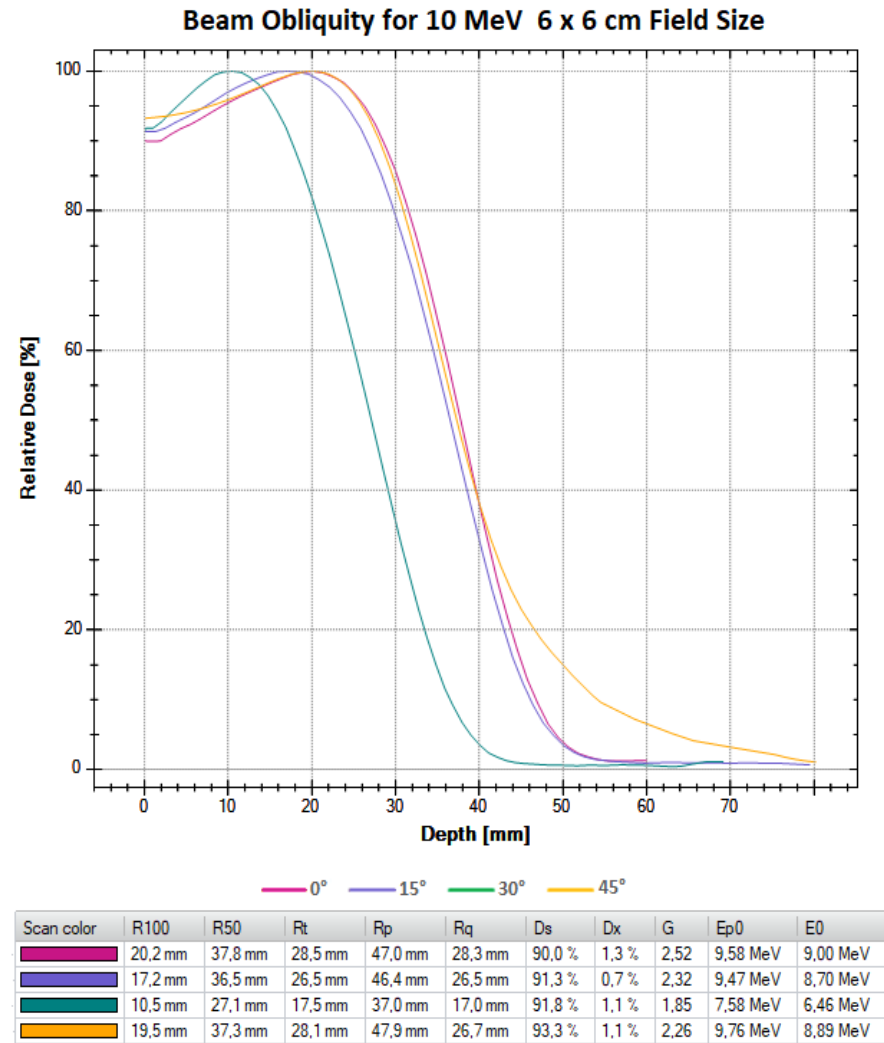
Figure 4.9 *Obliquity depth dose curves for (a) 5 MeV electron beam with 6 × 6 cm field size, (b) 10 MeV electron beam with 6 × 6 cm field size.*

Beam Obliquity for 14 MeV 6 x 6 cm Field Size

Legend: 0° | 15° | 30° | 45°

Scan color	R100	R50	Rt	Rp	Rq	Ds	Dx	G	Ep0	E0
	21,7 mm	48,5 mm	36,5 mm	59,5 mm	37,0 mm	94,8 %	1,9 %	2,64	12,10 MeV	11,56 MeV
	19,1 mm	46,5 mm	32,5 mm	58,9 mm	33,4 mm	95,0 %	1,8 %	2,31	11,98 MeV	11,06 MeV
	12,4 mm	34,6 mm	21,8 mm	48,0 mm	20,9 mm	94,9 %	0,8 %	1,77	9,78 MeV	8,24 MeV
	19,2 mm	36,6 mm	27,9 mm	46,5 mm	26,6 mm	90,5 %	1,3 %	2,34	9,47 MeV	8,71 MeV

(a)

Beam Obliquity for 5 MeV 8 x 8 cm Field Size

Legend: 0° | 15° | 30° | 45° | 60°

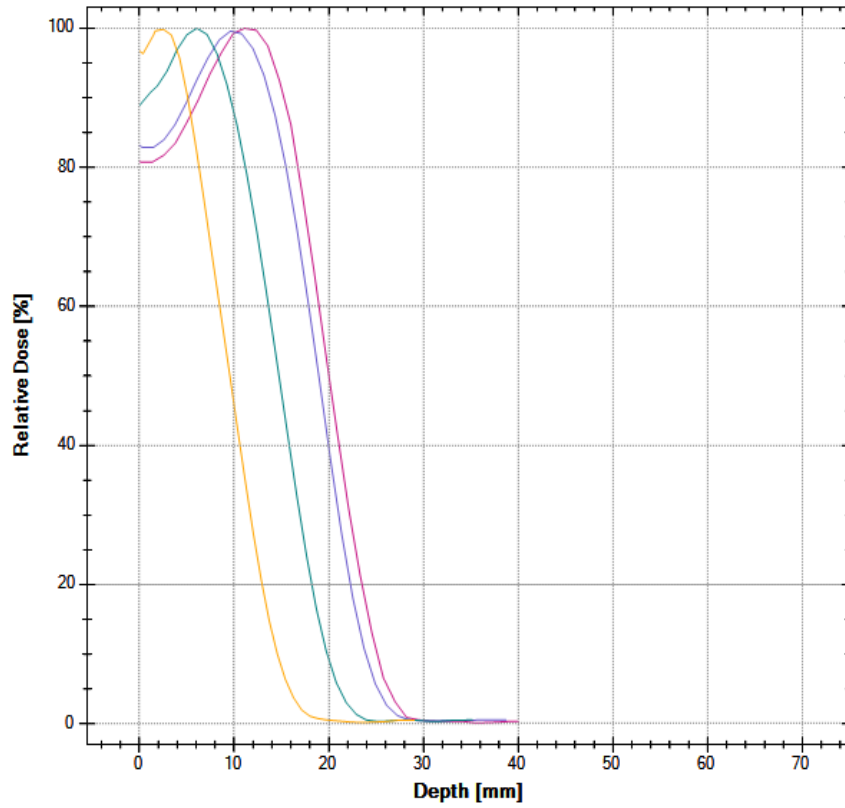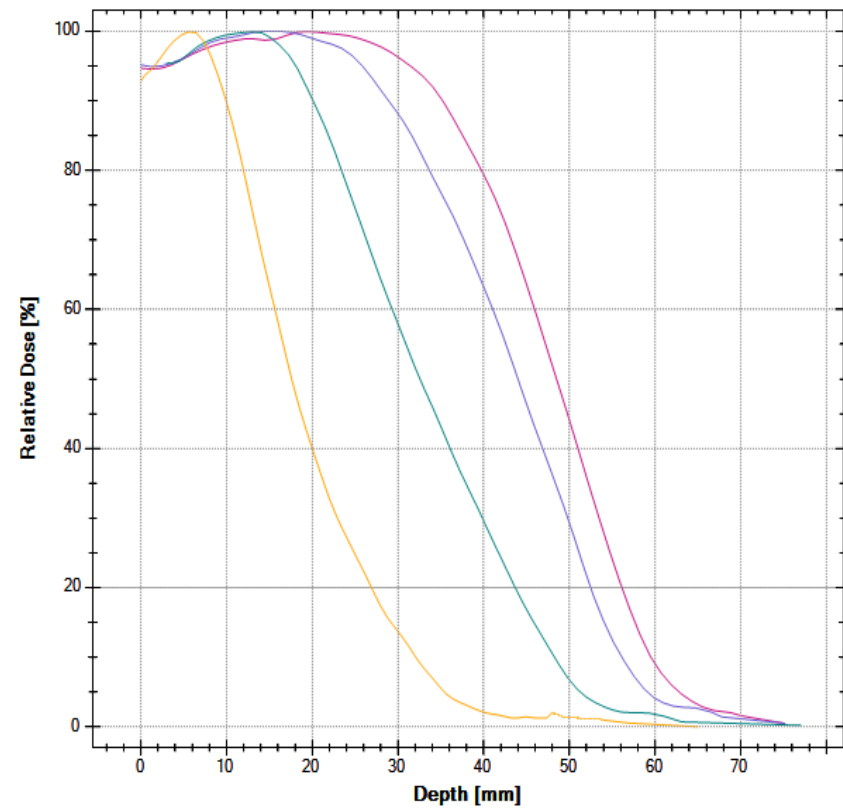| Scan color	R100	R50	Rt	Rp	Rq	Ds	Dx	G	Ep0
	12,0 mm	20.2 mm	15,2 mm	25,8 mm	14,6 mm	77,5 %	0,1 %	2,30	5,35 MeV
	9,9 mm	19.4 mm	14,3 mm	25,6 mm	13,6 mm	81,0 %	0,1 %	2,13	5,30 MeV
	7,5 mm	19.2 mm	12,1 mm	26,8 mm	12,0 mm	85,2 %	0,1 %	1,81	5,55 MeV
	5,0 mm	17.4 mm	9,3 mm	29,1 mm	7,6 mm	82,1 %	0,1 %	1,35	6,01 MeV
	2,0 mm	15.1 mm	6,3 mm	30,2 mm	1,8 mm	93,8 %	0,1 %	1,06	6,22 MeV

(b)

Figure 4.10 *Obliquity depth dose curves for 14 MeV electron beam with a 6 × 6 cm field size, (b) 5 MeV electron beam with 8 × 8 cm field size.*

Figure 4.11 *Obliquity depth dose curves for (a) 10 MeV electron beam with 8 × 8 cm field size, (b) 14 MeV electron beam with 8 × 8 cm field size.*

4.1.4 Effect of primary jaw field size on beam collimation

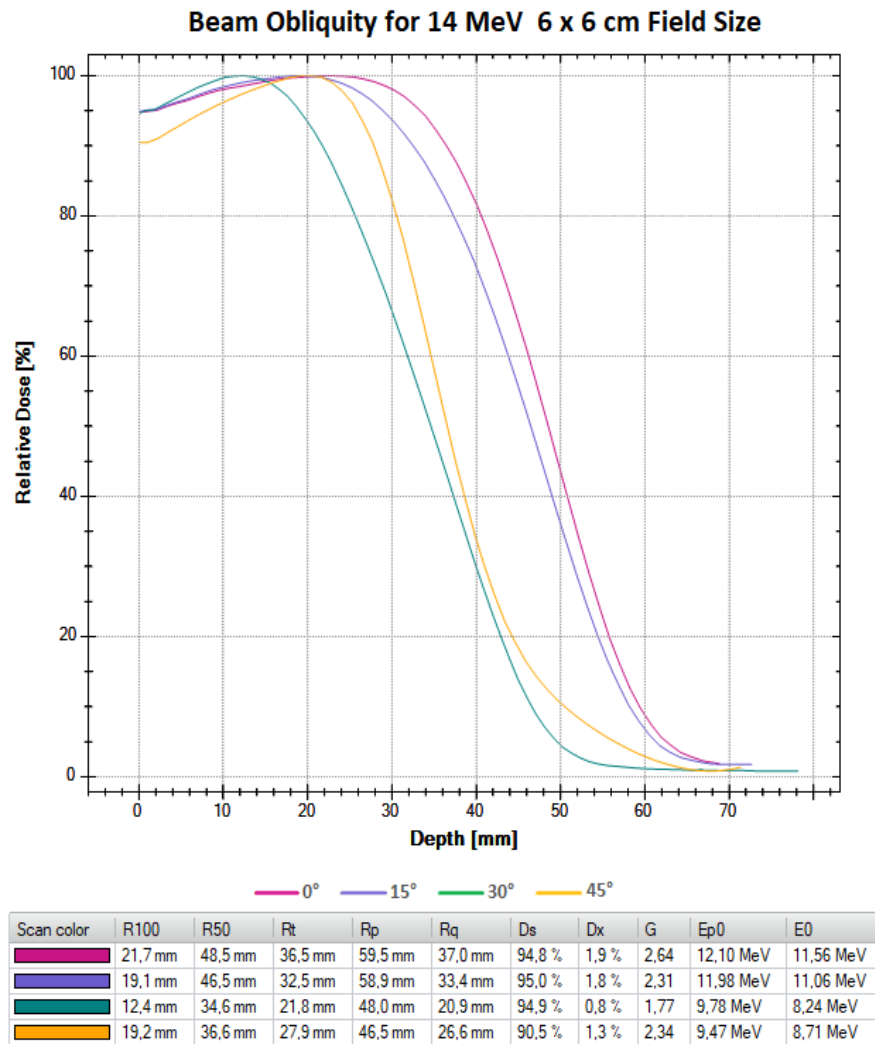The scatter from the photon collimator has a bearing on the profile of the electron beam. Measurements were conducted to determine the effect of the jaw field size as set by the primary jaws on the electron beam. Measurements were done for 10 × 10 cm, 15 × 15 cm, with the default setting of 19 × 19 cm and 22 × 22 cm primary jaw field sizes, for the lowest electron beam energy of 5 MeV, middle-range energy of 10 MeV and the highest available energy of 14 MeV. The applicator sizes were 2 × 2 cm, 4 × 4 cm, 6 × 6 cm and 8 × 8 cm field size. The results are shown in Figure 4.12 to Figure 4.35, with the normalized and unnormalized graphs for the various electron beam energies, jaw setting and collimator device settings.
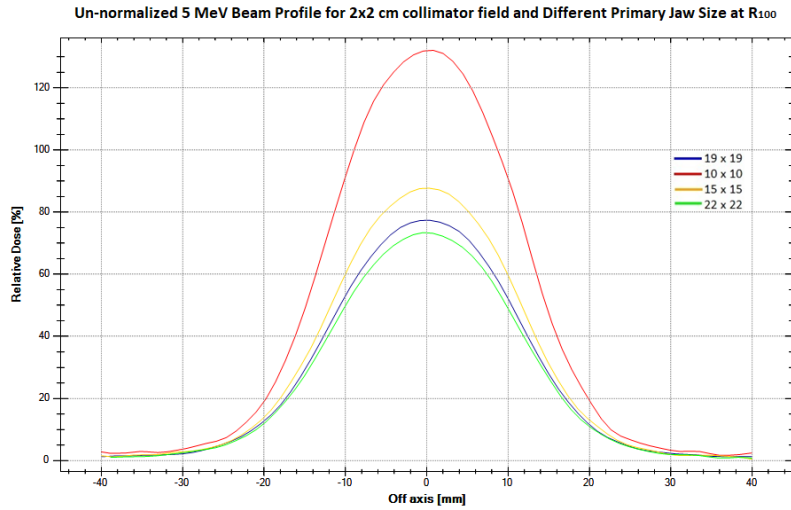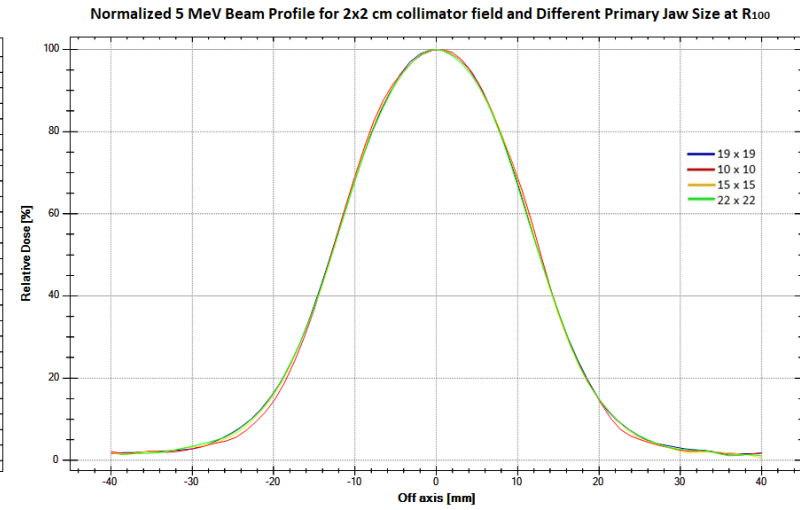
Figure 4.12 *Beam Profiles of 5 MeV electron beam for 2 × 2 cm field size at a depth of R_{100} for different primary jaw field settings. (a) Unnormalized (b) Normalized*

Figure 4.13 *Beam Profiles of 5 MeV electron beam for 2 × 2 cm field size at a depth of R_{90} for different primary jaw field settings. (a) Unnormalized (b) Normalized*

Figure 4.14 *Beam Profiles of 5 MeV electron beam for 2 × 2 cm field size at a depth of R_{50} for different primary jaw field settings. (a) Unnormalized (b) Normalized*

Figure 4.15 *Beam Profiles of 5 MeV electron beam for 4 × 4 cm field size at a depth of R_{100} for different primary jaw field settings. (a) Unnormalized (b) Normalized*

Figure 4.16 *Beam Profiles of 5 MeV electron beam for 4 × 4 cm field size at a depth of R_{90} for different primary jaw field settings. (a) Unnormalized (b) Normalized*
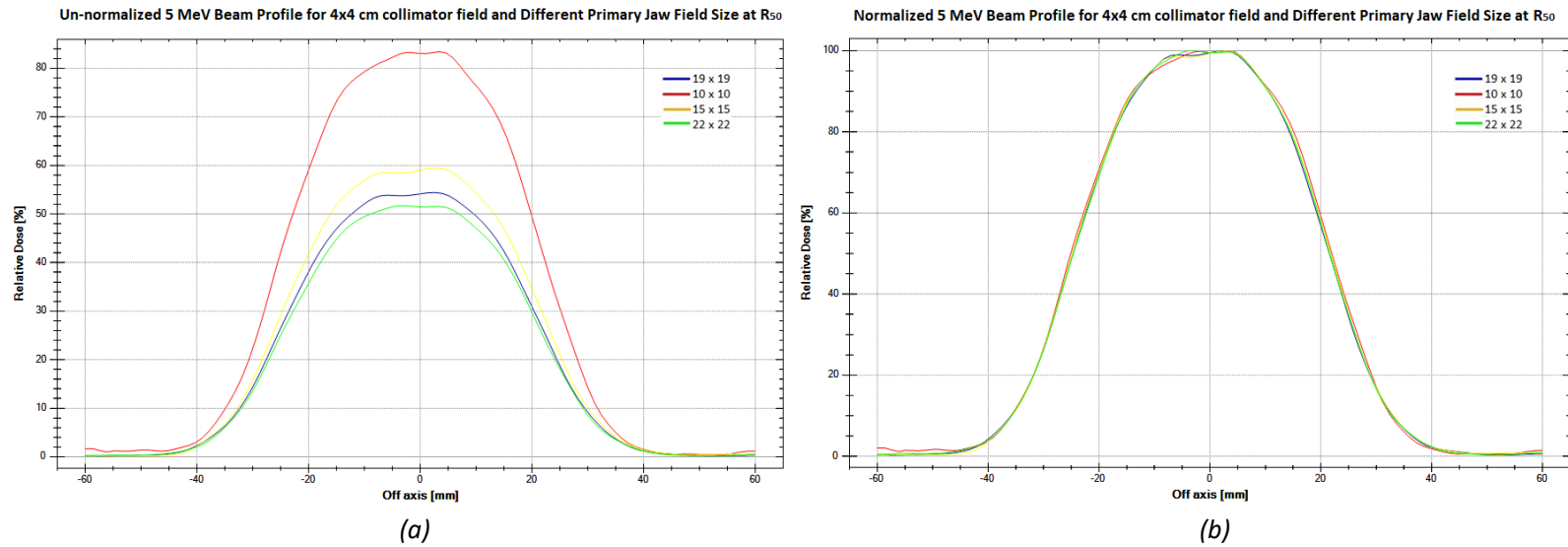
Figure 4.17 *Beam Profiles of 5 MeV electron beam for 4 × 4 cm field size at a depth of R_{50} for different primary jaw field settings. (a) Unnormalized (b) Normalized*
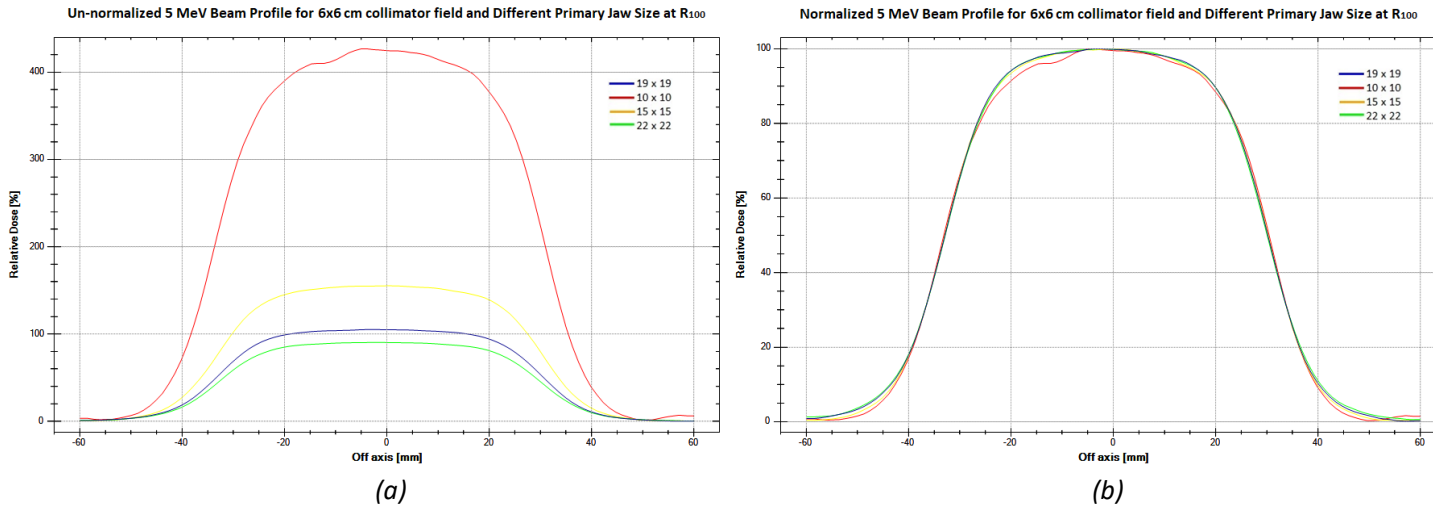
Figure 4.18 *Beam Profiles of 5 MeV electron beam for 6 × 6 cm field size at a depth of R_{100} for different primary jaw field settings. (a) Unnormalized (b) Normalized*
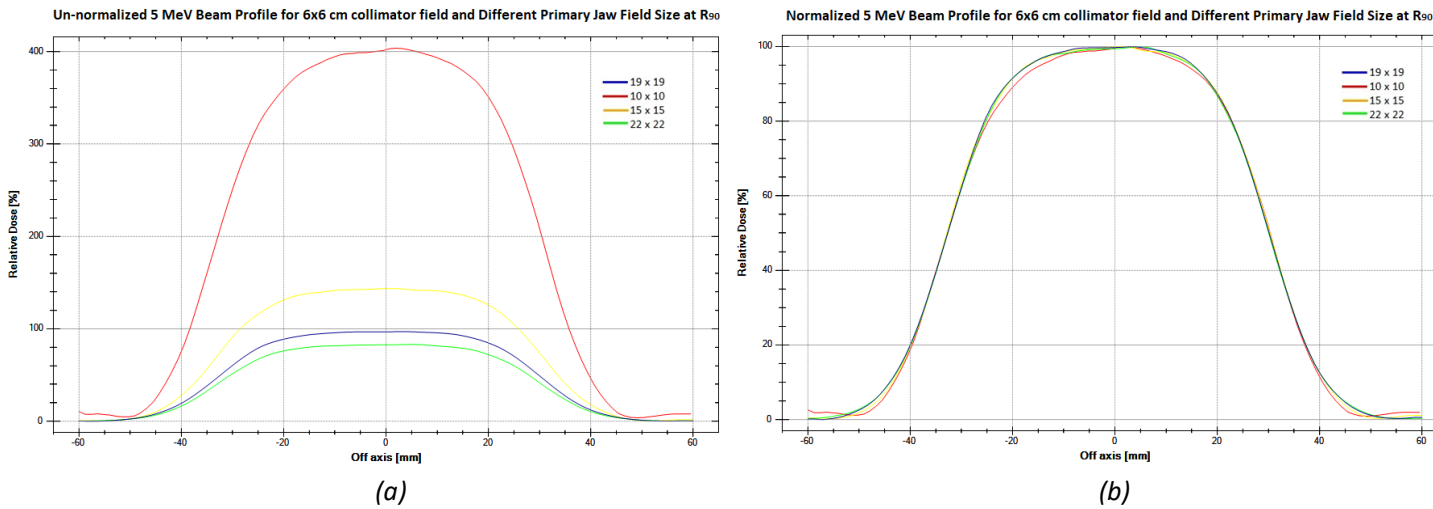
Figure 4.19 *Beam Profiles of 5 MeV electron beam for 6 × 6 cm field size at a depth of R_{90} for different primary jaw field settings. (a) Unnormalized (b) Normalized*
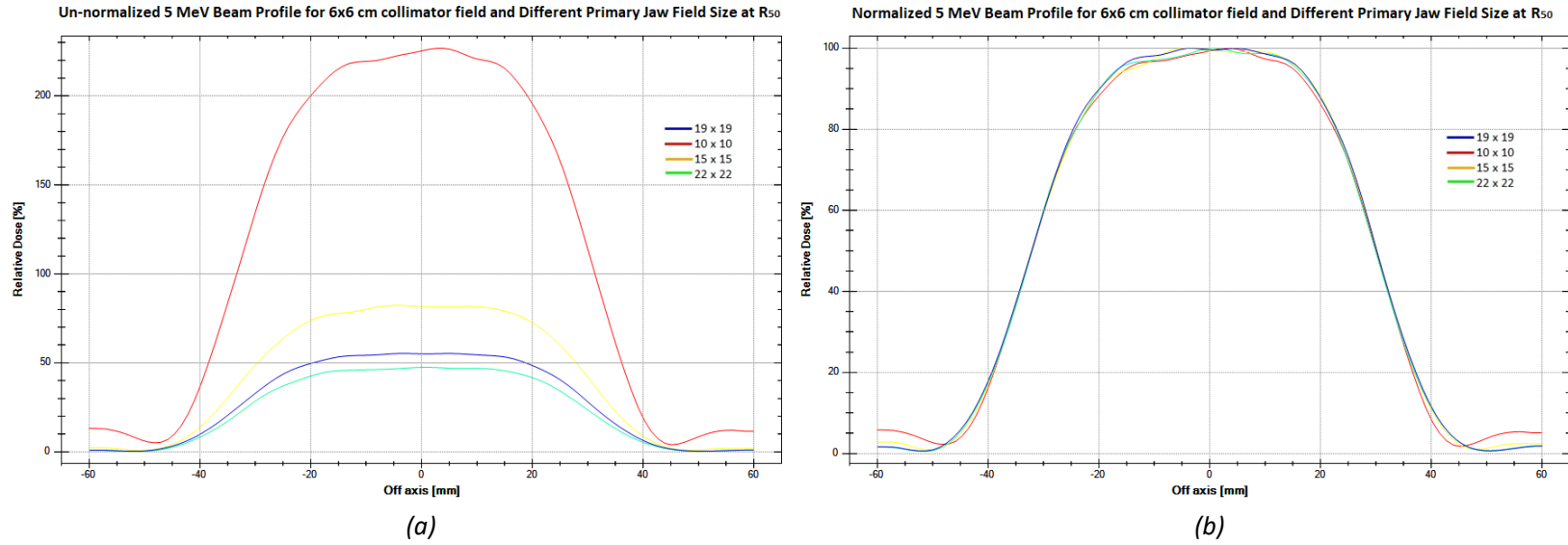
Figure 4.20 *Beam Profiles of 5 MeV electron beam for 6 × 6 cm field size at a depth of R_{50} for different primary jaw field settings. (a) Unnormalized (b) Normalized*
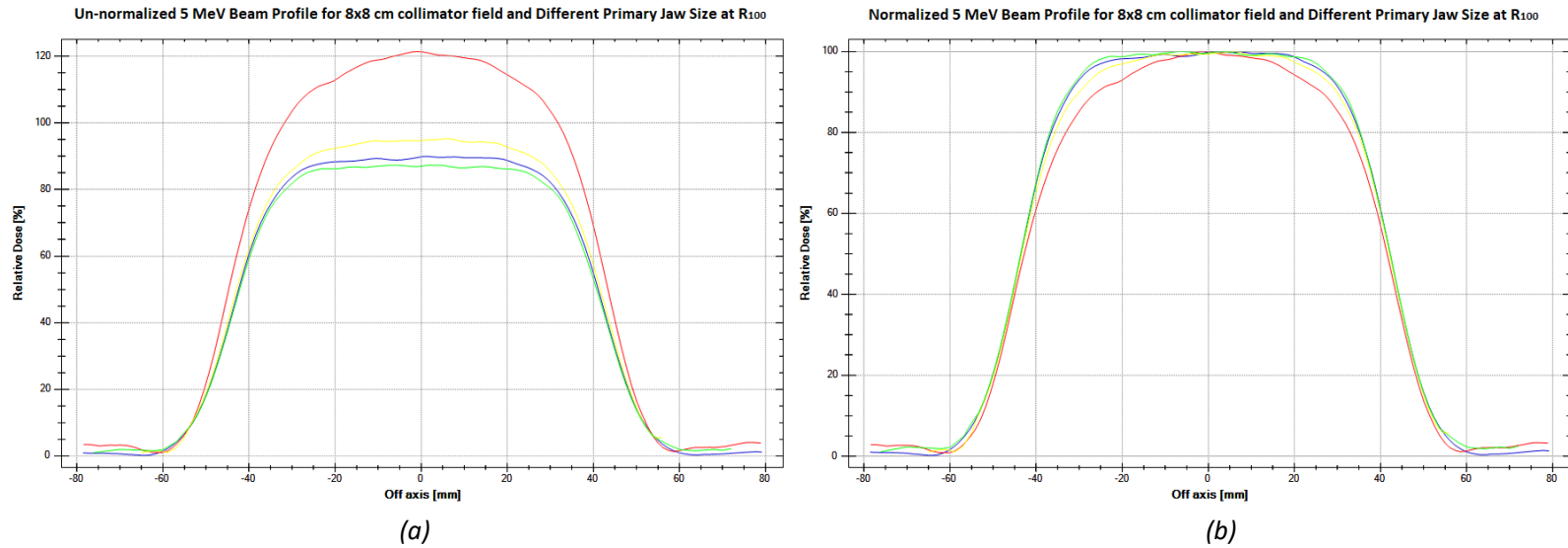
Figure 4.21 *Beam Profiles of 5 MeV electron beam for 8 × 8 cm field size at a depth of R_{100} for different primary jaw field settings. (a) Unnormalized (b) Normalized*
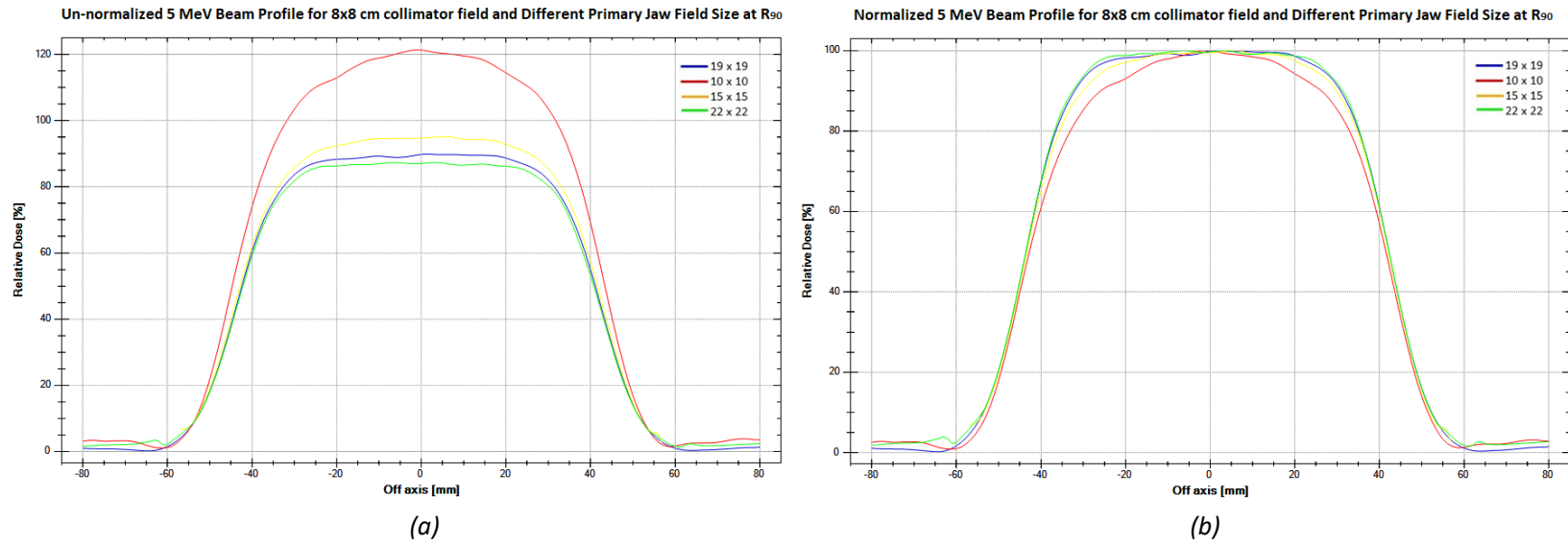
Figure 4.22 *Beam Profiles of 5 MeV electron beam for 8 × 8 cm field size at a depth of R_{90} for different primary jaw field settings. (a) Unnormalized (b) Normalized*
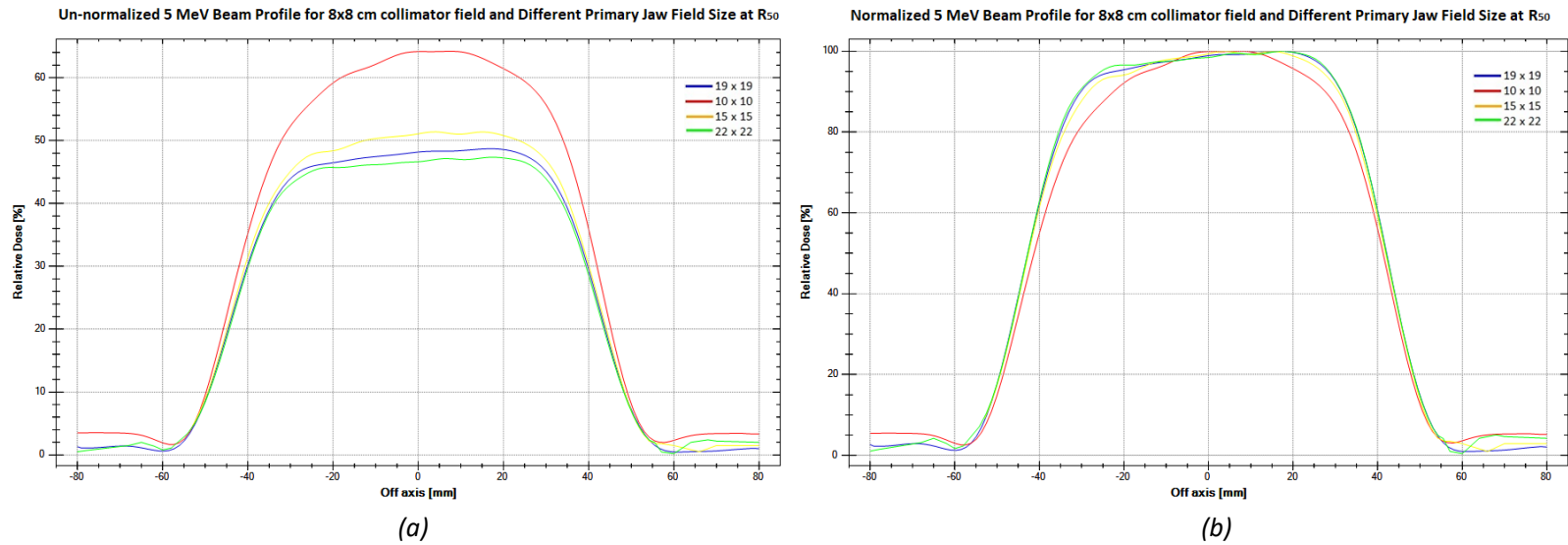
Figure 4.23 *Beam Profiles of 5 MeV electron beam for 8 × 8 cm field size at a depth of R_{50} for different primary jaw field settings. (a) Unnormalized (b) Normalized*
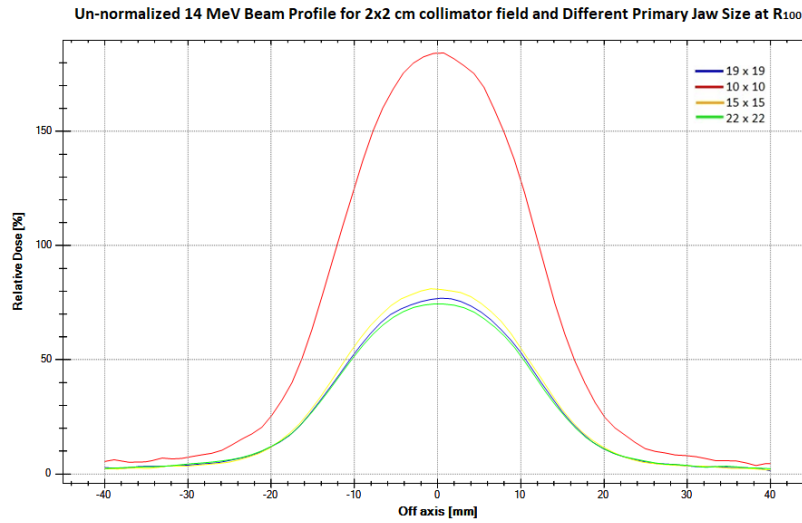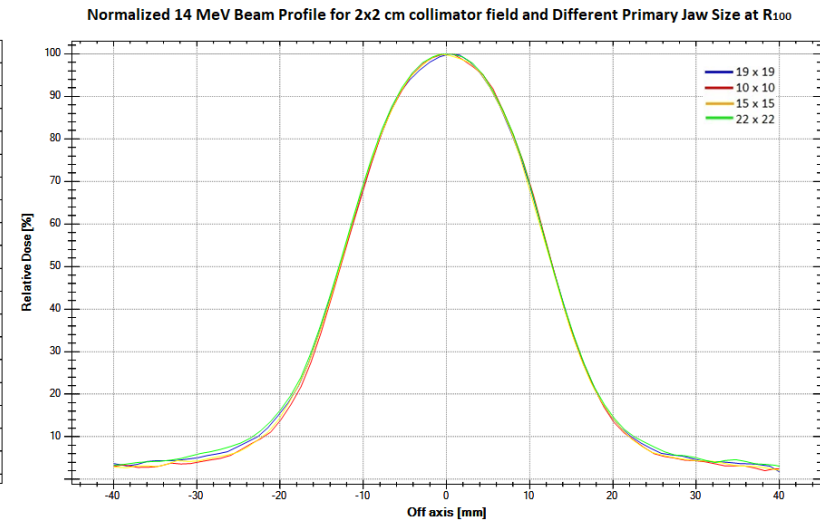
Figure 4.24 *Beam Profiles of 14 MeV electron beam for 2 × 2 cm field size at a depth of R_{100} for different primary jaw field settings. (a) Unnormalized (b) Normalized*
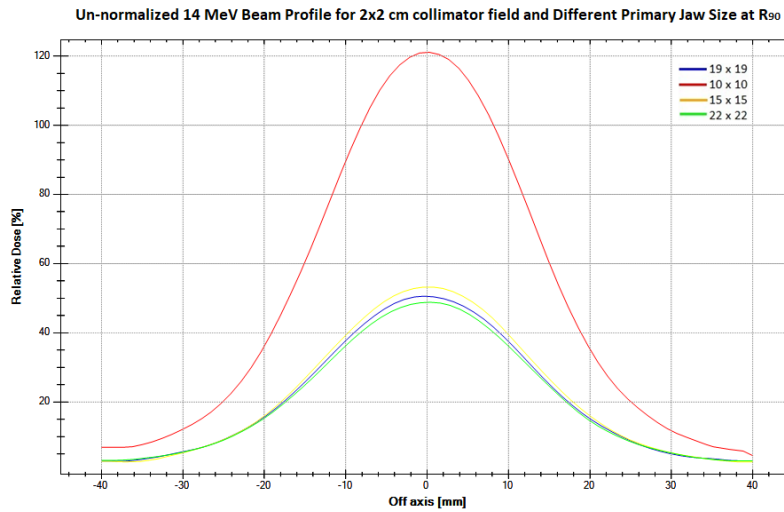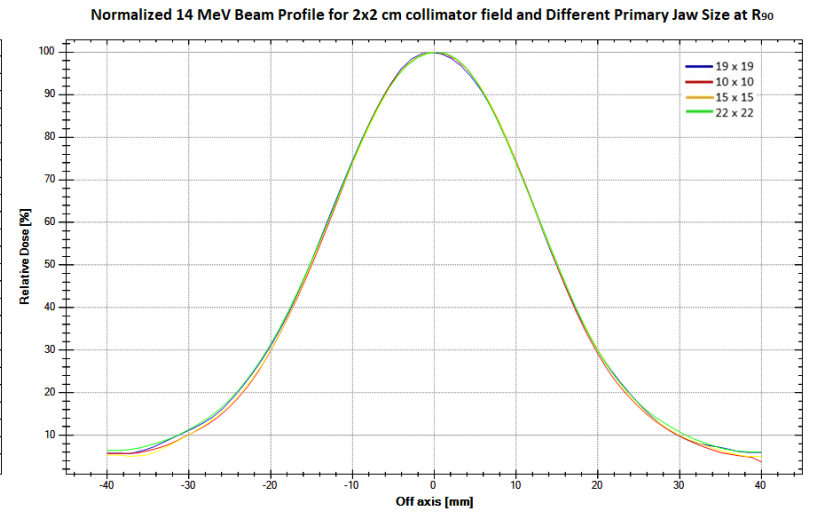
Figure 4.25 *Beam Profiles of 14 MeV electron beam for 2 × 2 cm field size at a depth of R_{90} for different primary jaw field settings. (a) Unnormalized (b) Normalized*
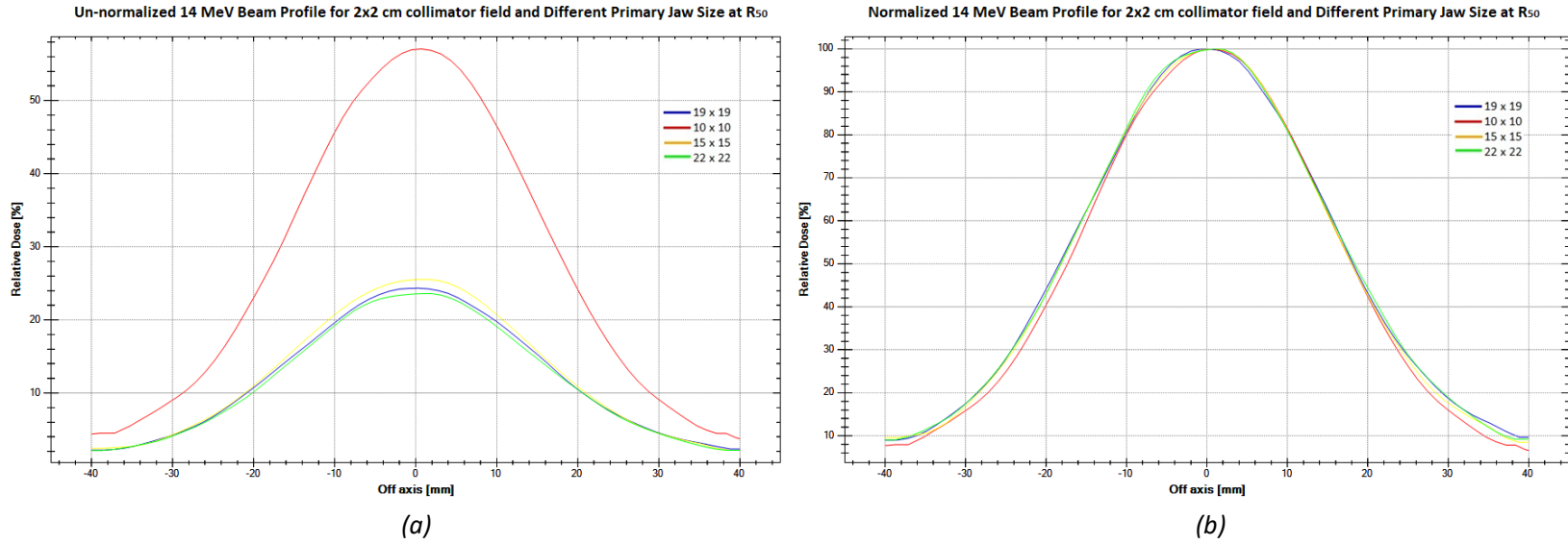
Figure 4.26 *Beam Profiles of 14 MeV electron beam for 2 × 2 cm field size at a depth of R_{50} for different primary jaw field settings. (a) Unnormalized (b) Normalized*
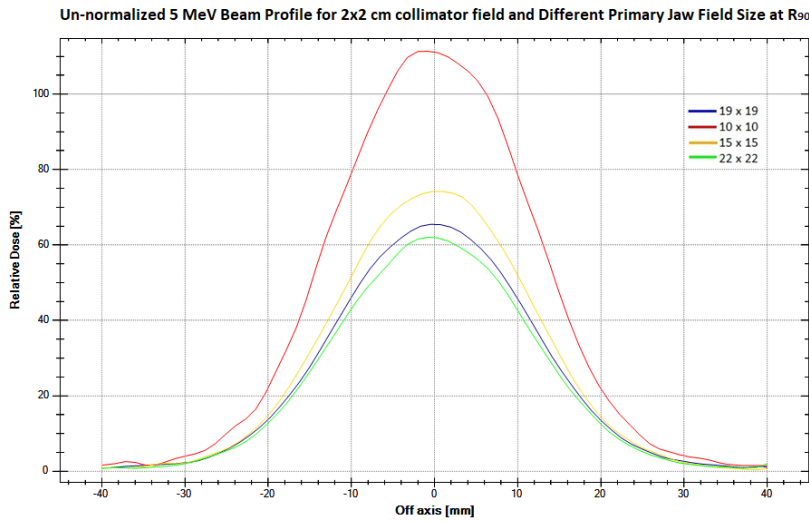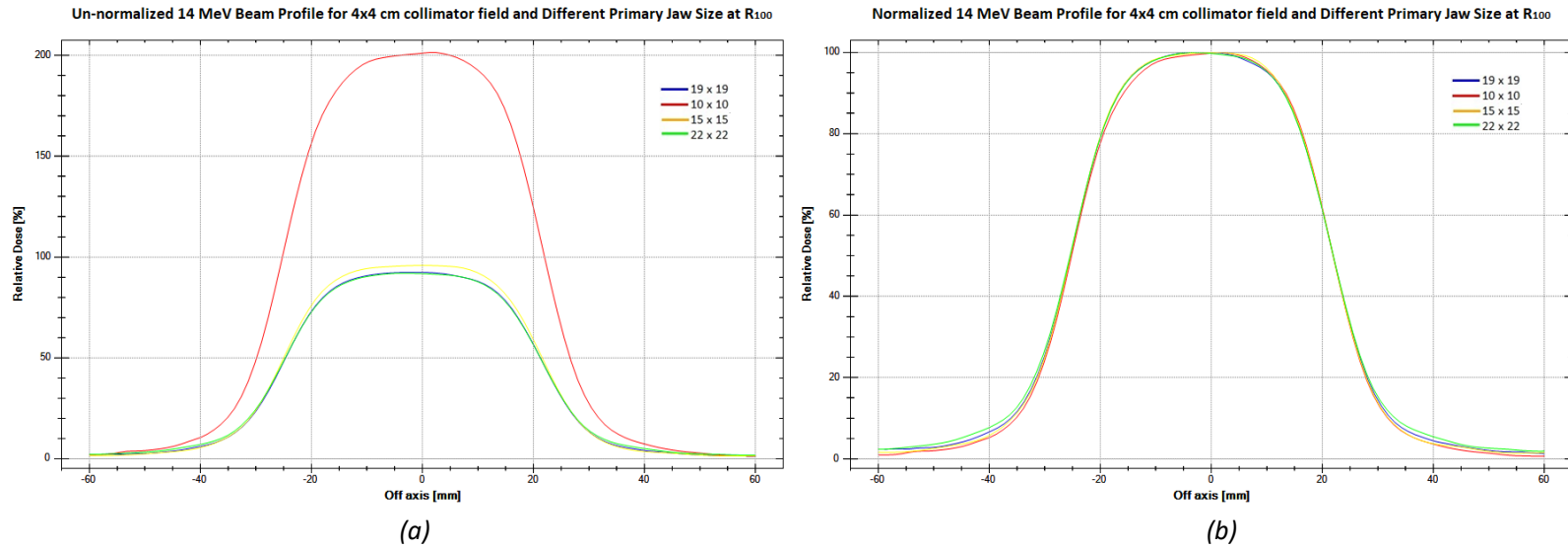

Figure 4.27 *Beam Profiles of 14 MeV electron beam for 4 × 4 cm field size at a depth of R_{100} for different primary jaw field settings. (a) Unnormalized (b) Normalized*
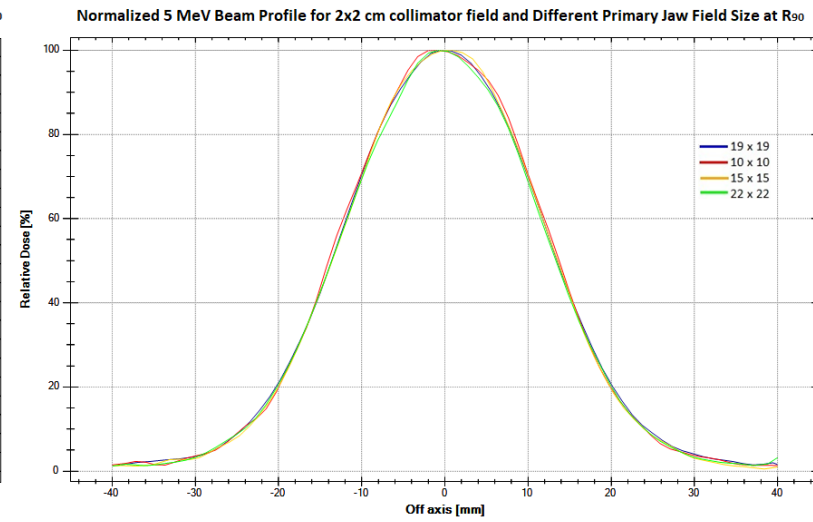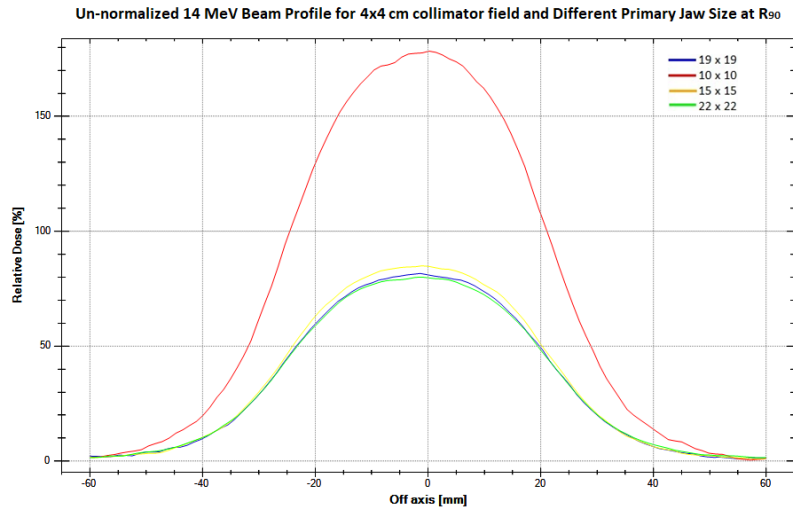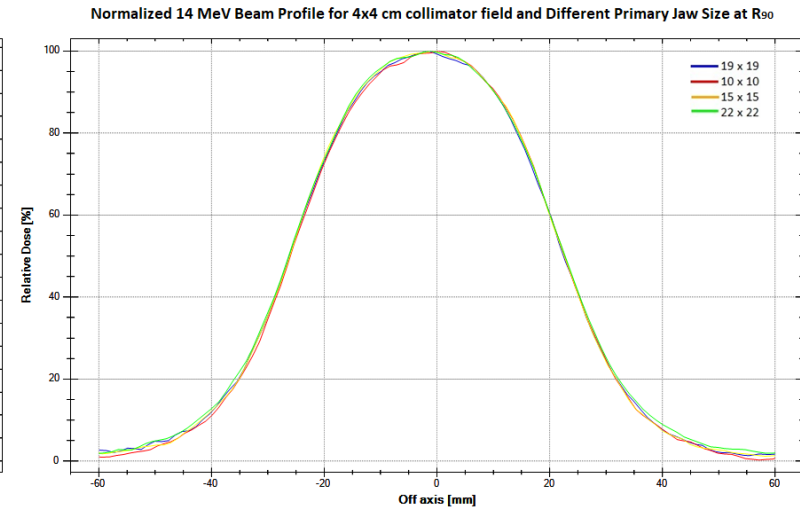
Figure 4.28 *Beam Profiles of 14 MeV electron beam for 4 × 4 cm field size at a depth of R_{90} for different primary jaw field settings. (a) Unnormalized (b) Normalized*
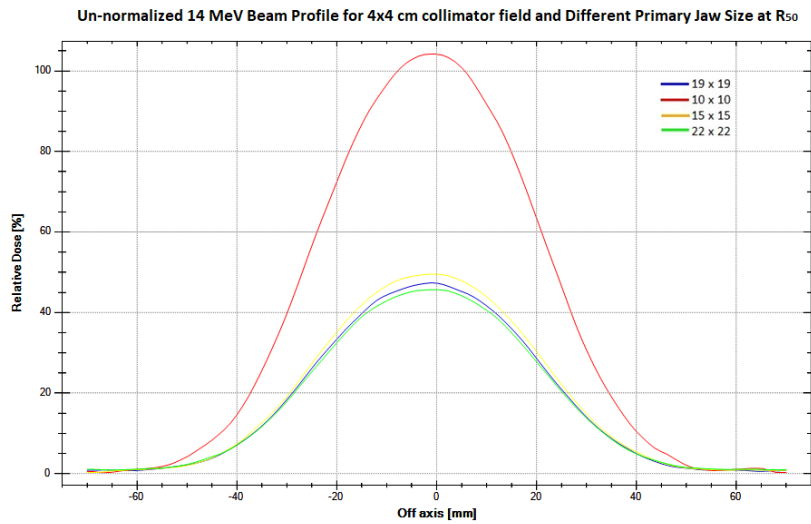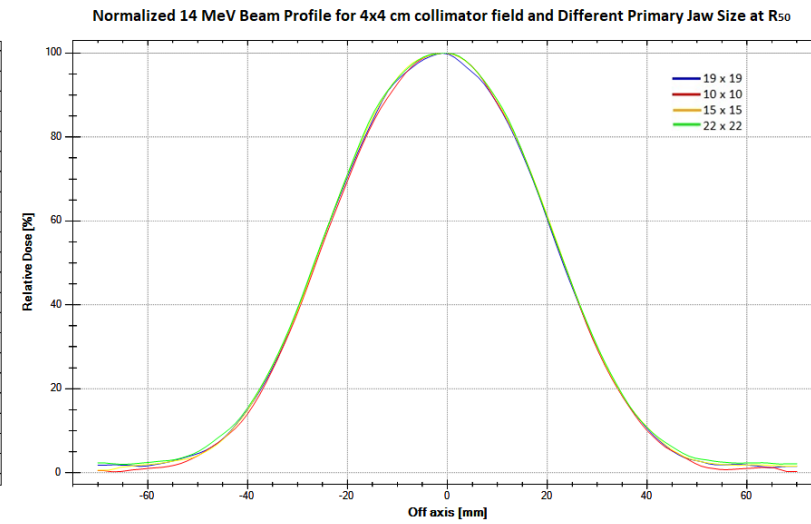
Figure 4.29 *Beam Profiles of 14 MeV electron beam for 4 × 4 cm field size at a depth of R_{50} for different primary jaw field settings. (a) Unnormalized (b) Normalized*
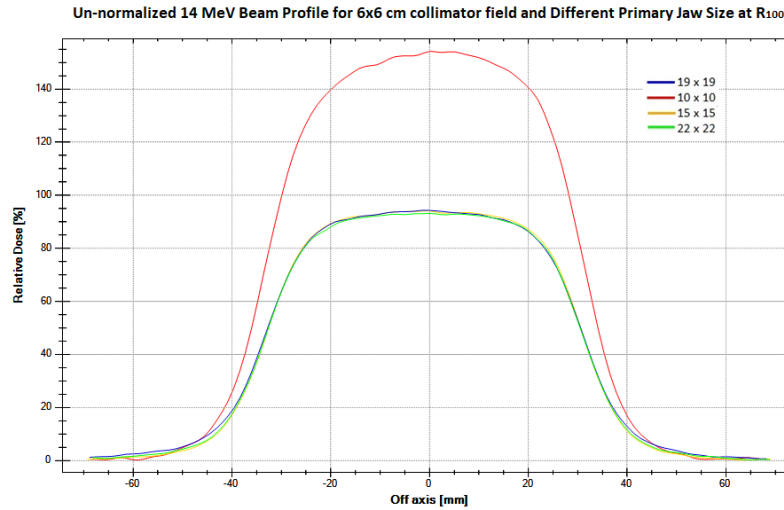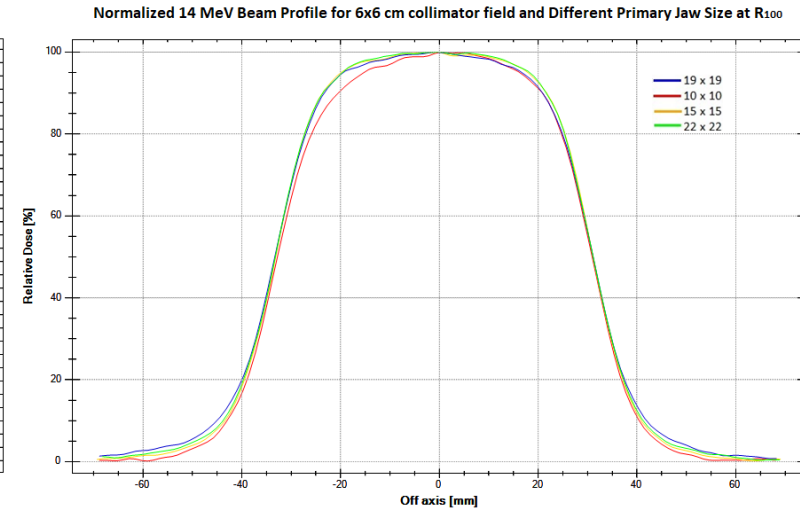
Figure 4.30 *Beam Profiles of 14 MeV electron beam for 6 × 6 cm field size at a depth of R_{100} for different primary jaw field settings. (a) Unnormalized (b) Normalized*
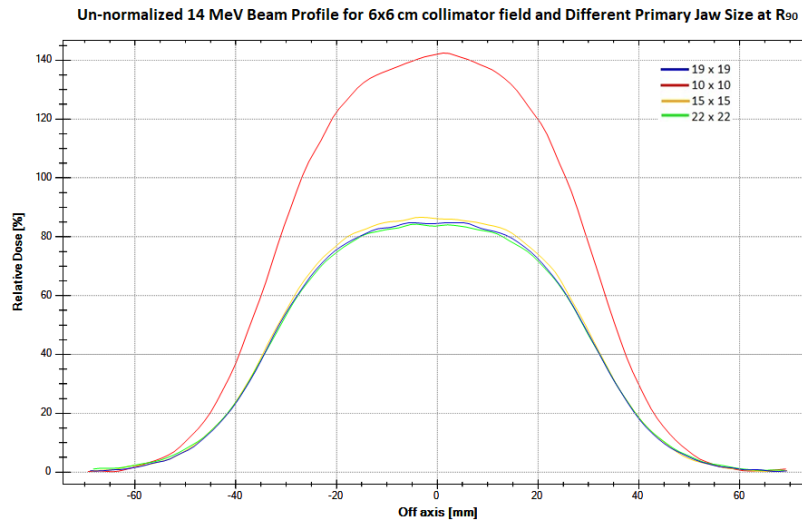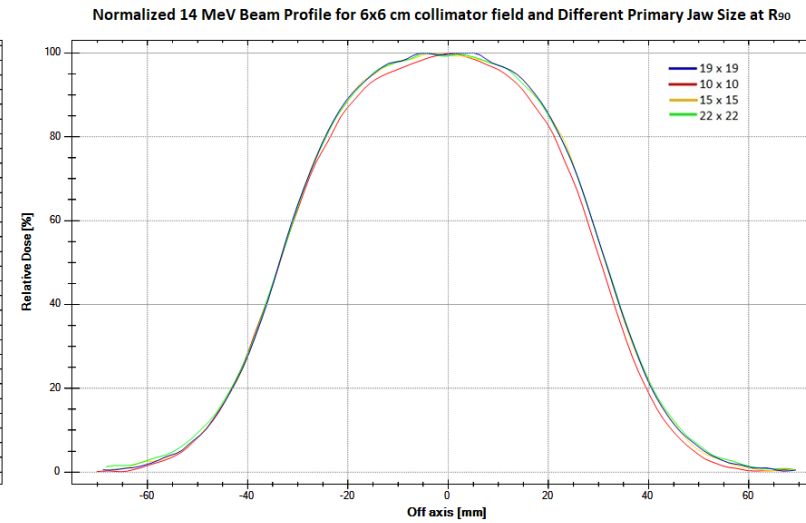
Figure 4.31 *Beam Profiles of 14 MeV electron beam for 6 × 6 cm field size at a depth of R_{90} for different primary jaw field settings. (a) Unnormalized (b) Normalized*
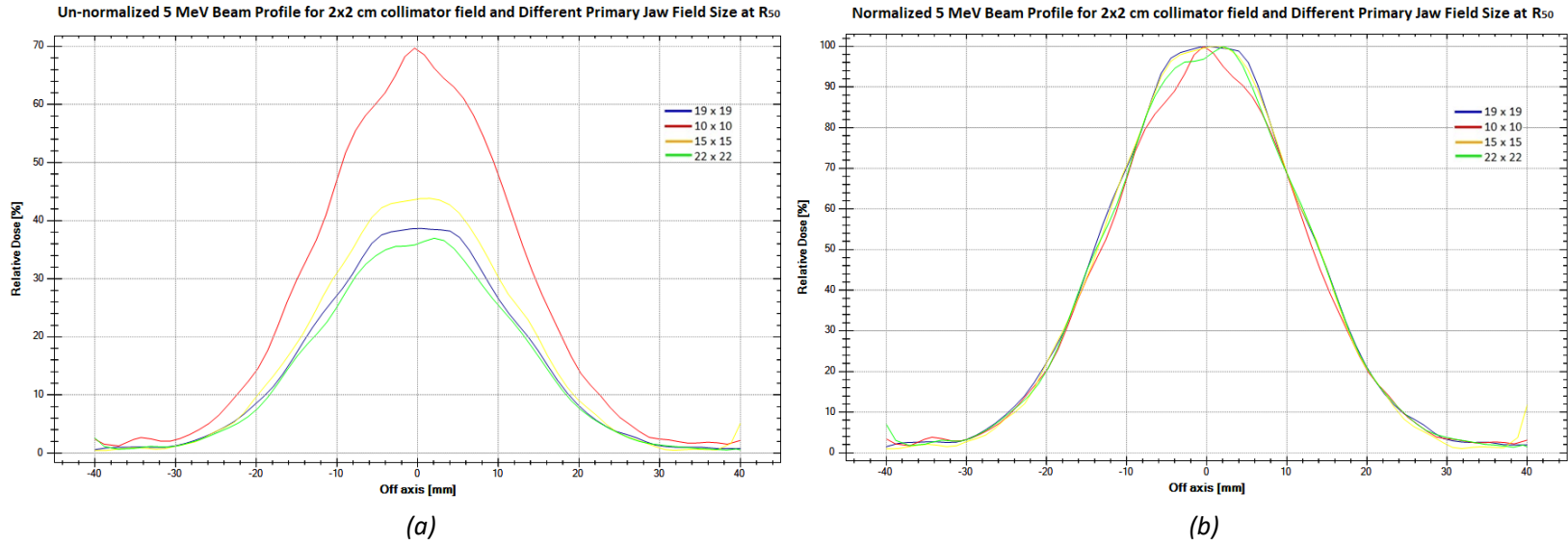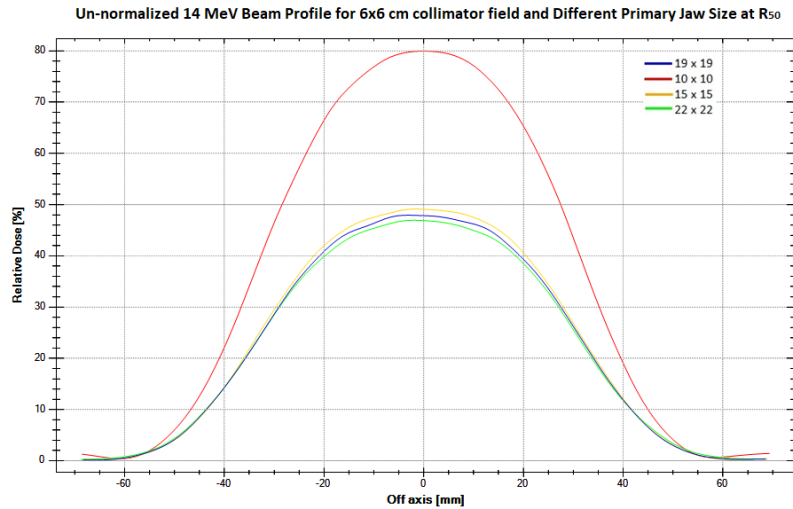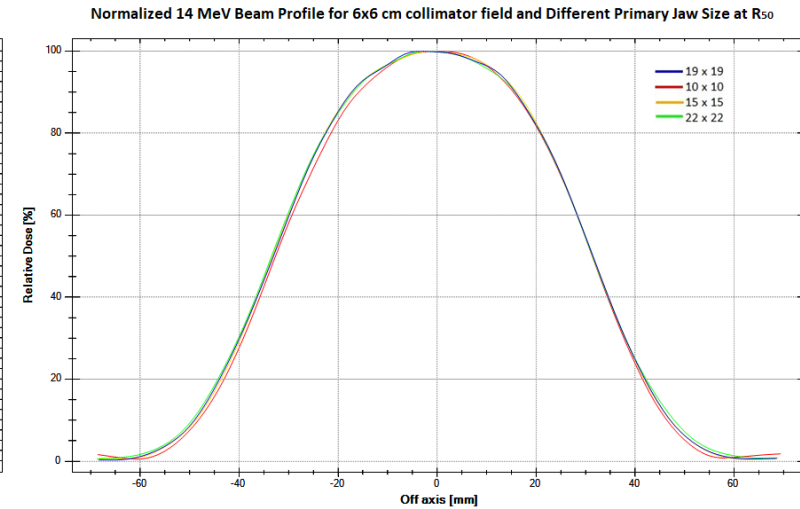
Figure 4.32 *Beam Profiles of 14 MeV electron beam for 6 × 6 cm field size at a depth of R_{50} for different primary jaw field settings. (a) Unnormalized (b) Normalized*
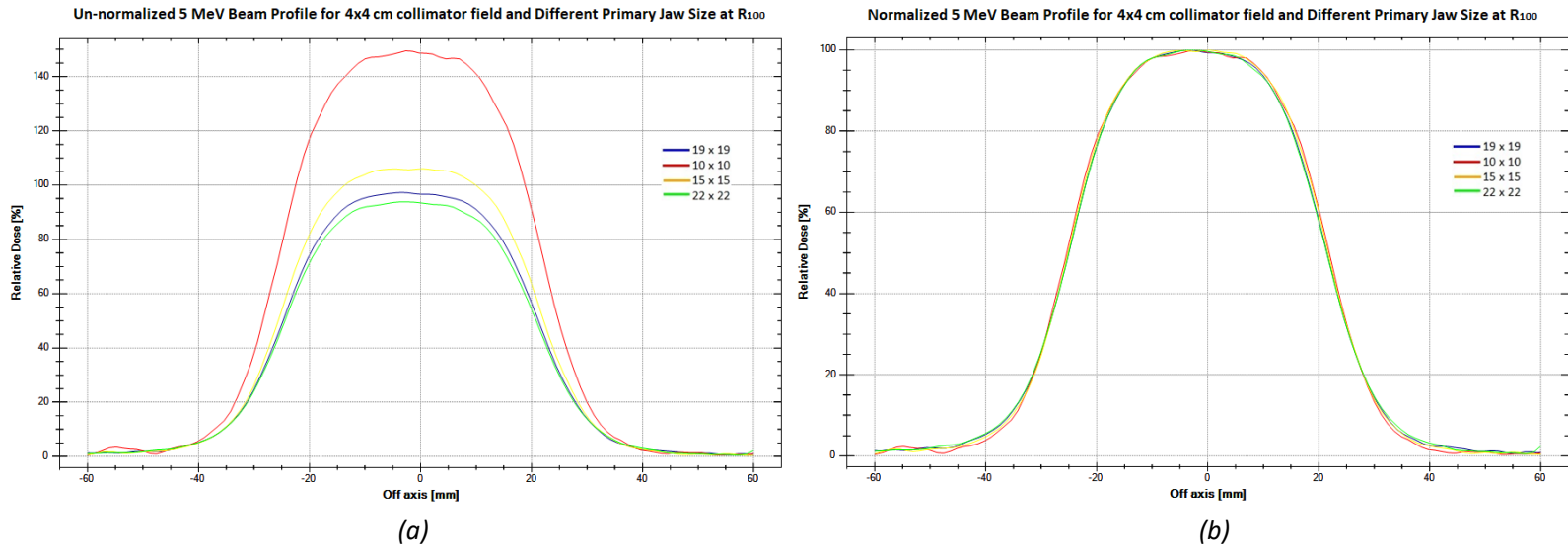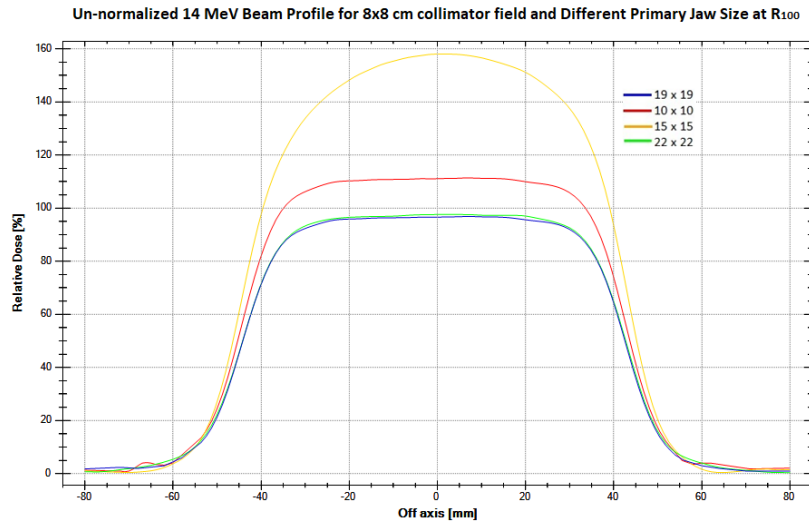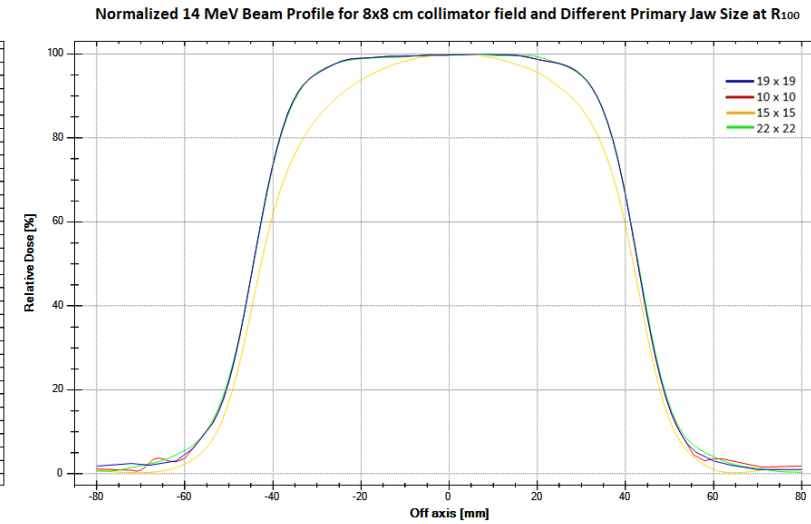

Figure 4.33 *Beam Profiles of 14 MeV electron beam for 8 × 8 cm field size at a depth of R_{100} for different primary jaw field settings. (a) Unnormalized (b) Normalized*
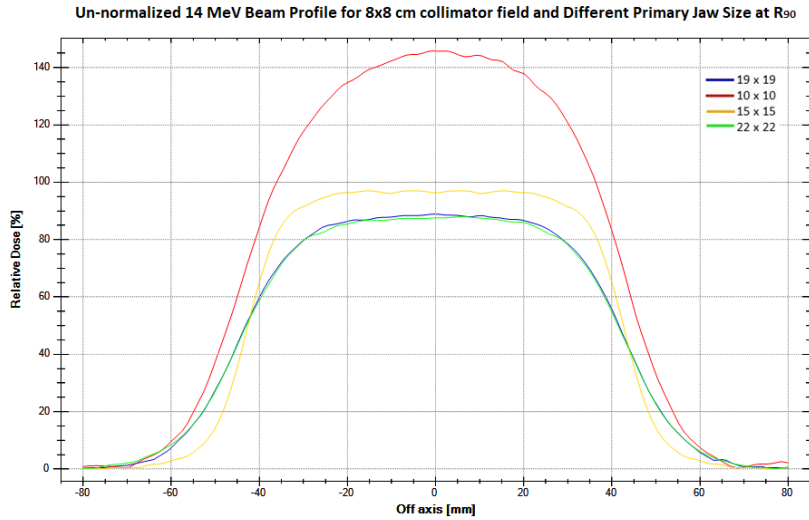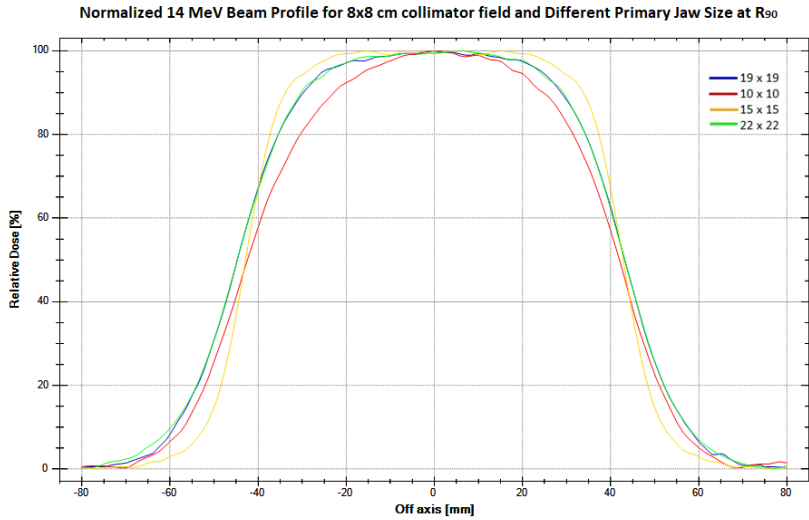
Figure 4.34 *Beam Profiles of 14 MeV electron beam for 8 × 8 cm field size at a depth of R_{90} for different primary jaw field settings. (a) Unnormalized (b) Normalized*
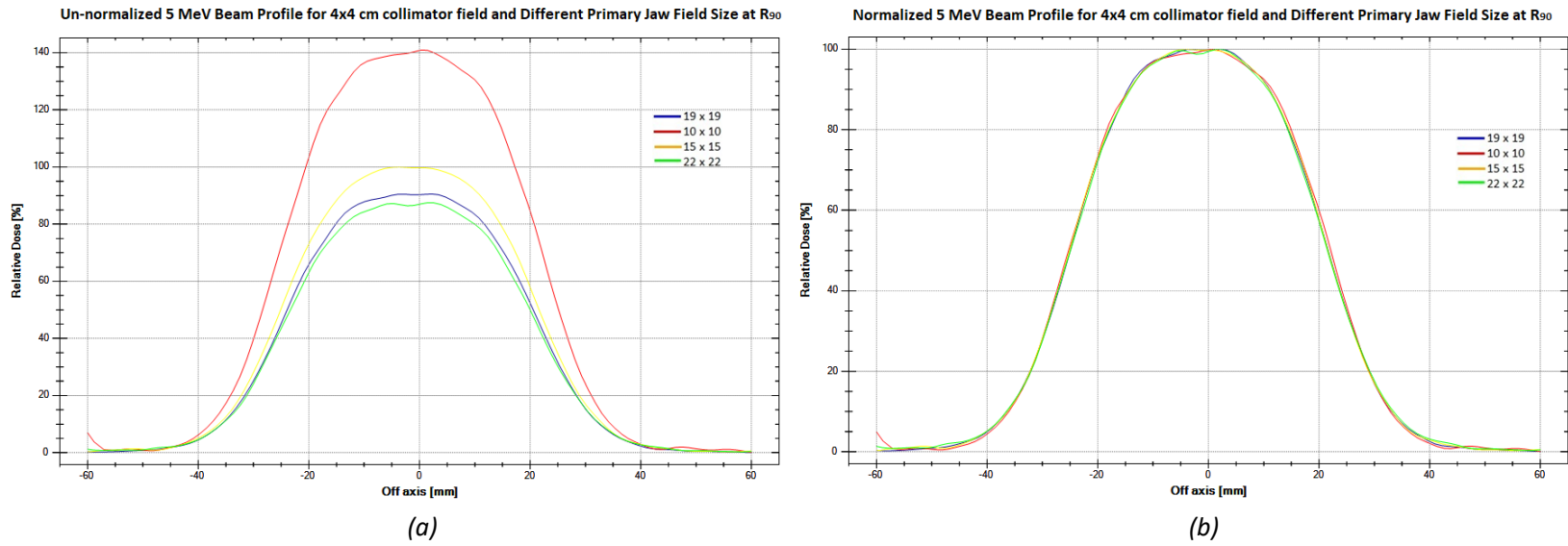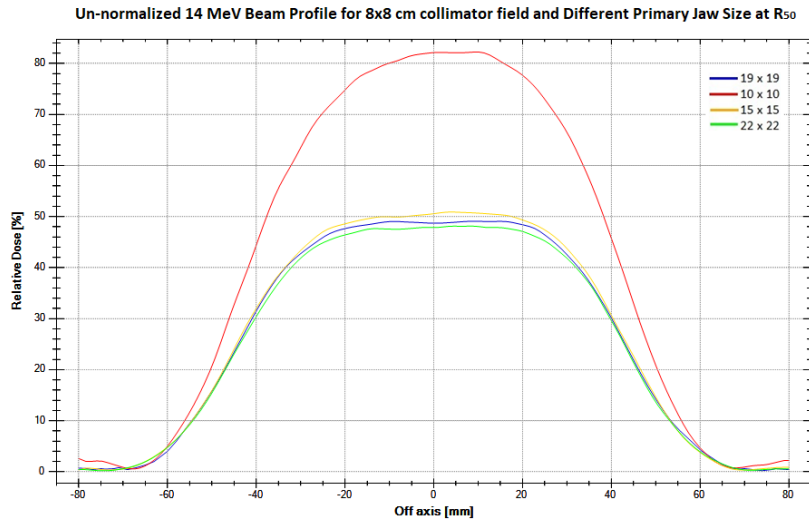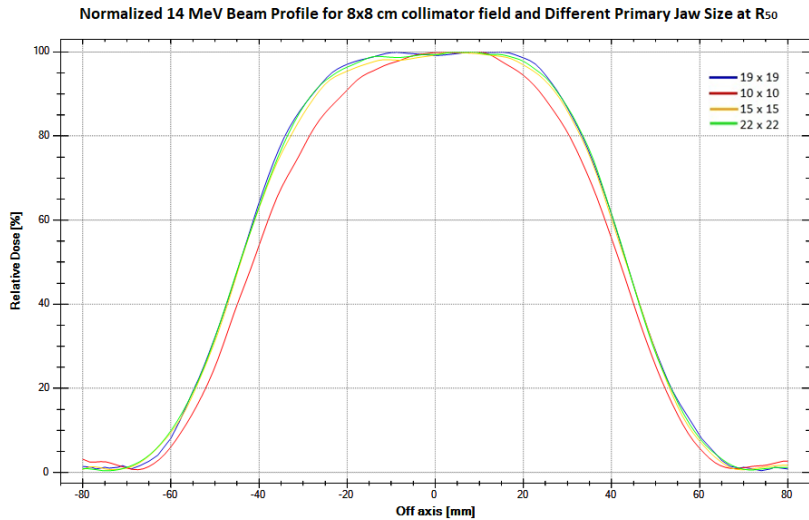

Figure 4.35 *Beam Profiles of 14 MeV electron beam for 8 × 8 cm field size at a depth of R_{50} for different primary jaw field settings. (a) Unnormalized (b) Normalized*

4.2 Virtual Source Position

4.2.1 Inverse Square Law Methods

The virtual source position is determined by plotting the inverse of the square root of the electrometer readings and finding the intercept of the straight line. The intercept indicates the virtual source position. The virtual source positions obtained using the inverse square method are shown in Table 4.2 below.

Table 4.2   *Comparison of virtual source positions obtained by the inverse slope (ISLP) method, inverse square law method and full-width at half-maximum (FWHM) method.*

Field Size																
	2x2				4x4				6x6				8x8			
Energy (MeV)	ISLP-Air	ISLP-Ph	ISQL	FWHM	ISLP-Air	ISLP-Ph	ISQL	FWHM	ISLP-Air	ISLP-Ph	ISQL	FWHM	ISLP-Air	ISQL	FWHM	ISLP-Air
5	15.7	19.7	17.5	16.7	22.4	39.8	45.1	45.5	56.7	57.0	52.5	79.1	60.4	68.7	59.2	86.7
7	20.4	25.7	21.7	24.3	26.1	51.7	56.1	66.6	59.8	64.7	63.5	80.3	79.4	73.6	71.3	89.9
8	24.6	30.0	26.1	28.1	28.6	58.5	62.1	72.7	62.7	67.7	65.3	81.3	82.8	75.5	77.6	92.7
10	32.3	39.5	33.8	39.2	32.3	66.1	63.2	86.9	63.3	71.6	72.1	84.4	84.3	78.0	80.7	94.2
12	38.6	43.1	40.3	48.5	38.6	69.0	64.1	92.3	65.8	72.2	75.7	96.4	86.2	78.9	82.8	95.2
14	41.5	45.9	43.4	55.6	41.5	71.3	67.8	93.8	69.7	72.5	77.4	96.5	89.5	79.6	85.1	95.2

Values are in cm. ISLP-Air: Inverse Slope in Air method, ISLP-Ph: Inverse Slope in a water Phantom method, ISQL: Inverse Square Law method and FWHM: Full-Width at Half-Maximum method.

The virtual source position is measured from the nominal source reference point. A comparison of the 8 × 8 cm field with the chamber start position at 5.0 cm from the end of the electron applicator and 0.0 cm from the applicator end is shown in Figure 4.36. Most studies indicate that measurements should be made 5 cm from the end of the applicator; if measurements also include the distance less than 5 cm, this has a bearing on the virtual source position.
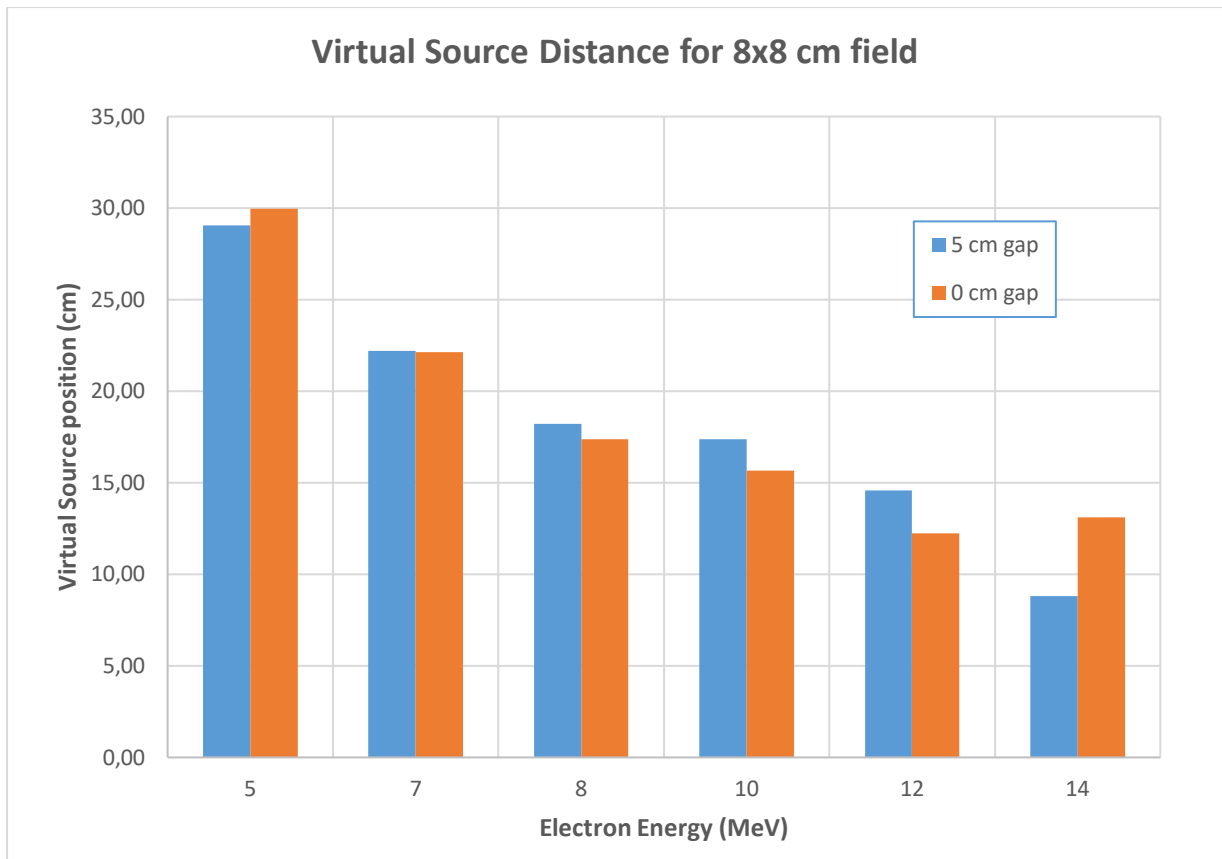
Figure 4.36 *Virtual source position for different field sizes and electron energies.*

4.2.2 Inverse Slope Methods

The plot of the square root of the charge quotient, $\sqrt{\frac{Q_0}{Q_s}}$, against the separation s, gives a linear plot whose inverse of the slope is related to the virtual source position, VSP_{eff}. The inverse of the slope of the plot of the square root of the charge quotient, $\sqrt{\frac{Q_0}{Q_s}}$, against the separation s, minus the depth of measurement, gives the virtual source position. A plot of the square root of the quotient of the charge with the chamber for in-air measurements is shown in Figure 4.37 to Figure 4.40. The linear plots of the quotient of the chamber charge readings against the air gap separation of the different electron beam energies and field sizes are shown in Figure 4.37 to Figure 4.40.
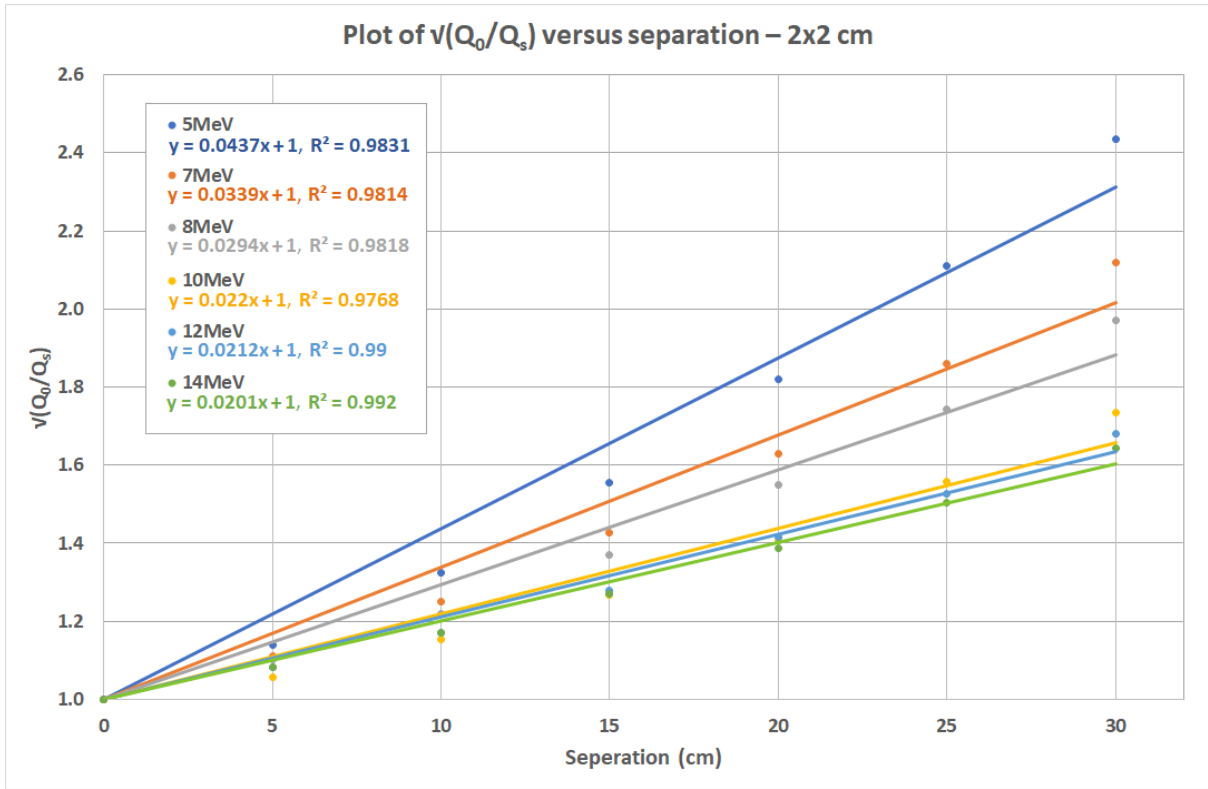
Figure 4.37 *Plot of the square root of the charge quotient with separation for 2 x 2 cm field.*
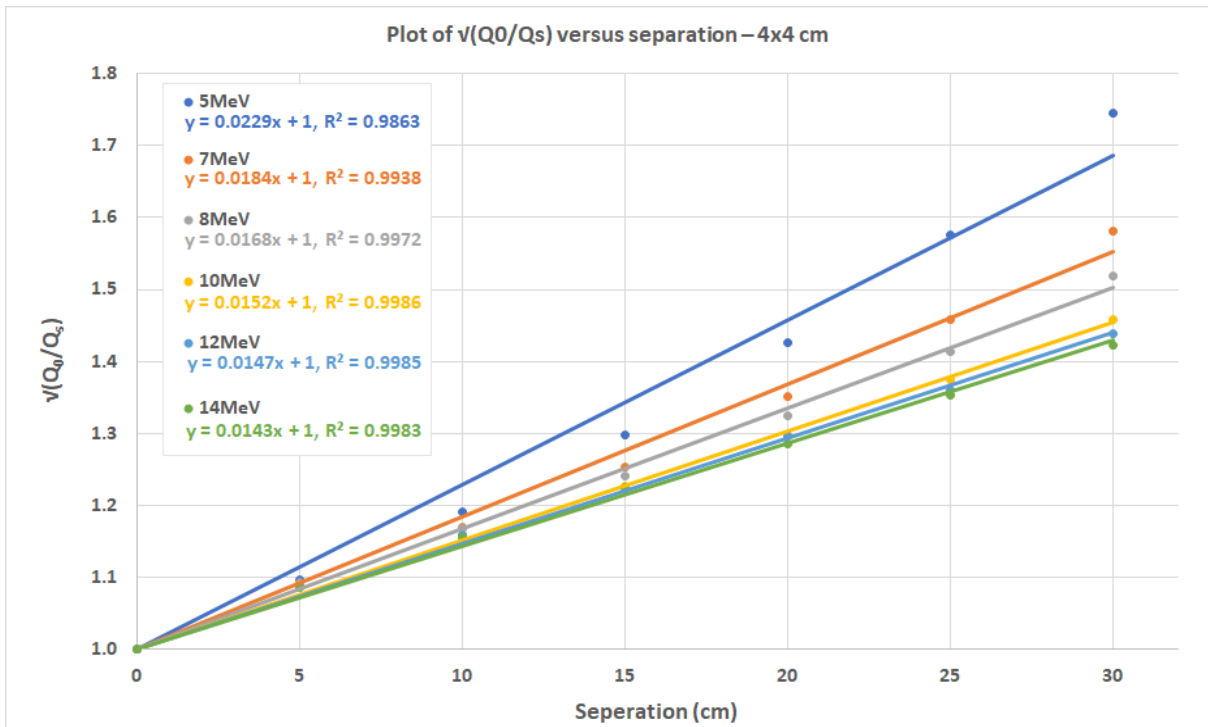
Figure 4.38 *Plot of the square root of the charge quotient with separation for 4 x 4 cm field.*
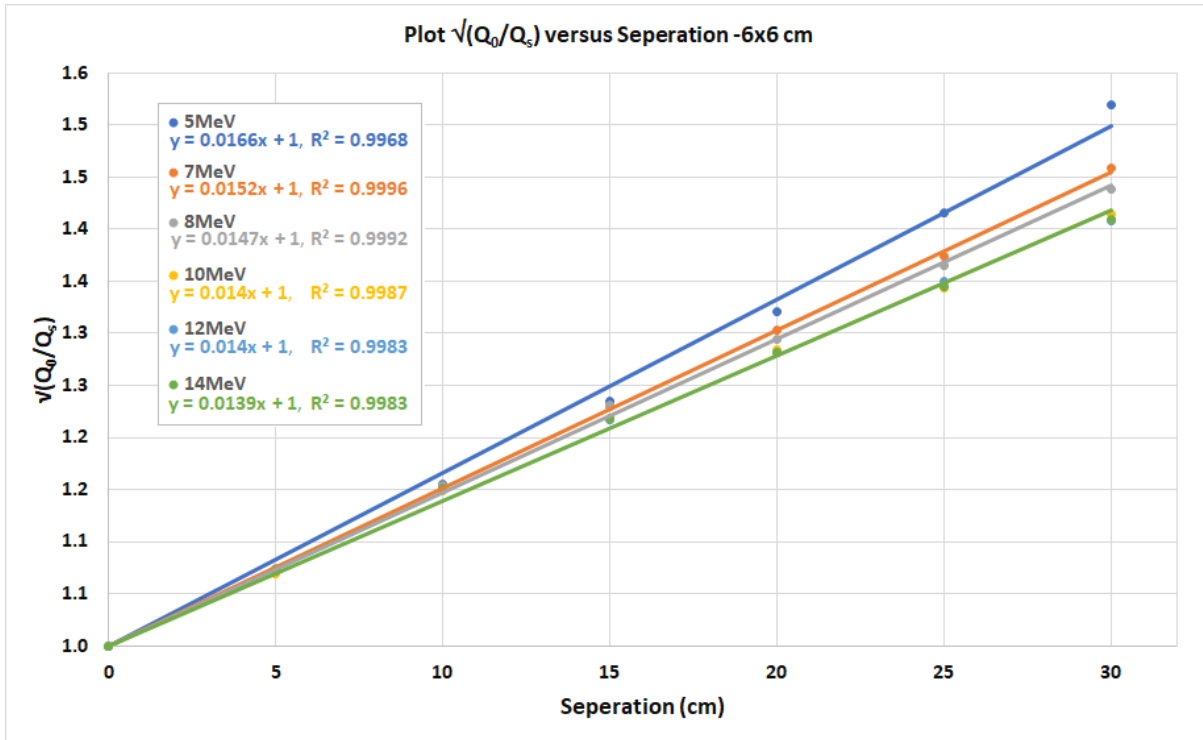
Figure 4.39 *Plot of the square root of the charge quotient with separation for 6 x 6 cm field.*
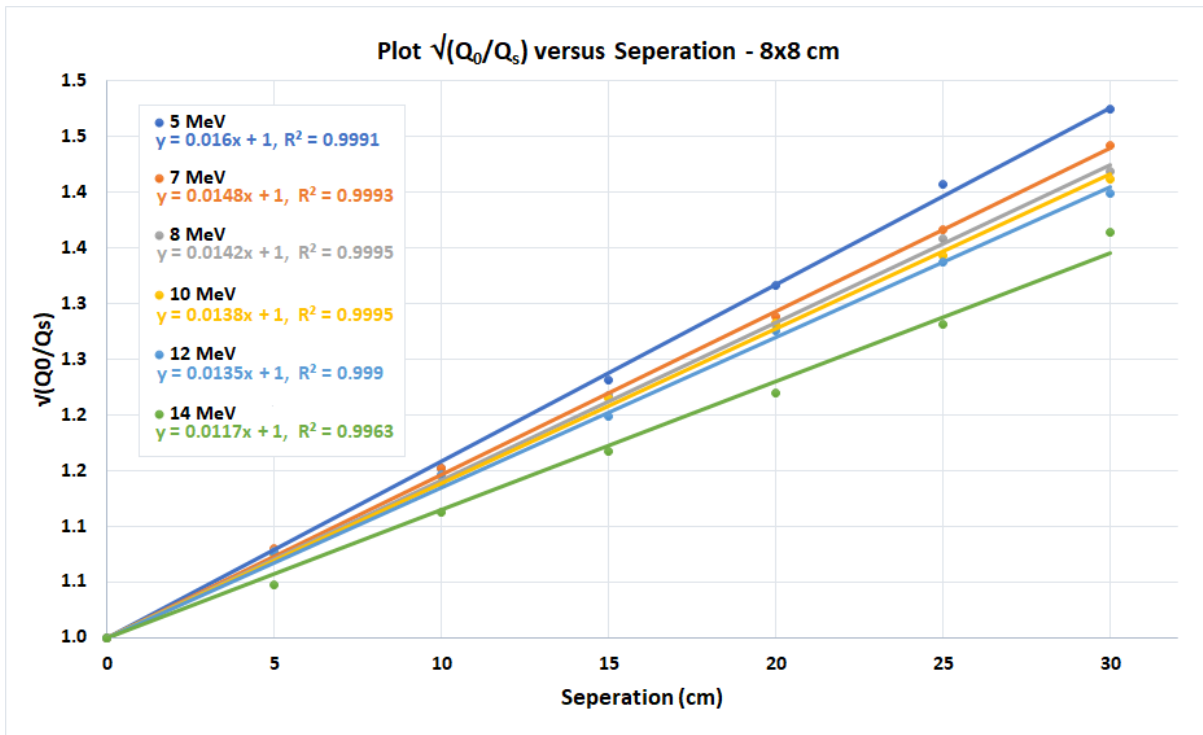
Figure 4.40 *Plot of the square root of the charge quotient with separation for 8 x 8 cm field.*

Figure 4.41 shows the virtual source position determined by using the inverse slope method for different field sizes and electron energies.
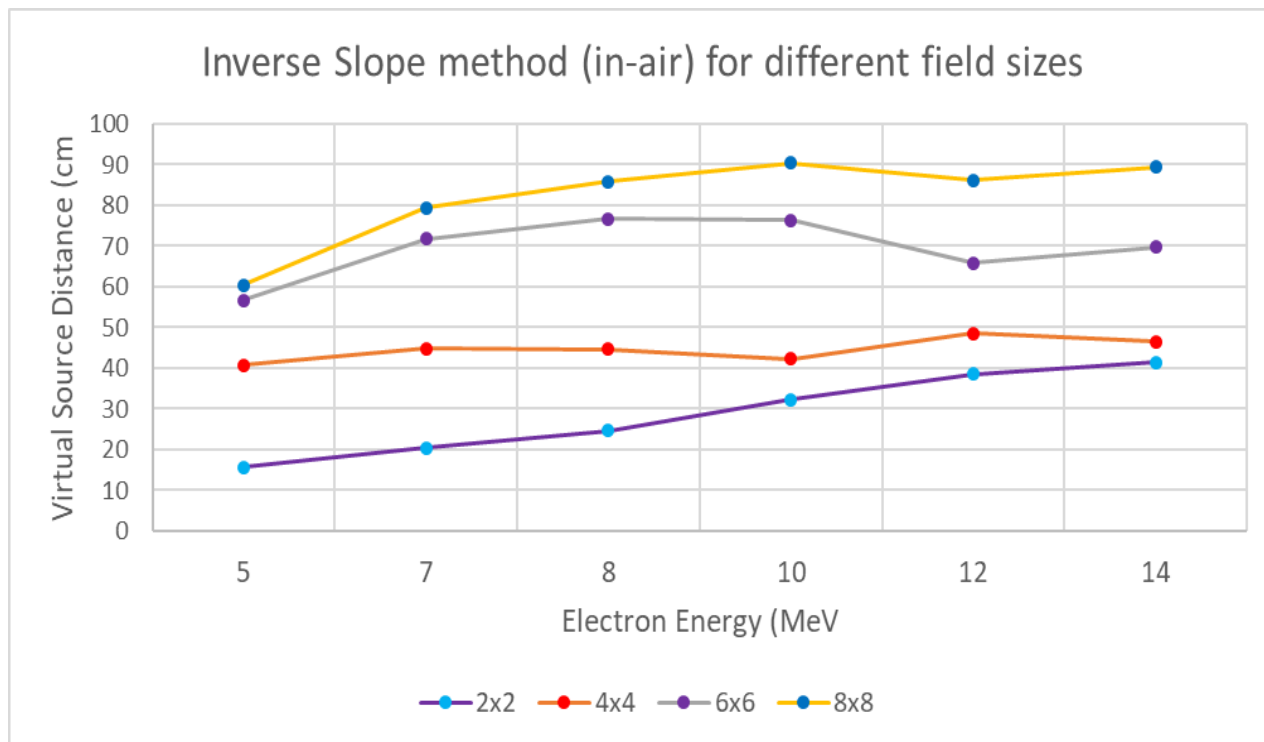
Figure 4.41 *Virtual source positions for different energies for different field sizes and energies using the in-air inverse slope method.*

4.2.2.1 Inverse Slope Method-in phantom

The inverse of the slope of the plot of the square root of the charge quotient, $\sqrt{\frac{Q_0}{Q_s}}$, against the separation s, where Q_0 is the collected charge with no separation, and Q_s is the collected charge with separation s, minus the depth of measurement, gives the virtual source position. The plot of the square root of the charge quotient, $\sqrt{\frac{Q_0}{Q_s}}$, against the separation s, for 6×6 cm field size and different electron beam energies is as shown in Figure 4.42.
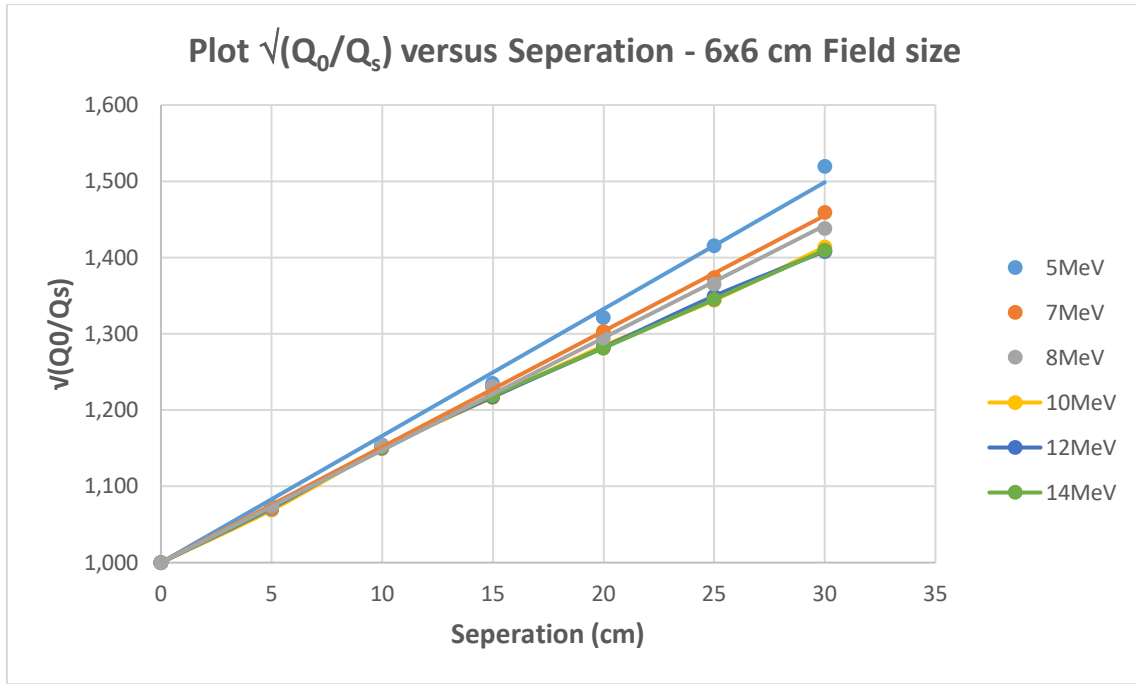
Figure 4.42 *The plot of the square root of the quotient of the charge against the separation.*

The inverse of the slope of the plot of the square root of the charge quotient, $\sqrt{\dfrac{Q_0}{Q_s}}$, against the separation s, minus the depth of measurement gives the virtual source position as shown in Figure 4.43.
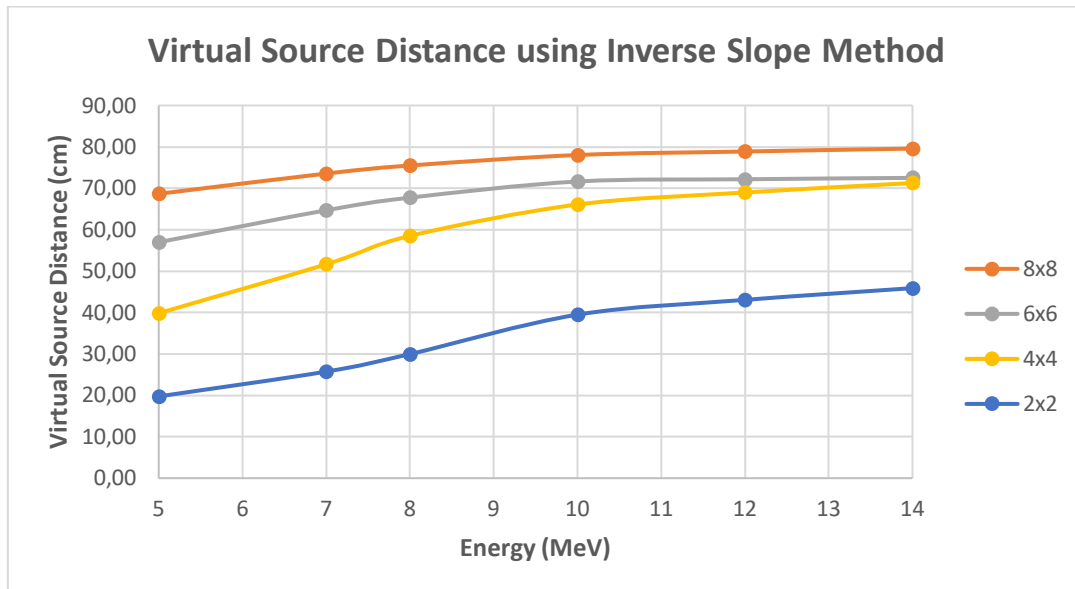
Figure 4.43 *The virtual source distances for different field sizes and energies using the inverse slope method.*

4.2.3 Full-Width Half-Maximum (FWHM) Method

The full-width half-maximum at different distances from the applicator was plotted against the SSD for each electron beam energy and field sizes, with the x-intercept indicating the virtual source position. Figure 4.44 shows the virtual source positions for different field sizes and different electron energies.
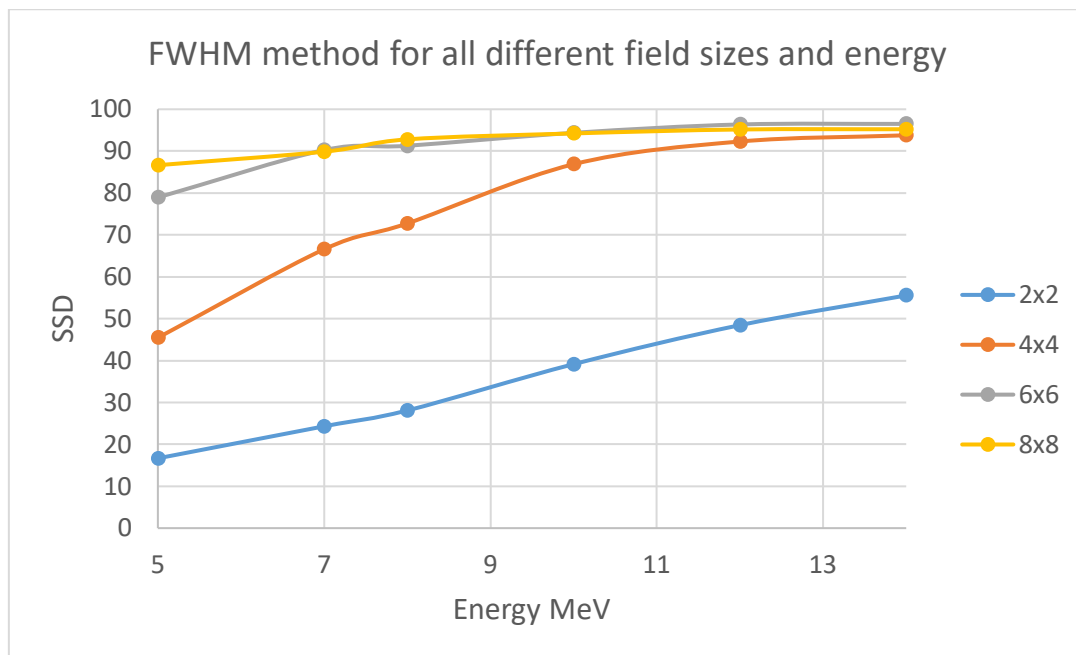
Figure 4.44 *Virtual source position for different field sizes and different electron energies, using the full-width half-maximum (FWHM) method.*

A comparison of the virtual source positions from the different methods that were used is presented in Table 4.2. The table provides the virtual source positions obtained from the inverse slope (ISLP) method, inverse square law method and the full-width at half-maximum (FWHM) method.

4.3 Variable field-shaping collimator

For the conceptual design, a 3-D model shown in Figure 4.45 was constructed using CAD software. A plastic model from the CAD design was initially fabricated using 3D printing as shown in Figure 4.46 below.
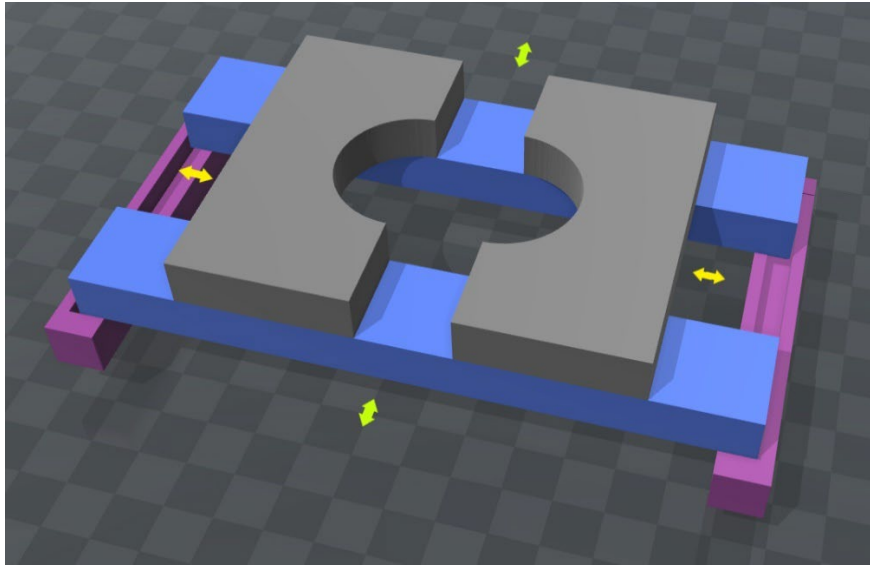
Figure 4.45 *3D model of the variable collimator, which was used for the fabrication of the collimator.*

An alternative design with the two upper jaws overlapping is shown in Figure 4.47; however, this design was not opted for in the final design. The variable collimator was designed to fit on a standard 10 × 10 cm electron applicator. When the upper circular jaws are closed, they form a 4 cm diameter circle with the lower jaw completely blocking the field when fully closed. A circular upper jaw was used to allow for the formation of squircular fields.
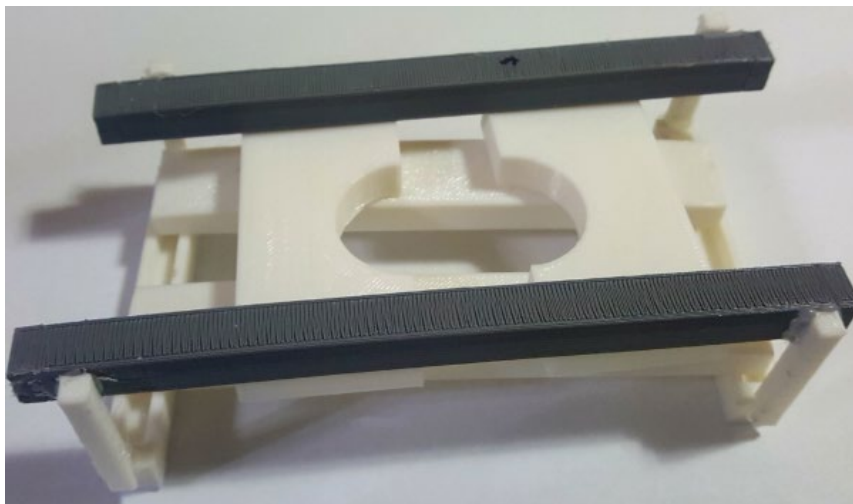
Figure 4.46 *3D printed model of the variable collimator.*

Mild steel was used for the construction of the prototype of the collimator. It was chosen because of its high tensile strength, good malleability and that it was not prohibitively expensive.
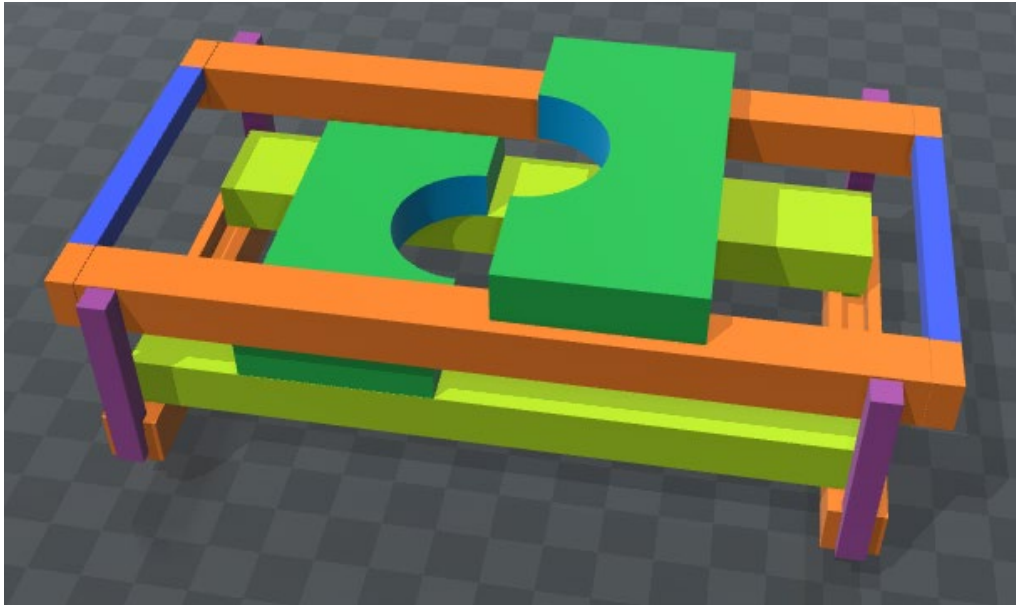
Figure 4.47 *3D model of variable collimator with overlapping jaws.*

The variable collimator made from steel is shown in Figure 4.47 below.
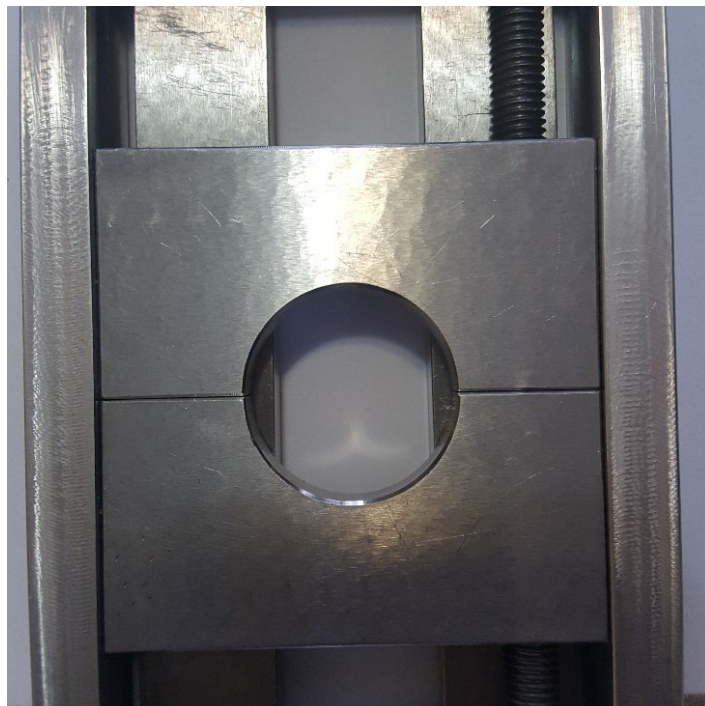
Figure 4.48 *Variable collimator.*

The results of the electron transmission are shown in Figure 4.49. As seen from the transmission curve, the TVT for the Cerrobend for a 14 MeV electron beam is 3.8 mm. From

Jayaraman and Lanzl (1996) and Tellili et al. (2017) the TVT for steel is about twice that of Cerrobend. Thus, a thickness of 10 mm for steel would be sufficient to prevent the transmission of 14 MeV electrons. 10 mm steel was used as this was readily available and was more suitable to work with in the construction of the variable applicator.
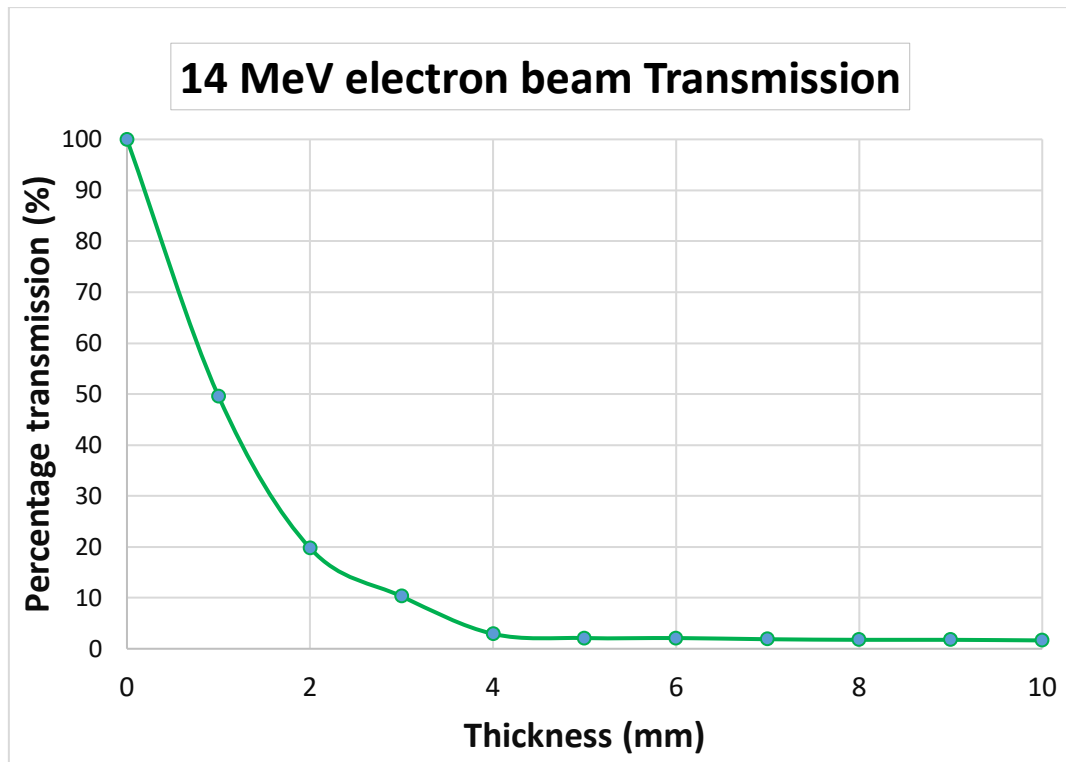
Figure 4.49 *Electron transmission curve for 14 MeV electrons.*

4.3.1 Motor Control for variable collimator

Four Maxon high-precision pencil motors were employed for moving the collimating jaws. The motors are the same as those that are used on the Siemens mlc. The motors were in turn driven by an Arduino Uno R3, which is an open-source microcontroller board based on the Microchip ATmega328P microcontroller (Arduino.cc, 2018).

4.4 Automated Couch Movement

Depending on the curvature and size of the scar, the scar was divided into segments, in which the gantry angle was varied for a particular segment. For each segment, the table was moved,

and the collimator angle changed accordingly to keep the beam perpendicular to the surface of the phantom. Positional commands for the lateral, longitudinal and vertical movements were sent to the couch; the position of the couch was then physically verified.

4.5 Collision Avoidance

The gantry and couch were rotated for all allowed couch and gantry rotations, to see possible collisions; the results of the collision avoidance chart for the couch rotation are shown in Figure 4.50.
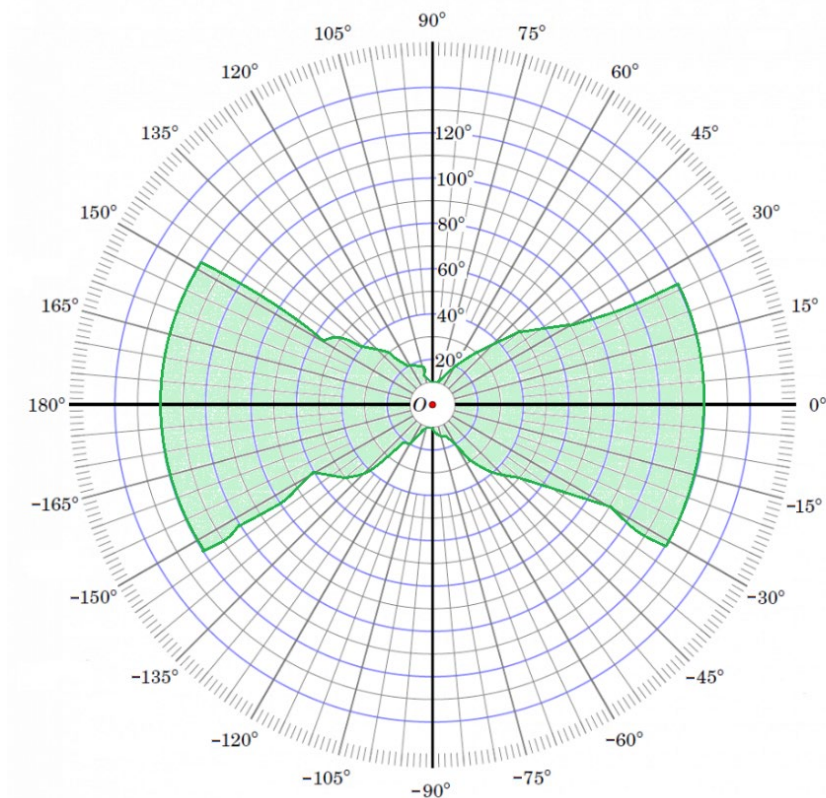
Figure 4.50 *Treatment couch vs gantry collision avoidance chart.*

4.6 Treatment of Rando phantom

The Alderson Rando phantom is made of tissue-equivalent material, which follows the ICRU-44 standards (ICRU, 1989). It was made up of 32 slices of 2.5 cm thickness. The chest part of the phantom, which has tissue and lung heterogeneity similar to an adult, was used

with GafChromic film placed in between the slices, as shown in Figure 4.51 and Figure 4.52. The film was placed in positions 16 to 20 of the Rando phantom, as indicated in Figure 4.51

Figure 4.51 *Rando phantom with a simulated scar and film slice position.*

The GafChromic RTQA2 film is a self-developing radiochromic quality assurance film; it was cut to conform to the curvature of the phantom.

Figure 4.52 *Radiochromic GafChromic films cut to the curvature of the Rando phantom and placed in-between the slices.*

A topogram of the scanned phantom is shown in Figure 4.53. The Rando phantom was placed on the treatment couch and treated using the treatment plan, with the couch moving to follow the length of a simulated mastectomy scar as shown in Figure 4.51.
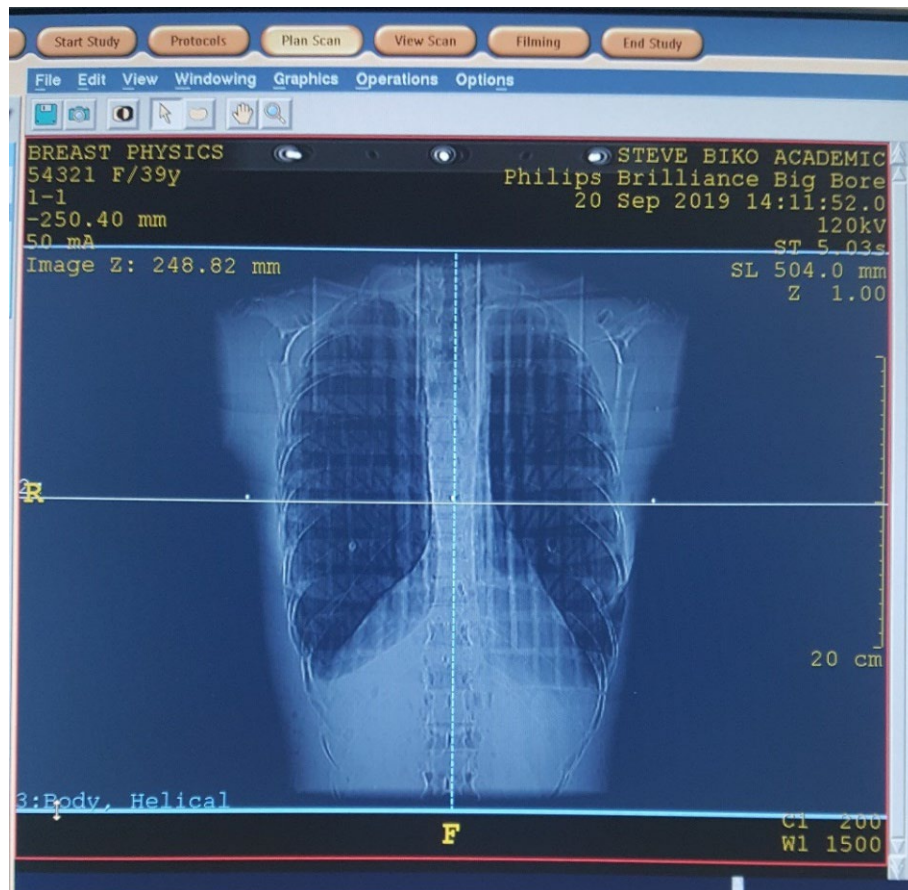
Figure 4.53 *CT topogram of the Rando phantom.*

The dose for the treatment plan was calculated using the electron Monte Carlo algorithm that comes with the Monaco treatment planning system. The GafChromic films were then scanned using the Canon Pixma MX494 4-in-1 Multifunction Printer, using the Canon IJ scan utility that came with the printer. The scanned film was processed and analyzed using the ImageJ 1.52p (Fiji) software. The scanned data images were saved in the TIFF image format. The ImageJ software is able to analyze the images in the red-green-blue (RGB) channels. The scans were analyzed using red channel data as recommended by the GafChromic EBT film manufacturer (Casanova Borca et al., 2013, Matney et al., 2010). The tools in the ImageJ software allowed for colour contours to be assigned to RGB image values using the dose calibration curve. The scanned images are indicated in Figure 4.54.

(a)
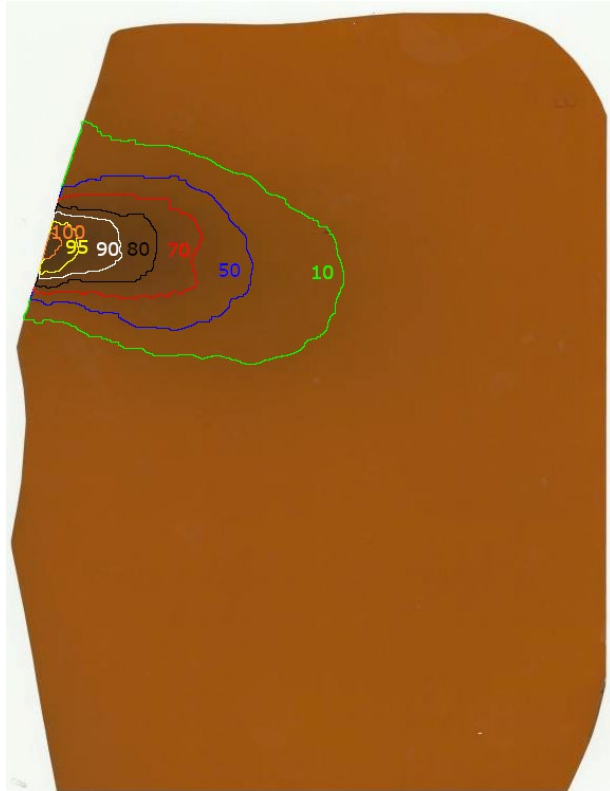
(b)
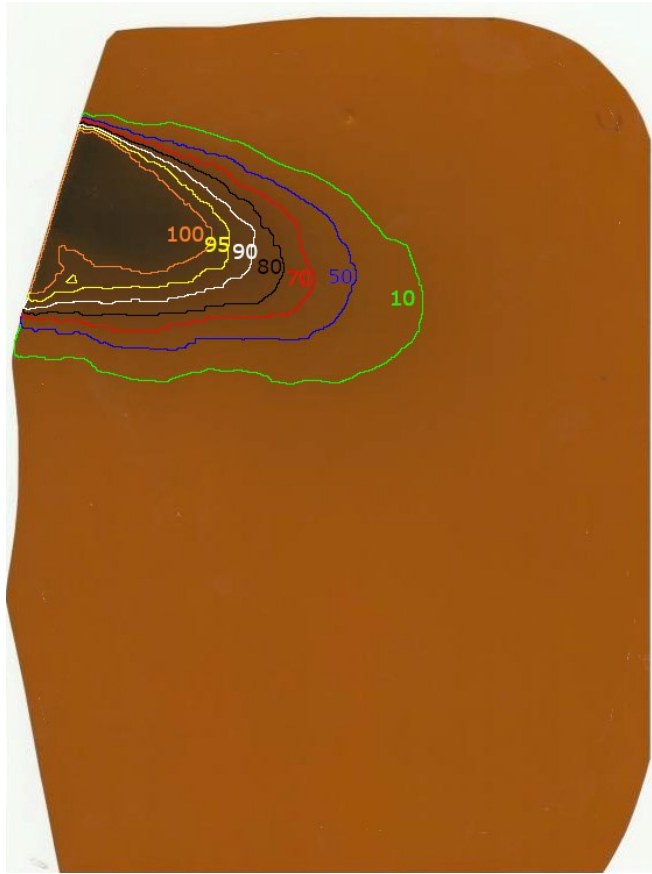
(c)
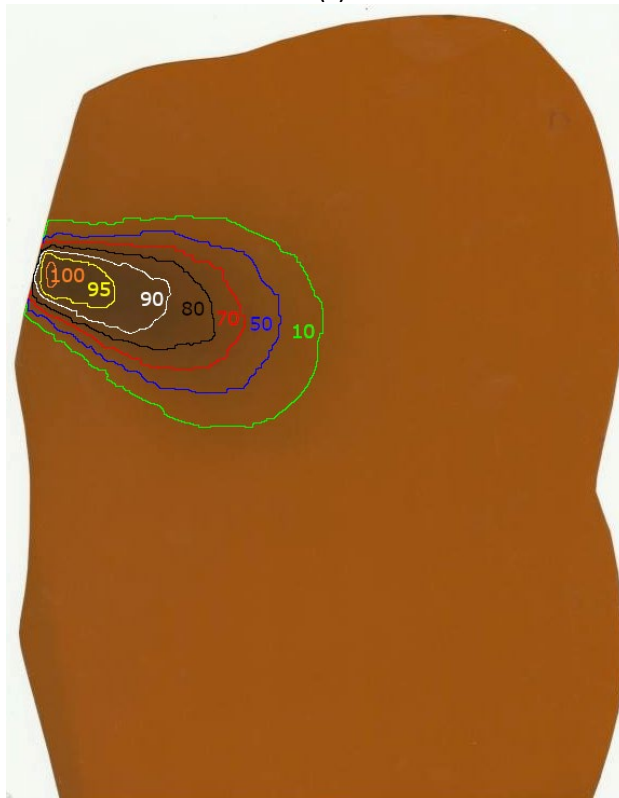
(d)

(e)

Figure 4.54 *Scanned GafChromic films with isodose lines indicating the dose distribution. Films were at different positions of the Rando phantom: (a) is at position 16, (b) is at position 17, (c) is at position 18, (d) is at position 19, (d) is at position 20.*

The isodose lines in Figure 4.54 are represented by the different coloured lines, indicating the dose distribution for the various sections of the phantom. The results in this section for the measurements that were conducted will now be discussed in the following section.

CHAPTER 5

DISCUSSION OF RESULTS

In this chapter, the results, as outlined in the previous chapter, Chapter 4, are discussed. In order to be able to deliver adequate radiotherapy treatment, it is essential to have an understanding of the beam delivery, the physical behaviour of the beam, how it interacts with matter and the various components that are involved in the treatment. The electron beam's behaviour is more complex than photon beams due to their size and being charged; some of these treatment aspects are discussed next.

5.1 Electron Beam Characteristics

The results of the electron beam measurements were consistent with those in the literature. It is known that electrons lose their energy continuously as they traverse matter and undergo substantial scatter due to their lightweight. Electrons are markedly different from photons due to numerous reasons already outlined, their interaction with the various components in the linac and phantom affects the dose distribution, and it is, therefore, important to characterise them. The interaction of the electrons with the primary jaws and the electron applicator, causes the electrons to undergo an increase in angular and energy spread. For broad fields, this has the effect of increasing the dose in the build-up region; however, this is not the case for small fields. Lax and Brahme (1980) showed that the lateral movement of the electrons in phantom and collimator had the effect of reducing the dose build-up and therapeutic range in the case of small fields; this can be seen in Table 4.1 as indicated by therapeutic range R_{90} and the peak dose R_{100}. It is desirable that the therapeutic range corresponds to the distal edge of the PTV, thus the minimum depth is 1.43 cm for the 5 MeV electron beam and the maximum is about 4 cm for the 14 MeV beam. Also, as the field size decreases, the R_{50} becomes more shallower, and there is an increase in the surface dose, with d_{max} moving closer to the surface. The choice of the energy of the electron beam is often determined by the depth of the lesion, and the depth of the 90 % isodose line, d_{90}., these values are shown in Table 4.1. It can also be seen from Table 4.1 that x-ray contamination due

to bremsstrahlung, indicated by Dx (%) for the lower electron beam energies, generally increases with increasing field size. This increase can be attributed to an increase in the surface area that the electrons interact with.

5.1.1 Beam Obliquity

It was shown that the effect of beam obliquity becomes more pronounced with an increasing beam angle of incidence. Electron beam obliquity has the effect of decreasing the penetration of the therapeutic depth dose, increasing the surface dose, and increasing the dose at depth of dose maximum. These effects can be seen in Figure 4.6 to Figure 4.11 for the different angles and field sizes. When prescribing electrons for treatment, the ICRU Report 71 (ICRU, 2004) states that, where possible large angles of incidence of the electron beam should be avoided, as the usefulness of the beam deteriorates with the increasing angle of incidence. The report also mentions that for the various levels of reporting, the patient curvature and beam obliquity need to be considered and corrected for electron beam therapy. It can also be seen that the effect of beam obliquity is more pronounced for smaller field sizes and the lower electron beam energies, as shown in Figure 4.6 (a), for a 5 MeV and 2 × 2 cm field size, as compared to a higher energy of 14 MeV and comparatively large field size of 8 × 8 cm shown in Figure 4.13, it is therefore necessary that when treating using oblique fields the obliquity effect be accounted for when calculating the dose to the target. Obliquity correction is required for monitor unit calculations when using manual calculations and for treatment planning systems using non-Monte Carlo based algorithms.

The chamber readings in the build-up regions could have been affected by detector volume averaging, which was more pronounced towards the surface. To verify this, comparison measurements using detectors such as the diode or diamond detectors would have assisted. These detectors have smaller sensitive volumes, with the PTW microSilicon diode detector having a nominal sensitive volume of 0.03 mm^3 and that of the PTW microDiamond detector having a nominal sensitive volume of 0.004 mm^3.

5.1.2 Effect of primary jaw field size

One of the desired characteristics for an electron beam is flatness across the beam field size and at different depths of measurement. The AAPM Report 34 by Khan et al. (1991) defines flatness for treatment fields that are equal to or greater than 10×10 cm^2. When considering the 5 MeV, the 15×15 cm, for the most part, offered a slightly more flat beam, compared to the other jaw settings. For the higher energy 14 MeV beam, it can be seen that for the 19×19 cm and 22×22 cm jaw settings, the profiles are similar to each other. Even though the relative ionisation was less for the default jaw field size of 19×19 cm, compared to that of 10×10 cm and 15×15 cm, the beam profile was more symmetrical and flatter. This can also be seen for the R_{50} for the various electron beam energies. Any gains that might arise with a smaller photon jaw collimator were not immediately visible. The default jaw setting of 19×19 cm was therefore the jaw setting of choice for all energies and variable collimator field sizes.

5.2 Virtual Source Position

The results showed that the field size and collimation had an effect on the virtual source position. The virtual source position is primarily affected by the collimation of the electron beam. As highlighted by Lax and Brahme (1980), there are four factors that are associated with collimation that contribute to the quality and characteristics of the electron beam. These factors are the presence of air, which scatters the electrons; the scattered electrons due to the collimating walls not being parallel to the direction of the beam; the contamination as a result of bremsstrahlung production; and contamination due to electrons being scattered back into the beam as they pass through the edges of the collimator. It can be seen that the virtual source position varies widely with the method used. Mayles et al. (2007) have stated that unlike for photons, where the virtual source is measured in air, in the case of electrons the measurements should be at d_{max} for the inverse square law analysis. For the in-air measurements, it was assumed that backscattered electrons were negligible since they only have a range of a few meters (Das et al., 1995). From literature, the inverse square in-phantom method is the preferred method. The standoff was kept at 5 cm, as there was no

advantage in using a larger standoff, rather there was a decrease in relative output as seen in Figure 4.1 to Figure 4.6

5.2.1 Inverse Square Law Methods

For the current study, the measurements were plotted with the distance to the nominal SSD on the x-axis and the inverse of the square root of the ionization on the y-axis, as shown in Figure 4.37 to Figure 4.40. The results show that the plot yields a straight line, which means that the radiation output obeys the inverse square law; a nonlinear plot would have meant that the radiation output does not comply with the inverse square law. The intercept with the x-axis indicates the position of the virtual source. The x-intercepts are positive; this means that virtual source positions are away from the nominal X-ray source and close to the patient. The virtual source positions are downstream from the scattering foil. A negative x-intercept shows that the virtual source position is more upstream.

It can be noted that for a particular electron beam energy and field size, the virtual source position does not vary with the reference depth of measurement. A single virtual source distance can thus be used for treating at different depths. It can also be seen that the virtual source position is dependent on the collimation and field size, which is a result of less side scatter contribution as the field size decreases. There is also a dependence of virtual source distance on electron beam energy, with it increasing with energy.

5.2.2 Inverse Slope Methods

As explained by Thomas (1988), a major contributing factor to the virtual source distance for different field sizes is scatter that is due to the applicator walls. For large field sizes at the centre of the field, there is less contribution from the scattered electrons. A reduction in field size has the effect of more scattered electrons reaching the center of the beam; however, this is offset by air scatter, which is more pronounced for lower energy electron beams. The net effect is a lower virtual source distance, as seen in Figure 4.41 and Figure 4.43. There was some variation between the virtual source position for the in-air and in-phantom measurements. However, the in-phantom measurements are preferred as they are more

representative of a clinical setup. The inverse of the slope of the plot of the square root of the quotient of the charge against the separation gap between the applicator and phantom surface, minus the depth of measurement, gave the virtual source position, as shown in Figure 4.43. There was a significant difference in the virtual source position between the in-air and in-phantom measurements. The largest difference was as high as 33.9 cm for the 8 MeV electron beam for the 4 × 4 cm field. The in-phantom virtual source position was higher than that of the in-air virtual source position for the 2 × 2 cm and 4 × 4 cm fields, and the in-air virtual source position was mostly higher than that of the in-phantom virtual source position for the 6 × 6 cm and 8 × 8 cm fields.

5.2.3 Full-Width Half-Maximum (FWHM) Method

The virtual source position was determined using the method described by Ravindran (1999). Figure 4.44 shows that for the 8 × 8 cm field size, the virtual source distance is almost the same for all electron beam energies. The field sizes of 4 × 4 cm, 6 × 6 cm and 8 × 8 cm seem to converge to the same value for a 14 MeV beam. This suggests that for field sizes greater than 2 × 2 cm, the collimator scatter at higher energies does not have a pronounced effect on the virtual distance. The results are similar to those of Jamshidi et al. (1986), of a shorter SSD than the nominal 100 cm. They found that as the electron beam energy decreases and the field size gets smaller, so does the SSD decrease. They found that for the smallest field size of 4 × 4 cm and energy of 6 MeV, the SSD was 55 cm; which is similar to the value that would be obtained for the interpolation of a 6 MeV beam in Figure 4.44. The results of Ravindran (1999) also showed a similar trend with the SSD decreasing with electron beam energy and field size.

Of the four methods used to determine the virtual source position the FWHM method had the highest value for the source position. The highest difference for the virtual source position of 54.6 cm was between the in-air inverse slope method and the FWHM method for the 10 MeV and 4 × 4 cm field. Ravindran (1999) also found that there was a significant disagreement between the inverse slope method and the FWHM method and concluded that the FWHM method was not suitable in a clinical setting. The in-phantom virtual source position is recommended as this is closest to clinical set-up conditions as advised by ICRU, 1984.

5.3 Electron Beam Collimation

Spirou and Chui (1994) developed an algorithm for generating arbitrary intensity profiles using dynamic jaws similar to the one by Convery and Rosenbloom (1992). The intensity distribution was taken to be piecewise linear and was evaluated as a minimization problem in linear programming. The collimation comprised of two jaws in the form of two solid blocks. The jaws used the sliding window technique, moving from one end at different speeds to the other unidirectionally, scanning an aperture of variable width. This concept was adopted for the current work.

5.3.1 Variable field-shaping collimator

For the conceptual design and initial testing of the collimating device, a plastic model was fabricated using 3D printing. A number of possible designs were considered, including one with the two upper jaws overlapping. The device was designed so that it fits on standard 10×10 cm^2 electron applicators that were available in the department. A prototype made of mild steel was then fabricated. For the purposes of this study, the thickness of the steel that was used was 1 cm, which was greater than the continuous slowing down approximation range for the clinical electron beams between 7 MeV and 14 MeV that were used. It can be seen from Figure 4.49 that a thickness of 4 mm of Cerrobend would have also sufficed.

A variable field-shaping collimator for the desired electron technique was developed. Mild steel was used for the construction of the prototype of the collimator. The use of high atomic number material such as mild steel has the effect of increasing the photon contamination, which can lead to more dose beyond the therapeutic depth of the electrons. The photon contamination can be seen as the 'tail' in Figure 4.49. To reduce the bremsstrahlung generated by the electron collimating device, the primary photon jaw mimics the electron collimator. Olofsson et al. (2005) looked at bremsstrahlung photon micro-leaf collimator (MLC) tracking for a 10×10 cm^2 electron field.
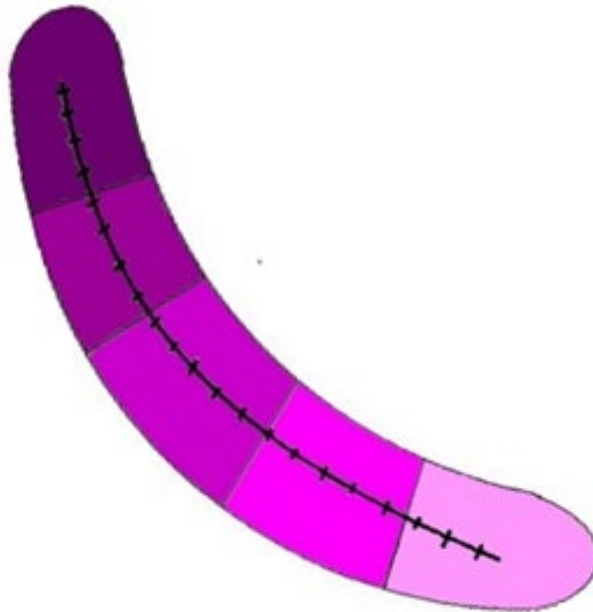
Figure 5.1 *Scar with a margin around it. Shaded areas indicate different segments, which can be treated with different electron beam energies to get the required dose distribution.*

The beam energy can be modulated in between segments to vary the depth being treated, as shown in Figure 5.1. Each of the segments is treated with a different electron beam energy to get the required dose distribution. The dose is delivered in automated segments, which can be delivered at higher dose rates to reduce the treatment times; however, this might not be the case, as pointed out by Ghasroddashti et al. (2012), as the overall treatment setup and delivery has to be considered. They found in the case of IMRT, increasing the dose rate leads to a 4% -7% increase in MU per 100 MU/min increase, which on its own led to an increase in treatment time; however, this was offset by the increased dose rate and reduced overall treatment time. The acceleration of the jaws takes a fraction of a second; the finite acceleration will thus have a negligible effect on the overall treatment time (Svensson et al., 1994). Thus, the dose delivered is dependent on the speed of the jaws.

5.3.2 Motor Control for variable collimator

For the motor selection a number of factors needed to be considered, with the four main factors being the speed of the motor, the torque of the motor and the position control and the frictional forces that the motor needed to overcome. The Maxon high precision pencil motors were used for drive the collimating jaws. These motors, in turn, were controlled by an

Arduino Uno R3. The Arduino Uno was used to control the speed for the jaw motors, through the L293D integrated circuit. The L293D is a monolithic integrated circuit (IC), high voltage, high current, push-pull 4-channel driver which can be used with DC motors and power supplies of up to 25 Volts. The L293D chip can supply a maximum current of 600mA per channel and is designed to accept standard diode-transistor logic (DTL) or transistor-transistor logic (TTL) levels. This IC is a type of H-Bridge, which is an electrical circuit that enables a voltage to be applied across a load in either direction to an inductive load such as relay solenoids and motor.

5.4 Automated Couch Movement

The concept that was proposed made use of an automated moving couch to position and move the "patient" (which in our experiments was the Rando phantom) into the required position during the course of treatment. For simulation purposes, the gantry and collimator movements were kept as small as possible. This is because the software that was developed was only for the treatment couch movements and did not incorporate the gantry and collimator positions. Bel et al. (2000) and Brock et al. (2002) have looked at the computer-controlled couch movement for "patient" setup adjustment. Even though the overall couch movements required for the new technique were much larger than those generally required for the setup corrections, the work done by Bel et al. (2000) and Brock et al. (2002) was used as a reference for the software design for the couch movements.

5.5 Collision avoidance

The treatment technique required the rotation of the treatment couch rotations as well as the rotation of the gantry in order to get the required dose distributions due to noncoplanar electron fields. It was also essential to determine what the limits are in the rotation of the couch and gantry, to avoid collision of the linac components and the patient. The approach taken was to create a visual collision avoidance chart, which would aid in the treatment planning process.

Although Becker et al. (2013) looked at the collision indicator charts for a Siemens linac. It was not easy to make a direct comparison with the work done here, as the linac and treatment table models and configurations were different. The attachment of the electron applicator was not part of the study by Becker et al. (2013). The collimator and treatment table considered by Becker et al. (2013) was a 160-leaf multileaf collimator and a 550 TXT table, in contrast to 58-leaf multileaf collimator and ZXT treatment table used in this study.

5.6 Treatment of Rando Phantom

When commissioning electron beams, water phantoms, which are homogeneous, are used because water is tissue equivalent and practical for acquiring beam data. However, the homogeneous media is quite different from the human body, which is made up of tissues of different densities and air cavities, which can result in the creation of hot or cold regions if not accounted for. Electrons tend to scatter more into low-density material, resulting in less dose in the adjacent high-density material, as much as 10% (Gerbi, 2006). As a result, heterogeneous corrections are required to get a more accurate dose distribution and raise the need for dosimetry measurements using the Rando phantom. Investigations were carried out using an anthropomorphic phantom for the dosimetric evaluation. This was done to check the adequacy of the electron dose distribution for the technique. Simulations of the actual treatment and testing of the technique were done using the anthropomorphic phantom, with the gantry and collimator being in the corresponding position. Due to a lack of lateral scatter of small fields and at the field edges, even for larger fields, the field size on the surface needs to be large enough to ensure that at depth, the target volume is covered by the 90% isodose curve, especially for high electron beam energies, as indicated in Figure 4.54. With the automated table movement, it was important to go into the treatment room and verify the "patient" position and manually adjust the gantry and collimator position.

CHAPTER 6

CONCLUSION AND RECOMMENDATIONS

Electron beam therapy continues to play an important role in the treatment of breast cancer, and more so in treating the mastectomy scar after surgery to decrease local resurgence.

The proof of concept was carried out in developing a technique for treating mastectomy scars that used a variable collimator and automated treatment table. This treatment technique is an alternative to conventional treatment techniques that use lead and Wood's alloy electron cut-outs. This technique does away with the need for a mould room with its associated challenges of staffing, health risks and financial burden. Cerrobend and mild steel are the two metals initially considered in developing the variable collimator. Mild steel was used for the construction of the prototype of the collimator as it was readily available in the department. Cerrobend would have required less thickness to limit the transmission of the electron beam; however, it is a soft metal which is not as strong as steel. The collimator was constructed from steel, which is stronger than Cerrobend. To optimize the collimator and make it more streamlined and efficient, the construction of the collimator using other metals, such as brass and aluminium, will have to be considered. The choice of metal will have to be such that it has the right atomic number so as not to contribute significantly to bremsstrahlung production and not too low to require increased thickness to limit the transmission of electrons.

Measurements were conducted to characterise the electron beam with the variable collimator, including dose profiles and virtual source position measurements. Large dosimetry errors can be introduced if the source is assumed to be at the electron window, scattering foil or any other component. For broad field sizes at high electron beam energies, the virtual source position does not vary significantly, however for small fields it does. Therefore, the virtual source position must be measured for all the energies and field sizes required for electron beam treatment.

The full integration of this technique with the planning system with an electron Monte Carlo algorithm will allow for more elegant treatment plans, to better conform the dose to the target volume and spare the treatment of normal tissue. For the technique to be fully integrated into the planning system, a required feature will be for the treatment planning system to track the moving collimator jaws. Also, certain aspects of this technique will have to be made generic to port the technique onto other platforms. Although the current study focused on the treatment of the mastectomy scar, the use of this technique can be extended to other treatment sites. The technique can be used as an adjunct or primary therapy however for this study, it was considered as a boost treatment. A radiation algorithm for breast cancer treatment is shown in Figure 6.1, to give a guide as to when the variable collimator can be used.

The comprehensive system development to include the synchronisation of the table movement with the rotation of the gantry and collimator movement was beyond the scope of this work. For this technique to have the full synchronisation of the table, collimator and gantry in delivering a given plan, will require the treatment planning system to incorporate this feature. The technique will require collision avoidance technologies to be utilised to ensure staff and patient safety and that equipment is not damaged. As part of this, collision avoidance charts can be incorporated into the treatment planning system software to assist the planner as they develop the treatment plan.

With this novel work, the next step would be the consideration of securing a patent; this phase was outside the scope of this work. The technique, with its various components, needs some modifications and refinements; however, the overall concept is sound and robust. In conclusion, the work done makes this treatment technique a viable treatment solution for patients who have undergone mastectomy and require radiotherapy treatment for the mastectomy scar. The technique can be used in place of electron cutouts, which are used for treating the mastectomy scar.
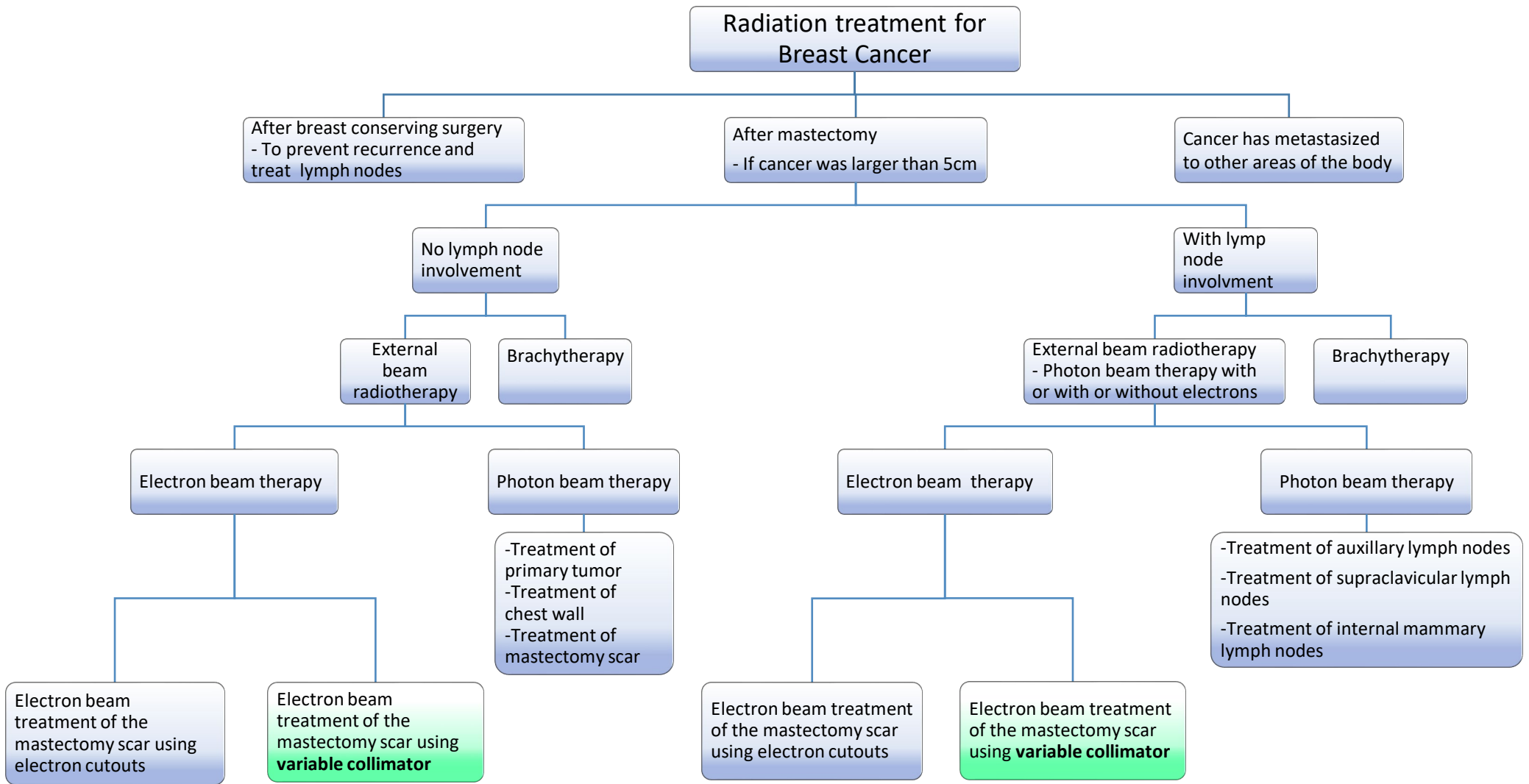
Figure 6.1 *Radiation algorithm of breast cancer treatment*

112

A limitation of this study was more work should have been done to determine dosimetric differences between square fields versus circular fields, including cross-plane and in-plane measurements for the beam profiles. Another shortcoming is that, for the most part, the Advanced Markus chamber was the detector that was used for measurements. Some of the measurements would have benefited from comparison measurements using detectors such as the diode or diamond detectors as well as film. Additional work will be required before the collimator is commissioned for clinical use.

REFERENCES

AAPM & IAEA 2017. Dosimetry of Small Static Fields Used in External Beam Radiotherapy. An International Code of Practice for Reference and Relative Dose Determination.

ADAMS, G., BERNIER, J., EUROPEAN SOCIETY FOR THERAPEUTIC, R. & ONCOLOGY 1995. *Radiation Oncology, 1895-1995 : A Century of Progress and Achievement,* Belgium, ESTRO.

AJITHKUMAR, T. V. & EADENS, M. 2011. Breast Cancer. *In:* AJITHKUMAR, T. V., COOK, N., BARRETT, A. & HATCHER, H. (eds.) *Oxford desk reference: oncology.* Oxford University Press.

AL-YAHYA, K., VERHAEGEN, F. & SEUNTJENS, J. 2007. Design and dosimetry of a few leaf electron collimator for energy modulated electron therapy. *Medical Physics,* 34**,** 4782.

AL ASMARY, M. & RAVIKUMAR, M. 2010. Position of effective electron source for shielded electron beams from a therapeutic linear accelerator. *Polish Journal of Medical Physics And Engineering,* 16**,** 11-21.

ALEXANDER, A., SOISSON, E., HIJAL, T., SARFEHNIA, A. & SEUNTJENS, J. 2011. Comparison of modulated electron radiotherapy to conventional electron boost irradiation and volumetric modulated photon arc therapy for treatment of tumour bed boost in breast cancer. *Radiotherapy and Oncology,* 100**,** 253-258.

ALFONSO, R., ANDREO, P., CAPOTE, R., HUQ, M. S., KILBY, W., KJÄLL, P., MACKIE, T., PALMANS, H., ROSSER, K. & SEUNTJENS, J. 2008. A new formalism for reference dosimetry of small and nonstandard fields. *Medical physics,* 35**,** 5179-5186.

ALLURI, P. & JAGSI, R. 2018. Postmastectomy Radiotherapy. *The Breast: Comprehensive Management of Benign and Malignant Diseases.* Elsevier.

ALMOND, P. 1976. Radiation physics of electron beams. *Clinical applications of the electron beam.* Wiley New York.

ALMOND, P. R., BIGGS, P. J., COURSEY, B. M., HANSON, W., HUQ, M. S., NATH, R. & ROGERS, D. 1999. AAPM's TG-51 protocol for clinical reference dosimetry of high-energy photon and electron beams. *Medical physics,* 26**,** 1847-1870.

ANDRES, A.-C. 2009. New perspectives for therapy choice. *In:* CASTIGLIONE, M. & PICCART, M. J. (eds.) *Adjuvant Therapy for Breast Cancer.* New York: Springer.

ARDUINO.CC. 2018. *Arduino* [Online]. Available: https://www.arduino.cc/ [Accessed 2018].

ARIEL, I. M. & CLEARY, J. B. 1987. *Breast cancer : diagnosis & treatment,* New York, McGraw-Hill.

ASHENAFI, M. M. S., BOYD, R. A. P. D., LEE, T. K. P. D., LO, K. K. M. D. P. D., GIBBONS, J. P. P. D., ROSEN, I. I. P. D., FONTENOT, J. D. P. D. & HOGSTROM, K. R. P. D. 2010. Feasibility of Postmastectomy Treatment With Helical TomoTherapy. *International Journal of Radiation Oncology, Biology, Physics,* 77**,** 836-842.

AZODI, M. Z., ARDESTANI, H., DOLAT, E., MOUSAVI, M., FAYAZFAR, S. & SHADLOO, A. 2012. Breast cancer: Genetics, risk factors, molecular pathology and treatment. *Journal of Paramedical Sciences,* 4.

BARRETT, A., DOBBS, J., MORRIS, S. & ROQUES, T. 2009. *Practical radiotherapy planning,* London, Hodder Arnold.

BARRIO, A. V. & CODY, H. S. 2018. Bilateral Breast Cancer. *The Breast: Comprehensive Management of Benign and Malignant Diseases.* Elsevier.

BAUM, M. 1986. The history of breast cancer. *In:* FORBES, J. F. (ed.) *Breast Disease.* Edinburgh ;: Churchill Livingstone.

BECKER, S. J. 2011. Collision indicator charts for gantry-couch position combinations for Varian linacs. *Journal of applied clinical medical physics,* 12**,** 16-22.

BECKER, S. J., CULBERSON, W. & FLYNN, R. T. 2013. Collision indicator charts for gantry-couch position combinations for Siemens ONCOR and Elekta Infinity linacs. *Journal of applied clinical medical physics,* 14**,** 278-283.

BEL, A., PETRASCU, O., VAN DE VONDEL, I., COPPENS, L., LINTHOUT, N., VERELLEN, D. & STORME, G. 2000. A computerized remote table control for fast on-line patient repositioning: Implementation and clinical feasibility. *Medical Physics,* 27**,** 354-358.

BELLON, J. R., WONG, J. S., MACDONALD, S. M. & HO, A. Y. 2016. *Radiation Therapy Techniques and Treatment Planning for Breast Cancer*, Springer International Publishing.

BIGGS, P. J., BOYER, A. L. & DOPPKE, K. P. 1978. Electron dosimetry of irregular fields on the clinac-18. *International Journal of Radiation Oncology, Biology, Physics: Supplement 2,* 4**,** 77-78.

BLAND, K. I., COPELAND III, E. M. & KLIMBERG, V. S. 2018. History of the therapy of breast cancer. *The Breast: Comprehensive Management of Benign and Malignant Diseases.* Elsevier.

BOVA, F. J. 1995. Clinical Electron Beam Physics. *In:* SMITH, A. R. (ed.) *Radiation Therapy Physics.* Springer.

BOYER, A., BIGGS, P., GALVIN, J., KLEIN, E., LOSASSO, T., LOW, D., MAH, K. & YU, C. 2001. Basic applications of multileaf collimators. American Association of Physicists in Medicine.

BOYLE, F. M. 2009. Multidisciplinary Care: Optimising team performance. *In:* CASTIGLIONE, M. & PICCART, M. J. (eds.) *Adjuvant Therapy for Breast Cancer.* New York: Springer.

BRAY, F., FERLAY, J., SOERJOMATARAM, I., SIEGEL, R. L., TORRE, L. A. & JEMAL, A. 2018. Global cancer statistics 2018: GLOBOCAN estimates of incidence and mortality worldwide for 36 cancers in 185 countries. *CA: a cancer journal for clinicians,* 68**,** 394-424.

BROCK, K. K., MCSHAN, D. L. & BALTER, J. M. 2002. A comparison of computer-controlled versus manual on-line patient setup adjustment. *J Appl Clin Med Phys,* 3**,** 241-7.

BUCHHOLZ, T. A. 2005. Breast Cancer. *In:* CHAO, K. S. C., APISARNTHANARAX, S. & OZYIGIT, G. (eds.) *Practical essentials of intensity modulated radiation therapy.* 2nd ed.

x, 362 pages : illustrations (some color) ; 29 cm ed. Philadelphia: Lippincott Williams & Wilkins.

BUCHHOLZ, T. A., STORM, E. A. & MCNEESE, M. D. 2010. The breast. *In:* COX, J. D. & ANG, K. K. (eds.) *Radiation oncology : rationale, technique, results.* 9th ed. / ed. Philadelphia: Mosby.

BUCHHOLZ, T. A., WAZER, D. E. & HAFFTY, B. G. 2013. Breast Cancer: Locally Advanced and Recurrent Disease, Postmastectomy Radiation, Systemic Therapies. *In:* HALPERIN, E. C., WAZER, D. E., PEREZ, C. A. & BRADY, L. W. (eds.) *Perez and Brady's Principles and Practice of Radiation Oncology.* 6 ed. Philadelphia, PA 19103 USA: Lippincott Williams & Wilkins.

CALVO, F. A., MEIRINO, R. M., MATA, M. D. D. L., SERRANO, F. J. & GALVEZ, M. 2008. Intraoperaive Radiotherapy. *In:* HALPERIN, E. C., PEREZ, C. A. & BRADY, L. W. (eds.) *Perez and Brady's Principles and Practice of Radiation Oncology.* Philadelphia, PA 19106 USA: Lippincott Williams & Wilkins.

CASANOVA BORCA, V., PASQUINO, M., RUSSO, G., GROSSO, P., CANTE, D., SCIACERO, P., GIRELLI, G., LA PORTA, M. R. & TOFANI, S. 2013. Dosimetric characterization and use of GAFCHROMIC EBT3 film for IMRT dose verification. *J Appl Clin Med Phys,* 14**,** 4111.

CHAO, K. C., PEREZ, C. A. & BRADY, L. W. 2002. *Radiation Oncology: Management Decisions,* Philadelphia, PA 19106 USA, Lippincott Williams & Wilkins.

CONVERY, D. & ROSENBLOOM, M. 1992. The generation of intensity-modulated fields for conformal radiotherapy by dynamic collimation. *Physics in medicine & biology,* 37**,** 1359.

COZZI, L., LOHR, F., FOGLIATA, A., FRANCESCHINI, D., DE ROSE, F., FILIPPI, A., GUIDI, G., VANONI, V. & SCORSETTI, M. 2017. Critical appraisal of the role of volumetric modulated arc therapy in the radiation therapy management of breast cancer. *Radiation Oncology,* 12**,** 200.

CRICHLOW, R. & EVANS, D. B. 1987. Cancer in the male breast. *In:* ARIEL, I. M. & CLEARY, J. B. (eds.) *Breast Cancer : Diagnosis & Treatment.* New York: McGraw-Hill.

DANDAPANI, S. V. 2017. Biomarkers and Radiotherapy. *In:* WONG, J. Y. C., SCHULTHESIS, T. E. & RADANY, E. H. (eds.) *Advances in Radiation Oncology.* Springer.

DAS, I. J., COIA, L. R. & TABATA, T. 1995. Harvesting Backscatter Electrons for Radiation Therapy. *Int J Radiat Oncol Biol Phys*.

DEL REGATO, J. A. 1996. One hundred years of radiation oncology. *In:* TOBIAS, J. & THOMAS, P. (eds.) *Current radiation oncology. Volume 2.* Great Britain: Edward Arnold.

DEPAUW, N., BATIN, E., DAARTZ, J., ROSENFELD, A., ADAMS, J., KOOY, H., MACDONALD, S. & LU, H.-M. 2015. A Novel Approach to Postmastectomy Radiation Therapy Using Scanned Proton Beams. *International Journal of Radiation Oncology*Biology*Physics,* 91**,** 427-434.

DIXON, J. M. & SAINSBURY, R. 2012. Breast Cancer: Treatment of elderly patients and uncommon conditions. *In:* DIXON, J. M. (ed.) *ABC of Breast Diseases.* 4th ed.: Wiley.

DONMEZ KESEN, N., CAKIR, A., OKUTAN, M. & BILGE, H. 2014. Research of dosimetry parameters in small electron beams. *Science and Technology of Nuclear Installations,* 2014.

DU PLESSIS, F. C. P., LEAL, A., STATHAKIS, S., XIONG, W. & MA, C. M. 2006. Characterization of megavoltage electron beams delivered through a photon multi-leaf collimator (pMLC). *Physics in Medicine and Biology,* 51**,** 2113-2129.

ELDIB, A., JIN, L., LI, J. & MA, C. M. 2013. Feasibility of replacing patient specific cutouts with a computer-controlled electron multileaf collimator. *Physics in Medicine and Biology,* 58**,** 5653-72.

ELENA, N., JAMES, L. B. & STEVE, W. 2003. Patient-specific planning for prevention of mechanical collisions during radiotherapy. *Physics in Medicine and Biology,* 48**,** N313-N321.

ENGENHART-CABILLIC, R. & WAMBERSIE, A. 1998. *Fast neutron and high-LET particles in cancer therapy,* Berlin ;, Springer.

EXPÓSITO, M. R., ROMERO-HERMIDA, M. I., TERRÓN, J. A., ESPOSITO, D., PLANES, D., LAGARES, J. I., SÁNCHEZ-NIETO, B., AMGAROU, K., DOMINGO, C., GÓMEZ, F., ROSELLÓ, J. & SÁNCHEZ-DOBLADO, F. 2013. Neutron Contamination in Medical Linear Accelerators Operating at Electron Mode. *World Congress on Medical Physics and Biomedical Engineering May 26-31, 2012, Beijing, China.* Springer Berlin Heidelberg : Berlin, Heidelberg.

FERLAY, J., SOERJOMATARAM, I., ERVIK, M., DIKSHIT, R., ESER, S., MATHERS, C., REBELO, M., PARKIN, D., FORMAN, D. & BRAY, F. 2013. GLOBOCAN 2012 v1.0, Cancer Incidence and Mortality Worldwide: IARC CancerBase No. 11 [Internet]. International Agency for Research on Cancer, Lyon, France.

FISHER, B., ANDERSON, S., BRYANT, J., MARGOLESE, R. G., DEUTSCH, M., FISHER, E. R., JEONG, J.-H. & WOLMARK, N. 2002. Twenty-year follow-up of a randomized trial comparing total mastectomy, lumpectomy, and lumpectomy plus irradiation for the treatment of invasive breast cancer. *New England Journal of Medicine,* 347**,** 1233-1241.

FOGLIATA, A., SEPPÄLÄ, J., REGGIORI, G., LOBEFALO, F., PALUMBO, V., DE ROSE, F., FRANCESCHINI, D., SCORSETTI, M. & COZZI, L. 2017. Dosimetric trade-offs in breast treatment with VMAT technique. *The British journal of radiology,* 90**,** 20160701.

FOWBLE, B., BEVAN, A., ALVARADO, M. & MELISKO, M. 2010. Cancer of the Breast. *In:* HOPPE, R., PHILLIPS, T. L. & ROACH, M. (eds.) *Leibel and Phillips Textbook of Radiation Oncology.* 3rd ed.: Elsevier-Saunders.

GAFFNEY, D. K. 2013. *Radiation oncology : imaging and treatment,* Salt Lake City, Utah, Amirsys.

GAFFNEY, D. K., LEAVITT, D. D., TSODIKOV, A., SMITH, L., WATSON, G., PATTON, G., GIBBS, F. A. & STEWART, J. R. 2001. Electron arc irradiation of the postmastectomy chest wall with CT treatment planning: 20-year experience. *International journal of radiation oncology, biology, physics,* 51**,** 994-1001.

GAUER, T., ALBERS, D., CREMERS, F., HARMANSA, R., PELLEGRINI, R. & SCHMIDT, R. 2006. Design of a computer-controlled multileaf collimator for advanced electron radiotherapy. *Physics in Medicine and Biology,* 51**,** 5987-6003.

GERBI, B. J. 2006. Clinical Applications of High-Energy Electrons. *In:* LEVITT, S. H., PURDY, J. A., PEREZ, C. A. & VIJAYAKUMAR, S. (eds.) *Technical Basis of Radiation Therapy: Practical Clinical Applications.* Germany: Springer.

GERBI, B. J., ANTOLAK, J. A., DEIBEL, F. C., FOLLOWILL, D. S., HERMAN, M. G., HIGGINS, P. D., HUQ, M. S., MIHAILIDIS, D. N., YORKE, E. D., HOGSTROM, K. R. & KHAN, F. M. 2009. Recommendations for clinical electron beam dosimetry: supplement to the recommendations of Task Group 25. *Medical physics,* 36**,** 3239-79.

GHASRODDASHTI, E., SMITH, W., QUIRK, S. & KIRKBY, C. 2012. Clinical consequences of changing the sliding window IMRT dose rate. *Journal of applied clinical medical physics,* 13**,** 4-12.

GIAP, H. & GIAP, B. 2012. Historical perspective and evolution of charged particle beam therapy. *Translational Cancer Research,* 1**,** 127-136.

GIBBONS, J. P., ANTOLAK, J. A., FOLLOWILL, D. S., HUQ, M. S., KLEIN, E. E., LAM, K. L., PALTA, J. R., ROBACK, D. M., REID, M. & KHAN, F. M. 2014. Monitor unit calculations for external photon and electron beams: Report of the AAPM Therapy Physics Committee Task Group No. 71. *Medical physics,* 41.

GOSSELIN, M., PODGORSAK, E. B. & EVANS, M. D. 1994. Dosimetry of centrally shielded electron beams. *Medical physics,* 21**,** 1245-1249.

GREENE, D. 1986. *Linear accelerators for radiation physics*, Adam Hilger Ltd.

GRIEM, K. L. & HARDIN, P. B. 1998. Breast Cancer. *In:* KHAN, F. M. & POTISH, R. A. (eds.) *Treatment planning in radiation oncology.* 1st Ed ed. Baltimore: Williams & Wilkins.

GUND, K. & PAUL, W. 1950. Experiments with a 6-MeV Betatron. *Nucleonics,* 7**,** 36-45.

GUNDERSON, L. L., HADDOCK, M. G., KAPP, D. S., MILLER, R. C., CALLISTER, M. D. & GOTTSCHALK, A. 2010. Intraoperative Radiation Therapy. *In:* HOPPE, R., PHILLIPS, T. L. & ROACH, M. (eds.) *Leibel and Phillips Textbook of Radiation Oncology.* Third ed.: Elsevier-Saunders.

HAAS, L. L., HARVEY, R. A., LAUGHLIN, J. S., BEATTIE, J. W. & HENDERSON, W. J. 1954. Medical aspects of high energy electron beams. *The American journal of roentgenology, radium therapy, and nuclear medicine,* 72**,** 250-9.

HAFFTY, B. G. 2003. The role of radiation therapy in breast cancer management. *In:* NABHOLTZ, J.-M., TONKIN, K., AAPRO, M. S. & REESE, D. M. (eds.) *Breast Cancer Management: Application of Clinical and Translational Evidence to Patient Care.* 2nd ed.: Lippincott Williams & Wilkins.

HARRIS, J. R., LIPPMAN, M. E., OSBORNE, C. K. & MORROW, M. 2012. *Diseases of the Breast*, Wolters Kluwer Health.

HAUG, E. 1975. Bremsstrahlung and pair production in the field of free electrons. *Zeitschrift für Naturforschung A,* 30, 1099-1113.

HAUSSMANN, J., CORRADINI, S., NESTLE-KRAEMLING, C., BÖLKE, E., NJANANG, F. J. D., TAMASKOVICS, B., ORTH, K., RUCKHAEBERLE, E., FEHM, T., MOHRMANN, S., SIMIANTONAKIS, I., BUDACH, W. & MATUSCHEK, C. 2020. Recent advances in radiotherapy of breast cancer. *Radiation Oncology,* 15**,** 71.

HOGSTROM, K. R. & ALMOND, P. R. 2006. Review of electron beam therapy physics. *Phys Med Biol,* 51**,** R455-89.

HOGSTROM, K. R., MILLS, M. D. & ALMOND, P. R. 1981. Electron beam dose calculations. *Physics in Medicine & Biology,* 26**,** 445.

HOGSTROM, K. R., STEADHAM, R. E., WONG, P.-F. & SHIU, A. S. 2000. Monitor Unit Calculations for Electron Beams. *In:* GIBBONS, J. P. & SOUTH EAST, A. C. S. (eds.) *Monitor Unit Calculations for External Photon and Electron Beams.* Madison, WI: Advanced Medical Pub.

HORST, K. C., HAFFTY, B. G., HARRIS, E. E. R., BAILEY, L., BELLON, J. R., CAREY, L., FREEDMAN, G. M., GOYAL, S., HALYARD, M. Y., MACDONALD, S. M., MORAN, M. S. & SUH, W. W. 2012. American College of Radiology ACR Appropriateness Criteria: PostmastectomyRadiotherapy.

HUIZENGA, H. & STORCHI, P. R. M. 1985. The Use of Computed-Tomography Numbers in Dose Calculations for Radiation-Therapy. *Acta Radiologica Oncology,* 24**,** 509-519.

HUMM, J. L., PIZZUTO, D., FLEISCHMAN, E. & MOHAN, R. 1995. Collision detection and avoidance during treatment planning. *International Journal of Radiation Oncology • Biology • Physics,* 33**,** 1101-1108.

HUSTON, T. L. & SIMMONS, R. M. 2005. Emerging Local Treatment Modalities for Breast Cancer. *In:* ROSES, D. F. (ed.) *Breast cancer.* 2nd ed. ed. Edinburgh: Churchill Livingstone.

IARC 2018. Latest global cancer data: Cancer burden rises to 18.1 million new cases and 9.6 million cancer deaths in 2018. *International Agency for Research on Cancer,* World Health Organisation: PRESS RELEASE N° 263.

ICRU 1970. Linear Energy Transfer, Report No. 16. *International Commission on Radiation Units and Measurements, Washington, DC*.

ICRU 1974. *Radiation dosimetry : electrons with initial energies between 1 and 50 MeV, Report 21,* Washington, D.C., International Commission on Radiation Units and Measurements.

ICRU 1984. Radiation Dosimetry: Electron Beams with Energies Between 1 and 50 MeV, Report 35. Bethesda, Maryland, USA: International Commission on Radiation Units and Measurements.

ICRU 1989. *Tissue Substitutes in Radiation Dosimetry and Measurement*, International Commission on Radiation Units and Measurements.

ICRU 2004. Prescribing, recording, and reporting electron beam therapy, Report 71. International Commission on Radiation Units.

IKTUEREN, B., BILGE, H., KARACAM, S. & ATKOVAR, G. 2012. The peripheral dose outside the applicator in electron beams of Oncor linear accelerator. *Radiation protection dosimetry,* 150**,** 192-7.

ITO, S., PARKER, B. C., LEVINE, R., SANDERS, M. E., FONTENOT, J., GIBBONS, J. & HOGSTROM, K. 2011. Verification of calculated skin doses in postmastectomy helical tomotherapy. *International Journal of Radiation Oncology* Biology* Physics,* 81**,** 584-591.

JAIN, S. & GRADISHAR, W. J. 2018. Male breast cancer. *The Breast.* Elsevier.

JAMSHIDI, A., KUCHNIR, F. T. & REFT, C. S. 1986. Determination of the source position for the electron beams from a high-energy linear accelerator. *Medical physics,* 13**,** 942-948.

JANSSON, T., LINDMAN, H., NYGÅRD, K., DAHLGREN, C. V., MONTELIUS, A., ÖBERG-KREUGER, C., ASPLUND, S. & BERGH, J. 1998. Radiotherapy of breast cancer after breast-conserving surgery: an improved technique using mixed electron–photon beams with a multileaf collimator. *Radiotherapy and Oncology,* 46**,** 83-89.

JAYARAMAN, S. & LANZL, L. H. 1996. *Clinical Radiotherapy Physics: Treatment Planning and Radiation Safety*, Taylor & Francis.

JIMENEZ, R. B., GOMA, C., NYAMWANDA, J., KOOY, H. M., HALABI, T., NAPOLITANO, B. N., MCBRIDE, S. M., TAGHIAN, A. G., LU, H.-M. & MACDONALD, S. M. 2013. Intensity modulated proton therapy for postmastectomy radiation of bilateral implant reconstructed breasts: A treatment planning study. *Radiotherapy and Oncology,* 107**,** 213-217.

JIN, L., MA, C. M., FAN, J., ELDIB, A., PRICE, R. A., CHEN, L., WANG, L., CHI, Z., XU, Q., SHERIF, M. & LI, J. S. 2008. Dosimetric verification of modulated electron radiotherapy delivered using a photon multileaf collimator for intact breasts. *Phys Med Biol,* 53**,** 6009-25.

JOHNS, H. & CUNNINGHAM, J. 1983. *The Physics of Radiology 4th edn (Springfield, IL: Thomas)*.

KARZMARK, C. & PERING, N. C. 1973. Electron linear accelerators for radiation therapy: history, principles and contemporary developments. *Physics in Medicine & Biology,* 18**,** 321.

KEYNES, G. 1928. Radium Treatment of Primary Carcinoma of the Breast. *The Lancet,* 212**,** 108-111.

KHAN, F. M. 2003. *The Physics of Radiation Therapy,* Philadelphia, PA 19106 USA, Lipincott Williams & Wilkins.

KHAN, F. M. (ed.) 2007. *Treatment Planning in Radiation Oncology,* Philadelphia, PA 19106 USA: Lippincott Williams & Wilkins.

KHAN, F. M., DOPPKE, K. P., HOGSTROM, K. R., KUTCHER, G. J., NATH, R., PRASAD, S. C., PURDY, J. A., ROZENFELD, M. & WERNER, B. L. 1991. Clinical electron-beam dosimetry: Report of AAPM Radiation Therapy Committee Task Group No. 25. *Medical Physics,* 18**,** 73-109.

KHAN, F. M., HIGGINS, P. D., GERBI, B. J., DEIBEL, F. C., SETHI, A. & MIHAILIDIS, D. N. 1998. Calculation of depth dose and dose per monitor unit for irregularly shaped electron fields. *Physics in Medicine and Biology,* 43**,** 2741-2754.

KHAN, F. M. & MCNEESE, M. D. 1999. Electron Beam Therapy. *In:* LEVITT, S. H., PURDY, J. A., PEREZ, C. A. & VIJAYAKUMAR, S. (eds.) *Technical Basis of Radiation Therapy: Practical Clinical Applications.* 3rd, illustrated ed.

KHAN, F. M., SEWCHAND, W. & LEVITT, S. H. 1978. Effect of air space on depth dose in electron beam therapy. *Radiology,* 126**,** 249-251.

KIROVA, Y. M., CAMPANA, F., FOURNIER-BIDOZ, N., STILHART, A., DENDALE, R., BOLLET, M. A. & FOURQUET, A. 2007. Postmastectomy Electron Beam Chest Wall Irradiation in Women With Breast Cancer: A Clinical Step Toward Conformal Electron Therapy. *International Journal of Radiation Oncology, Biology and Physics,* 69.

KLEIN, E. E. & KASHANI, R. 2013. Electron-Beam Therapy Dosimetry, Treatment Planning, and Techniques. *In:* HALPERIN, E. C., WAZER, D. E., PEREZ, C. A. & BRADY, L. W. (eds.) *Perez and Brady's Principles and Practice of Radiation Oncology.* 6 ed. Philadelphia, PA 19103 USA: Lippincott Williams & Wilkins.

KLEVENHAGEN, S. 1985. Physics of electron beam therapy.

KLEVENHAGEN, S. C. 1993. *Physics and dosimetry of therapy electron beams,* Madison, Wis., Medical Physics Pub.

KÖHN, C., EBERT, U. & MANGIAROTTI, A. 2014. The importance of electron–electron bremsstrahlung for terrestrial gamma-ray flashes, electron beams and electron–positron beams. *Journal of Physics D: Applied Physics,* 47.

KUDCHADKER, R. J., HOGSTROM, K. R., GARDEN, A. S., MCNEESE, M. D., BOYD, R. A. & ANTOLAK, J. A. 2002. Electron conformal radiotherapy using bolus and intensity modulation. *International Journal of Radiation Oncology*Biology*Physics,* 53**,** 1023-1037.

KUNKLER, I. H. 2003. Breast. *In:* BOMFORD, C. K., KUNKLER, I. H. & WALTER, J. (eds.) *Walter and Miller's textbook of radiotherapy : radiation physics, therapy and oncology ; foreword by B.W. Hancock.* 6th ed. / ed. Edinburgh: Churchill Livingstone.

KUNKLER, I. H. 2012. Breast. *In:* SYMONDS, P., DEEHAN, C., MILLS, J., MEREDITH, C., WALTER, J. & BOMFORD, C. K. (eds.) *Walter and Miller's Textbook of radiotherapy : radiation physics, therapy, and oncology.* 7th ed. ed. Edinburgh: Elsevier Ltd.

KURUP, R., GLASGOW, G. & LEYBOVICH, L. 1993. Design of electron beam wedges for increasing the penumbra of abutting fields. *Physics in Medicine & Biology,* 38**,** 667.

KURUP, R. G., GLASGOW, G. P. & LEYBOVICH, L. 1995. Output factors for irregularly shaped electron fields. *Medical Dosimetry,* 20**,** 155-159.

LACEY, J. V., JR., KREIMER, A. R., BUYS, S. S., MARCUS, P. M., CHANG, S. C., LEITZMANN, M. F., HOOVER, R. N., PROROK, P. C., BERG, C. D. & HARTGE, P. 2009. Breast cancer epidemiology according to recognized breast cancer risk factors in the Prostate, Lung, Colorectal and Ovarian (PLCO) Cancer Screening Trial Cohort. *BMC Cancer,* 9**,** 84.

LARAMORE, G. E., PHILLIPS, M. H. & DELANEY, T. F. 2008. Particle Beam Radiotherapy. *In:* HALPERIN, E. C., PEREZ, C. A. & BRADY, L. W. (eds.) *Perez and Brady's Principles and Practice of Radiation Oncology.* 5 ed. Philadelphia, PA 19106 USA: Lippincott Williams & Wilkins.

LAX, I. & BRAHME, A. 1980. Collimation of high energy electron beams. *Acta Radiologica: Oncology,* 19**,** 199-207.

LIEF, E. P., DEWYNGAERT, J. K. & LYMBERS, S. C. 2005. Accelerated concomitant boost. Emerging technology. *In:* MUNDT, A. J. & ROESKE, J. C. (eds.) *Intensity Modulated Radiation Therapy: A Clinical Perspective.* BC Decker Inc London.

LIEF, E. P., LO, Y.-C. & HUMM, J. L. 1998. Electron wedges for radiation therapy. *International Journal of Radiation Oncology* Biology* Physics,* 40**,** 233-243.

LIEF, E. P. & LUTZ, W. R. 2000. Determination of effective electron source size using multislit and pinhole cameras. *Medical physics,* 27**,** 2372-2375.

LILLICRAP, S. C., WILSON, P. & BOAG, J. W. 1975. Dose distributions in high energy electron beams: Production of broad beam distributions from narrow beam data. *Physics in Medicine and Biology,* 20**,** 30-38.

LIN, K.-H., HUANG, C.-Y., LIN, J.-P. & CHU, T.-C. 2002. Surface dose with grids in electron beam radiation therapy. *Applied Radiation and Isotopes,* 56**,** 477-484.

LIU, M., WANG, Q., LIU, B., GAO, L., WU, D., YANG, S., LIU, B. & DONG, L. 2015. Male breast carcinoma: radiotherapy contributed to favorable local control in two cases and related literature review. *European journal of medical research,* 20**,** 94.

LOGANADANE, G., XI, Z., XU, H. P., GRELLIER ADEDJOUMA, N., BAZIRE, L., FOURQUET, A. & KIROVA, Y. M. 2017. Patterns of loco regional failure in women with breast cancer treated by Postmastectomy Conformal Electron Beam Radiation Therapy (PMERT): Large scale single center experience. *Clinical and Translational Radiation Oncology,* 4**,** 46-50.

LOMAX, T., PERDRONI, E., CORAY, D., GOITEIN, G. & JERMANN, M. 2005. Intensity-Modulated Proton Therapy. *In:* MUNDT, A. J. & ROESKE, J. C. (eds.) *Intensity Modulated Radiation Therapy: A Clinical Perspective.* BC Decker Inc London.

LOVE, R. R. 2008. Defining a global research agenda for breast cancer. *Cancer,* 113**,** 2366-2371.

LOW, D. A., STARKSCHALL, G., BUJNOWSKI, S. W., WANG, L. L. & HOGSTROM, K. R. 1992. Electron bolus design for radiotherapy treatment planning: Bolus design algorithms. *Medical Physics,* 19**,** 115-124.

MA, C.-M., DING, M., LI, J. S., LEE, M. C., PAWLICKI, T. & DENG, J. 2003. A comparative dosimetric study on tangential photon beams, intensity-modulated radiation therapy (IMRT) and modulated electron radiotherapy (MERT) for breast cancer treatment. *Physics in Medicine and Biology,* 48**,** 909.

MA, L. 2004. Dosimetric properties of magnetically collimated electron beams for radiation therapy: Magnetically collimated electron beams. *Medical physics,* 31**,** 2973-2977.

MACDONALD, S. M., PATEL, S. A., HICKEY, S., SPECHT, M., ISAKOFF, S. J., GADD, M., SMITH, B. L., YEAP, B. Y., ADAMS, J., DELANEY, T. F., KOOY, H., LU, H.-M. & TAGHIAN, A. G. 2013. Proton Therapy for Breast Cancer After Mastectomy: Early Outcomes of a Prospective Clinical Trial. *International Journal of Radiation Oncology*Biology*Physics,* 86**,** 484-490.

MAGEE, B., RIBEIRO, G., WILLIAMS, P. & SWINDELL, R. 1991. Use of an electron beam for post-mastectomy radiotherapy: 5-year follow-up of 500 cases. *Clinical oncology,* 3**,** 310-314.

MAHDAVI, H., JABBARI, K. & ROAYAEI, M. 2016. Evaluation of various boluses in dose distribution for electron therapy of the chest wall with an inward defect. *Journal of Medical Physics/Association of Medical Physicists of India,* 41**,** 38.

MATNEY, J. E., PARKER, B. C., NECK, D. W., HENKELMANN, G. & ROSEN, I. I. 2010. Evaluation of a commercial flatbed document scanner and radiographic film scanner for radiochromic EBT film dosimetry. *Journal of applied clinical medical physics,* 11**,** 198-208.

MAUGHAN, R. L. & YUDELEV, M. 1999. Neutron therapy. *In:* VAN DYK, J. (ed.) *The modern technology of radiation oncology : a compendium for medical physicists and radiation oncologists.* Madison, Wis.: Medical Physics Pub.

MAYLES, P., NAHUM, A. E. & ROSENWALD, J.-C. 2007. *Handbook of radiotherapy physics : theory and practice,* New York, Taylor & Francis.

MCNEESE, M. D., STORM, E. A., BUCHHOLZ, T. A., LEVITT, S. H. & KHAN, F. M. 1999. Breast Cancer. *In:* LEVITT, S. H., PURDY, J. A., PEREZ, C. A. & VIJAYAKUMAR, S. (eds.) *Technical Basis of Radiation Therapy: Practical Clinical Applications.* 3rd, illustrated ed.: Lippincott Williams & Wilkins.

MILLS, M. D., HOGSTROM, K. R. & ALMOND, P. R. 1982. Prediction of electron beam output factors. *Medical physics,* 9**,** 60-68.

MOHAN, R. & GROSSHANS, D. 2017. Proton therapy − Present and future. *Advanced Drug Delivery Reviews,* 109**,** 26-44.

MONTAGUE, E. D., DELCLOS, L., LICHTMAN, R. R., TAYLOR, S. E. & WOOD, J. V. 1988. Breast. *In:* WITHERS, H. R. & PETERS, L. J. (eds.) *Innovations in Radiation Oncology.* Springer Berlin Heidelberg : Berlin, Heidelberg.

MONTEMAGGI, P., GUERRIERI, P., FEDERICO, M. & MORTELLARO, G. 2008. Clinical Applications of Brachytherapy: Low-Dose-Rate and Pulse-Dose-Rate. *In:* HALPERIN, E. C., PEREZ, C. A. & BRADY, L. W. (eds.) *Perez and Brady's Principles and Practice of Radiation Oncology.* 5 ed. Philadelphia, PA 19106 USA: Lippincott Williams & Wilkins.

MOTWANI, S. B., STROM, E. A., MCNEESE, M. D. & BUCHHOLZ, T. A. 2006. Breast Cancer. *In:* LEVITT, S. H., PURDY, J. A., PEREZ, C. A. & VIJAYAKUMAR, S. (eds.) *Technical Basis of Radiation Therapy: Practical Clinical Applications.* 4, illustrated ed.

NAG, S. & SCRUGGS, G. R. 2013. Clinical Aspects and Applications of High-Dose-Rate Brachytherapy. *In:* HALPERIN, E. C., WAZER, D. E., PEREZ, C. A. & BRADY, L. W. (eds.) *Perez and Brady's Principles and Practice of Radiation Oncology.* 6 ed. Philadelphia, PA 19103 USA: Lippincott Williams & Wilkins.

NAM, J. & MARKS, L. B. 2009. Radiotherapy Techniques. *In:* BLAND, K. I. & COPELAND, E. M. I. (eds.) *The Breast : comprehensive management of benign and malignant diseases. Volume two.* 4th ed. ed. Philadelphia: Saunders/Elsevier.

NAQA, I. E., LI, R. & MURPHY, M. J. 2015. *Machine Learning in Radiation Oncology: Theory and Applications*, Springer International Publishing.

NAROD, S. A. 2014. Bilateral breast cancers. *Nature Reviews Clinical Oncology,* 11**,** 157.

NATIONAL CANCER REGISTRY (NCR) 2014. Cancer in South Africa, 2014 Report.

NATIONAL CANCER REGISTRY (NCR) 2016. Cancer in South Africa, 2016 Report.

NATIONAL CANCER REGISTRY, N. 2018. Cancer in South Africa, 2018 NCR Report.

NATIONAL CANCER REGISTRY, N. 2019. Cancer in South Africa 2019-NCR- Report.

NCRP 1984. Neutron contamination from medical electron accelerators : recommendations of the National Council on Radiation Protection and Measurements. Bethesda, Md.: National Council on Radiation, Protection

Measurements.

NICHOLS, G. P., FONTENOT, J. D., GIBBONS, J. P. & SANDERS, M. E. 2014. Evaluation of volumetric modulated arc therapy for postmastectomy treatment. *Radiation Oncology,* 9**,** 66.

NIEDERHUBER, J. E. 2005. Multimodality Treatment of Breast Cancer. *In:* ROSES, D. F. (ed.) *Breast cancer.* 2nd ed. ed. Edinburgh: Churchill Livingstone.

OLOFSSON, L., KARLSSON, M. G. & KARLSSON, M. 2005. Effects on electron beam penumbra using the photon MLC to reduce bremsstrahlung leakage for an add-on electron MLC. *Physics in medicine and biology,* 50**,** 1191.

PALTA, J. R., BIGGS, P. J., HAZLE, J. D., HUQ, M. S., DAHL, R. A., OCHRAN, T. G., SOEN, J., DOBELBOWER JR, R. R. & MCCULLOUGH, E. C. 1995. Intraoperative electron beam radiation therapy: Technique, dosimetry, and dose specification: Report of task force 48 of the radiation therapy committee, American Association of Physicists in Medicine. *International Journal of Radiation Oncology*Biology*Physics,* 33**,** 725-746.

PERKINS, G. H., MCNEESE, M. D., ANTOLAK, J. A., BUCHHOLZ, T. A., STROM, E. A. & HOGSTROM, K. R. 2001. A custom three-dimensional electron bolus technique for optimization of postmastectomy irradiation. *International Journal of Radiation Oncology* Biology* Physics,* 51**,** 1142-1151.

PIERQUIM, B. & GRIMARD, L. 1989. Radiation therapy as primary treatment. *In:* HOOGSTRATEN, B., BURN, I. & BLOOM, H. J. G. (eds.) *Breast Cancer.* Berlin ;: Springer-Verlag.

POORTMANS, P. 2007. Evidence based radiation oncology: Breast cancer. *Radiotherapy and Oncology,* 84**,** 84-101.

RAGAZ, J., OLIVOTTO, I. A., SPINELLI, J. J., PHILLIPS, N., JACKSON, S. M., WILSON, K. S., KNOWLING, M. A., COPPIN, C. M. L., WEIR, L., GELMON, K., LE, N., DURAND, R., COLDMAN, A. J. & MANJI, M. 2005. Locoregional Radiation Therapy in Patients With High-Risk Breast Cancer Receiving Adjuvant Chemotherapy: 20-Year Results of the British Columbia Randomized Trial. *Journal of the National Cancer Institute,* 97**,** 116-126.

RAVINDRAN, B. P. 1999. A study on virtual source position for electron beams from a Mevatron MD linear accelerator. *Phys Med Biol,* 44**,** 1309-15.

RAVINDRAN, B. P., SINGH, I. R., BRINDHA, S. & SATHYAN, S. 2002. Manual multi-leaf collimator for electron beam shaping--a feasibility study. *Physics in medicine and biology,* 47**,** 4389-96.

RECHT, A. 2009. Postmastectomy Radiotherapy. *In:* BLAND, K. I. & COPELAND, E. M. I. (eds.) *The Breast : comprehensive management of benign and malignant diseases. Volume two.* 4th ed. ed. Philadelphia: Saunders/Elsevier.

RICHERT, J. D., HOGSTROM, K. R., FIELDS, R. S., II, K. L. M. & BOYD, R. A. 2007. Improvement of field matching in segmented-field electron conformal therapy using a variable-SCD applicator. *Physics in Medicine and Biology,* 52**,** 2459.

RODRIGUES, A., YIN, F.-F. & WU, Q. 2013. Dynamic electron arc radiotherapy (DEAR): a feasibility study. *Physics in Medicine & Biology,* 59**,** 327.

RONG, Y., YADAV, P., WELSH, J. S., FAHNER, T. & PALIWAL, B. 2012. Postmastectomy radiotherapy with integrated scar boost using helical tomotherapy. *Medical dosimetry : official journal of the American Association of Medical Dosimetrists,* 37**,** 233-9.

ROSENBERG, I. 2007. Relative dose measurements and commissioning. *In:* MAYLES, P., NAHUM, A. E. & ROSENWALD, J.-C. (eds.) *Handbook of radiotherapy physics : theory and practice.* New York: Taylor & Francis.

ROSES, D. F. 2005. Development of Mordern Breast Cancer Treatment. *In:* ROSES, D. F. (ed.) *Breast Cancer.* 2nd ed. ed. Edinburgh: Churchill Livingstone.

SALGUERO, F. J., PALMA, B., ARRANS, R., ROSELLO, J. & LEAL, A. 2009. Modulated electron radiotherapy treatment planning using a photon multileaf collimator for post-mastectomized chest walls. *Radiotherapy Oncology,* 93**,** 625-32.

SANDISON, G. & HUDA, W. 1989. Is the'fictitious' virtual source a redundant concept for scanned therapeutic electron beams? *Physics in Medicine & Biology,* 34**,** 369.

SCHAEFFER, R., REEVES, H. & ORLAND, H. 1982. Electrodisintegration and photodisintegration of nuclei. *The Astrophysical Journal,* 254**,** 688.

SCHRÖDER-BABO, P. 1983. Determination of the virtual electron source of a betatron. *Acta radiologica. Supplementum,* 364**,** 7-10.

SEDLMAYER, F., DUBOIS, J.-B., REITSAMER, R., FASTNER, G., OLILLA, D. & ORECCHIA, R. 2011. Breast Cancer. *In:* GUNDERSON, L. L., WILLETT, C. G., CALVO, F. A. & HARRISON, L. B. (eds.) *Intraoperative Irradiation: Techniques and Results.* Humana Press.

SELTZER, S. M. & BERGER, M. J. 1985. Bremsstrahlung Spectra from Electron Interactions with Screened Atomic Nuclei and Orbital electrons. *Nuclear Instruments & Methods in Physics Research Section B-Beam Interactions with Materials and Atoms,* 12**,** 95-134.

SHAH, C., AL-HILLI, Z. & VICINI, F. 2021. Advances in Breast Cancer Radiotherapy: Implications for Current and Future Practice. *JCO oncology practice,* 17**,** 697-706.

SHIU, A. S., TUNG, S. S., NYERICK, C. E., OCHRAN, T. G., OTTE, V. A., BOYER, A. L. & HOGSTROM, K. R. 1994. Comprehensive analysis of electron beam central axis dose for a radiotherapy linear accelerator. *Medical Physics,* 21**,** 559-566.

SIEMENS MEDICAL SOLUTIONS USA 2004. ZXT Treatment Table Service. *In:* SIEMENS-MEDICAL-SOLUTIONS-USA (ed.) Service Manual ed.

SIEMENS MEDICAL SOLUTIONS USA 2005. PRIMUS & PRIMUS^PLUS Linear Accelerator User Manual.

SMYTH, G., BAMBER, J. C., EVANS, P. M. & BEDFORD, J. L. 2013. Trajectory optimization for dynamic couch rotation during volumetric modulated arc radiotherapy. *Physics in Medicine & Biology,* 58**,** 8163.

SPIROU, S. V. & CHUI, C. S. 1994. Generation of arbitrary intensity profiles by dynamic jaws or multileaf collimators. *Medical physics,* 21**,** 1031-1041.

STERN, R. L., HEATON, R., FRASER, M. W., GODDU, S. M., KIRBY, T. H., LAM, K. L., MOLINEU, A. & ZHU, T. C. 2011. Verification of monitor unit calculations for non-IMRT clinical radiotherapy: report of AAPM Task Group 114. *Medical physics,* 38**,** 504-530.

STEVENS, R. E. 2005. Radiotherapy for in situ, stage I, stage II breast cancer. *In:* ROSES, D. F. (ed.) *Breast Cancer.* 2nd ed. ed. Edinburgh: Churchill Livingstone.

STEWART, A. J., HALLOWAY, C. L. & DEVLIN, P. M. 2013. Clinical Applications of Brachytherapy: Low Dose Rate and Pulsed-Dose Rate. *In:* HALPERIN, E. C., WAZER, D. E., PEREZ, C. A. & BRADY, L. W. (eds.) *Perez and Brady's Principles and Practice of Radiation Oncology.* 6 ed. Philadelphia, PA 19103 USA: Lippincott Williams & Wilkins.

STEWART, B. & WILD, C. P. 2014. *World cancer report 2014,* World Health Organization.

STRYDOM, W., PARKER, W. & OLIVARES, M. 2005. Electron beams: physical and clinical aspects. *In:* PODGORSAK, E. (ed.) *Radiation oncology physics: a handbook for teachers and students/EB Podgorsak.–Vienna: International Atomic Energy Agency.*

SU, F.-C., LIU, Y., STATHAKIS, S., SHI, C., ESQUIVEL, C. & PAPANIKOLAOU, N. 2007. Dosimetry characteristics of GAFCHROMIC® EBT film responding to therapeutic electron beams. *Applied Radiation and Isotopes,* 65**,** 1187-1192.

SU, S., MORAN, K. & ROBAR, J. L. 2014. Design and production of 3D printed bolus for electron radiation therapy. *Journal of applied clinical medical physics,* 15**,** 194-211.

SUIT, H. 2002. The Gray Lecture 2001: coming technical advances in radiation oncology. *International journal of radiation oncology, biology, physics,* 53**,** 798-809.

SUNG, H., FERLAY, J., SIEGEL, R. L., LAVERSANNE, M., SOERJOMATARAM, I., JEMAL, A. & BRAY, F. 2021. Global Cancer Statistics 2020: GLOBOCAN Estimates of Incidence and Mortality Worldwide for 36 Cancers in 185 Countries. *CA: A Cancer Journal for Clinicians,* 71**,** 209-249.

SVENSSON, R., KALLMAN, P. & BRAHME, A. 1994. An analytical solution for the dynamic control of multileaf collimators. *Physics in Medicine & Biology,* 39**,** 37.

SWEENEY, L. E., GUR, D. & BUKOVITZ, A. G. 1981. Scatter component and its effect on virtual source and electron beam quality. *International Journal of Radiation Oncology Biology Physics,* 7**,** 967-971.

TELLILI, B., ELMAHROUG, Y. & SOUGA, C. 2017. Investigation on radiation shielding parameters of cerrobend alloys. *Nuclear Engineering and Technology,* 49**,** 1758-1771.

THOMAS, S. J. 1988. Virtual Source Distances for Electron-Beams between 5 and 20 Mev. *Physics in Medicine and Biology,* 33**,** 1325-1328.

TOSCAS, J. I., LINERO, D., RUBIO, I., HIDALGO, A., ARNALTE, R., ESCUDÉ, L., COZZI, L., FOGLIATA, A. & MIRALBELL, R. 2010. Boosting the tumor bed from deep-seated tumors in early-stage breast cancer: A planning study between electron, photon, and proton beams. *Radiotherapy and Oncology,* 96**,** 192-198.

TRUMP, J., VAN DE GRAAFF, R. & CLOUD, R. 1940. Cathode rays for radiation therapy. *Am. J. Roentgenol. Radium Therapy & Nuclear Med,* 43**,** 728-734.

TUBIANA, M. & SARRAZIN, D. 1987. The role of postoperative radiotherapy in breast cancer. *In:* ARIEL, I. M. & CLEARY, J. B. (eds.) *Breast Cancer : Diagnosis & Treatment.* New York: McGraw-Hill.

ULIN, K. & PALISCA, M. 1996. The use of scattering foil compensators in electron beam therapy. *International journal of radiation oncology, biology, physics,* 35**,** 785-92.

VAN DER MERWE, D. G. 1994. *The effect of tissue inhomogeneities on the energy spectrum and dosimetry in electron radiation therapy.* University of the Witwatersrand.

VAN DYK, J. 2005. *The modern technology of radiation oncology : a compendium for medical physicists and radiation oncologists,* Madison, Wis., Medical Physics Pub.

VASSIL, A. D. & TENDULKAR, R. D. 2012. Breast Radiotherapy. *In:* VASSIL, A. D. & VIDETIC, G. M. M. (eds.) *Handbook of Treatment Planning in Radiation Oncology.* Special Pharma ed.: Demos Medical Publishing.

VATANEN, T., TRANEUS, E., VÄÄNÄNEN, A. & LAHTINEN, T. 2009. The effect of electron collimator leaf shape on the build-up dose in narrow electron MLC fields. *Physics in Medicine and Biology,* 54**,** 7211-7226.

VINÉS, E., LE PÉCHOUX, C. & ARRIAGADA, R. 2003. Radiation therapy for breast cancer: Radiotherapy techniques to decrease treatment morbidity. *In:* NABHOLTZ, J.-M., TONKIN, K., AAPRO, M. S. & REESE, D. M. (eds.) *Breast Cancer Management: Application of Clinical and Translational Evidence to Patient Care.* 2nd ed.: Lippincott Williams & Wilkins.

WANG, J., HU, W., YANG, Z., CHEN, X., WU, Z., YU, X., GUO, X., LU, S., LI, K. & YU, G. 2017. Is it possible for knowledge-based planning to improve intensity modulated radiation therapy plan quality for planners with different planning experiences in left-sided breast cancer patients? *Radiation oncology (London, England),* 12**,** 85-85.

WAZER, D. E. & ARTHUR, D. W. 2013. Breast Cancer: Stage Tis. *In:* HALPERIN, E. C., WAZER, D. E., PEREZ, C. A. & BRADY, L. W. (eds.) *Perez and Brady's Principles and Practice of Radiation Oncology.* 6 ed. Philadelphia, PA 19103 USA: Lippincott Williams & Wilkins.

WCRF INTERNATIONAL, W. C. R. F. I. 2023. *Breast cancer statistics* [Online]. Available: https://www.wcrf.org/cancer-trends/breast-cancer-statistics/ [Accessed 23 March 2023 2023].

WHEELER, J. A. & LAMB JR, W. E. 1939. Influence of atomic electrons on radiation and pair production. *Physical Review,* 55**,** 858.

WHO. 2015. *Breast cancer: prevention and control* [Online]. World Health Organisation. Available: http://www.who.int/cancer/detection/breastcancer/en/index1.html [Accessed 19/03/2015 2015].

WHO, W. H. O. 2021. Breast Cancer Fact Sheet. *In:* ORGANIZATION, W. H. (ed.). World Health Organization.

WILSON, R. R. 1946. Radiological use of fast protons. *Radiology,* 47**,** 487-491.

WORLD CANCER RESEARCH FUND & AMERICAN INSTITUTE FOR CANCER RESEARCH 2018. *Food, nutrition, physical activity, and the prevention of cancer: a global perspective*, Amer Inst for Cancer Research.

XIA, P., GODLEY, A., SHAH, C., GREGORY M. M. VIDETIC, M. D. C. M. F. & SUH, J. 2018. *Strategies for Radiation Therapy Treatment Planning*, Springer Publishing Company.

XU, Z., WALSH, S. E., TELIVALA, T. P., MEEK, A. G. & YANG, G. 2009. Evaluation of the eclipse electron Monte Carlo dose calculation for small fields. *Journal of applied clinical medical physics,* 10**,** 75-85.

YU, E., SUZUKI, H., YOUNUS, J., ELFIKI, T., STITT, L., YAU, G., VUJOVIC, O., PERERA, F., LOCK, M. & TAI, P. 2012. The impact of post-mastectomy radiation therapy on male breast cancer patients—a case series. *International Journal of Radiation Oncology* Biology* Physics,* 82**,** 696-700.

YUDELEV, M., TATCHER, M., MANDELZWEIG, Y. & KUTEN, A. Behaviour of the virtual electron source of the Philips SL 75-10 linear accelerator. The Nuclear Societies of Israel, Joint annual meeting 1982 Transactions, v 10, 1982 Israel. Israel Atomic Energy Commission; Tel-Aviv University, 191-194.

ZACKRISSON, B. & KARLSSON, M. 1996. Matching of electron beams for conformal therapy of target volumes at moderate depths. *Radiotherapy and Oncology,* 39**,** 261-270.

ZAGARS, G. K. 2010. Principles of Combining Radiation Therapy and Surgery. *In:* COX, J. D. & ANG, K. K. (eds.) *Radiation oncology : rationale, technique, results.* 9th ed. / ed. Philadelphia: Mosby.